
Site U1370¹

Expedition 329 Scientists²

Chapter contents

Background and objectives	1
Operations	2
Lithostratigraphy	3
Paleontology and biostratigraphy	7
Physical properties	8
Paleomagnetism	11
Biogeochemistry	11
Microbiology	15
References	17
Figures	19
Tables	57

Background and objectives

Integrated Ocean Drilling Program (IODP) Site U1370 (proposed Site SPG-11B) was selected as a drilling target because

- Its microbial activities and cell counts were expected to be characteristic of the southern gyre edge,
- Its basement age (~75 Ma) renders it a reasonable location for quantifying the extent to which relatively old and deeply buried sedimentary microbial communities may be sustained by hydrogen from water radiolysis, and
- Its basement age also makes it a reasonable location for testing the extent of sediment-basement interaction in a moderately sedimented region of relatively old basaltic basement (D'Hondt et al., 2010).

The principal objectives at Site U1370 are

- To document the habitats, metabolic activities, genetic composition, and biomass of microbial communities in subseafloor sediment with very low total activity;
- To test how oceanographic factors control variation in sedimentary habitats, activities, and communities from gyre center to gyre margin;
- To quantify the extent to which these sedimentary microbial communities may be supplied with electron donors by water radiolysis; and
- To determine how sediment-basement exchange and potential activities in the basaltic basement vary with basement age and hydrologic regime (from ridge crest to abyssal plain).

Site U1370 (5074 meters below sea level) is in the South Pacific Gyre within a region of abyssal hill topography trending northeast-southwest (065°) with relief ranging from 50 to 100 m (Fig. F1). Abyssal hill spacing is ~5–8 km with a relatively subdued fabric that has been smoothed by sedimentation. Two seamounts (500 m high; 6 km wide) are at the eastern limit of the survey area. The largest seamount is ~10 km east of the coring site. The closest previous drilling site is Ocean Drilling Program Leg 181 Site 1123, 810 nmi away.

The coring site is within magnetic polarity Chron 33n, so the crustal age may range from 73.6 to 79.5 Ma (Gradstein et al., 2004). Based on a tectonic reconstruction of the region by Larson et al. (2002), the crust was accreted along the Pacific-Phoenix spreading center at ~75 Ma.

¹Expedition 329 Scientists, 2011. Site U1370. In D'Hondt, S., Inagaki, F., Alvarez Zarikian, C.A., and the Expedition 329 Scientists, *Proc. IODP, 329*: Tokyo (Integrated Ocean Drilling Program Management International, Inc.).
doi:10.2204/iodp.proc.329.108.2011

²Expedition 329 Scientists' addresses.



Many geological and geophysical characteristics of the target site were characterized by the 2006/2007 KNOX-02RR survey expedition (D'Hondt et al., 2011) (Figs. F1, F2, F3, F4, F5, F6). The shallow sediment (0–5.6 meters below seafloor [mbsf]) consists of brown clay with frequent round mottles of very pale brown (D'Hondt et al., 2009). Smear slides are barren of microfossils. Manganese nodules occur at the sediment/water interface.

D'Hondt et al. (2009) documented the presence of microbial cells and oxic respiration throughout the uppermost 3 m of sediment at Site U1370. Cell concentrations were approximately three orders of magnitude lower than at similar depths in previously drilled marine sediment of other regions. Net respiration was similarly much lower than at previously drilled sites. From extrapolation of dissolved oxygen content in the uppermost 3 m of sediment, Fischer et al. (2009) predicted that dissolved oxygen penetrates the entire sediment column, from seafloor to basement.

Operations

Transit to Site U1370

After a 56.5 h transit from Site U1369, covering 625 nmi and averaging 11.1 kt, the speed was reduced and thrusters were lowered. Dynamic positioning was initiated over Site U1370 at 1602 h on 26 November 2010. The position reference was a combination of GPS signals. No acoustic beacon was deployed, but a beacon remained on standby in the event of a loss of GPS satellite coverage. While automatic input into the dynamic positioning system was not possible because of a system malfunction, it was possible to manually hold the vessel in position to clear the seafloor with the bottom-hole assembly if necessary.

All times in this section are given in local ship time unless otherwise noted. For most of the expedition, local time was Universal Time Coordinated – 10 h.

Site U1370

Six holes were drilled or cored at Site U1370 (Table T1). The first hole was a washdown hole drilled with the center bit in order to establish the sediment depth of 66.7 mbsf and any hard layers (chert) throughout the formation. Hole U1370B had one mudline core taken before coring problems forced abandonment of the hole. Hole U1370C was drilled to 7.8 mbsf, and the attempt to take a piston core failed. The last three holes were cored successfully with the advanced piston corer (APC) system. The advanced piston corer temperature tool (APCT-3)

was deployed four times on Holes U1370D and U1370E. Perfluorocarbon tracer (PFT) for contamination testing was pumped from Hole U1370C onward until the last core was on deck. A total of 26 cores were attempted while coring 206.3 m. The total length of core recovered at this site was 214.59 m. The overall recovery for Site U1370 using the APC coring system was 104%.

Hole U1370A

Rig floor operations commenced at 1602 h on 26 November 2010. The trip to the seafloor was uneventful. The top drive was picked up, the drill string was spaced out, and the hole was spudded at 0230 h on 27 November. The washdown hole was drilled to determine depth of basement. Mudline was established as 5085.7 meters below rig floor (mbrf) using an offset depth from Hole U1370B. After drilling down, basement was established at 5150.4 mbrf (64.7 mbsf). Basement depth was verified by drilling two additional meters into the basement. The bit was pulled back above the seafloor, clearing the seafloor at 0620 h and ending Hole U1370A.

Hole U1370B

After clearing the seafloor, the center bit was pulled by wireline, the vessel was offset 20 m west, and the drill string was spaced out to spud Hole U1370B. After making up the first APC core barrel, the core barrel was run to bottom on the wireline and Hole U1370B was spudded at 0745 h on 27 November. Seafloor depth was established at 5085.7 mbrf with a mudline core. APC coring was terminated after the second core attempt. It appeared as if there was something blocking the seal-bore collar that was preventing the core barrel from seating. The center bit was deployed in order to verify a clean seal-bore assembly and to check flow against the slow circulating rates taken at the start of the hole. Subsequent problems determined that it was most likely the shear pins failing during the deployment of the core barrel. The hole was terminated and several remedial measures were implemented. One core was taken with a total recovery of 7.81 m (100.1%). After Core 329-U1370B-1H was recovered, the bit was tripped back to just above the seafloor, ending Hole U1370B at 1000 h on 27 November.

Hole U1370C

Hole U1370C began at 1000 h when the APC assembly cleared the seafloor after completing Hole U1370B. After offsetting the vessel 20 m north, an attempt to spud Hole U1370C was made. After multiple wireline runs and multiple attempts to spud Hole U1370C, the hole was spudded at 1810 h in an

attempt to advance the hole and coring began. During the effort to continue coring, several remediation efforts were attempted. The root problem seemed to be shear pin failure during the wireline trip into the hole. Rig instrumentation indicated that the core line received increasingly high tension variation as the core line was run to greater depth. Variations were ~2500 lb of force. An extra shear pin was added to the system in an effort to land the core barrel with the shear pin assembly intact. This still failed. A 90° heading change was made to try to reduce the overall heave of the vessel. Decreasing weather and the heading change successfully reduced the heave by over a meter. In an attempt to dampen the tension variation, the compensator was opened for core barrel deployment. After a drilled advance of 7.8 m, the core barrel was finally deployed without the shear pin failure that had been experienced all day. With three shear pins installed and the core barrel landed, the mud pump pressure was insufficient to shear the pins and shoot the APC core barrel. Consequently, the core barrel was pulled to the surface and redressed with new shear system components and two shear pins. Hole U1370C was abandoned and the bit cleared the seafloor at 2000 h on 27 November, ending Hole U1370C.

Hole U1370D

Hole U1370D began at 2000 h, when the APC assembly cleared the seafloor after completing Hole U1370C. After offsetting the vessel 20 m east, Hole U1370D was spudded at 2115 h on 27 November. Seafloor depth was established with a mudline core at 5084.7 mbrf. An APCT-3 measurement was taken on Core 329-U1370D-4H. The APC coring system was used to take eight cores to 68.2 mbsf with 70.2 m recovery (103%). After Core 8H, the bit was advanced and rotated into basement to verify basement depth (68.2 mbsf) and the bit was tripped back to just above the seafloor, ending Hole U1370D at 1250 h on 28 November.

Hole U1370E

Hole U1370E began at 1250 h when the APC assembly cleared the seafloor after completing Hole U1370D. After offsetting the vessel 20 m east, Hole U1370E was spudded at 1445 h on 28 November. Seafloor depth was established with a mudline core at 5085.3 mbrf. An APCT-3 measurement was taken on Cores 329-U1370E-3H, 5H, and 6H. The APC system was used to take nine cores to 65.6 mbsf with a 70.2 m recovery (107%). PFT was mixed with the drilling fluid (seawater) and pumped on all cores for contamination testing. After Core 9H, the bit was advanced and rotated into basement to verify base-

ment depth (65.6 mbsf) and the bit was tripped back to just above the seafloor, ending Hole U1370E at 0855 h on 29 November.

Hole U1370F

Hole U1370F began at 0855 h when the APC assembly cleared the seafloor after completing Hole U1370E. The vessel was offset 20 m south of Hole U1370E. After making up the first APC core barrel, the core barrel was run to bottom on the wireline and Hole U1370F was spudded at 1010 h. Seafloor depth was established with a mudline core at 5084.8 mbrf. The APC system was used to take eight cores to 64.7 mbsf with a 66.32 m recovery (102.5%). PFT was mixed with the drilling fluid (seawater) and pumped on all cores for contamination testing. After Core 329-U1370F-8H, the bit was advanced and rotated into basement to verify basement depth (64.7 mbsf). The drill string was tripped to the surface, clearing the rotary table at 0530 h on 30 November. The rig floor was secured for the 499 nmi transit to the next site, ending Hole U1370F and Site U1370 at 0600 h.

Lithostratigraphy

The sediment at Site U1370 is ~70 m thick. The dominant lithology is zeolitic metalliferous pelagic clay. The strata also contain a relatively short (30 cm to 2.9 m) interval of very pale brown to pale yellow nannofossil ooze that divides the clay into upper and lower units. The principal components of the clay are red-brown to yellow-brown semiopaque oxide (RSO), phillipsite, and smectite (see Site U1370 smear slides in “[Core descriptions](#)”; Fig. F7).

Lithologic Unit I lies between the sediment/water interface and the top of the nannofossil ooze at ~61 mbsf. Modal abundances of RSO, phillipsite, and clay are 36%, 29%, and 27%, respectively. Based on smear slide analyses, the ooze (Unit II) contains 96% coccolithophores, 3% phillipsite, and 1% clay. The lower clay (Unit III) is thin; it contains 88% RSO, 12% clay, and 0% phillipsite and directly overlays the basaltic basement. Volcanic glass is locally abundant (~43%) in Unit I; however, its overall abundance is only 7% and it is completely absent in Units II and III. Manganese nodules were not recovered in mudline cores. A large, fragmented nodule was recovered in Hole U1370D at 10 mbsf, and fragments of manganese-encrusted hardground were recovered in Hole U1370F at 52 mbsf.

The overall structure of the dark brown pelagic clay and pale yellow nannofossil ooze at Site U1370 is massive, although occasional laminations and thin beds are visible in the lower half of Unit I. *Planolites*

(horizontal) burrows are faintly visible in most of the mottled clay and are occasionally highlighted by very pale ellipses in the upper part of Unit I. *Trichichnus* (vertical) burrows blend the upper and lower contacts of the pale yellow nannofossil ooze and the over- and underlying metalliferous clay. Lithostratigraphic correlation among Site U1370 holes shows that sediment thickness and composition are uniform (Fig. F8).

The pelagic sediment rests on altered basalt that was recovered in small fragments in Cores 329-U1370D-8H (~68 mbsf) and 329-U1370F-8H (~65 mbsf).

Description of units

Unit I

Subunit IA

Intervals: 329-U1370D-1H-1, 0 cm, to 6H-CC, 22 cm; 329-U1370E-1H-1, 0 cm, to unrecovered (see below); 329-U1370F-1H-1, 0 cm, to 6H-CC, 24 cm

Depths: Hole U1370D = 0–53.9 mbsf, Hole U1370E = 0 to >51.6 mbsf (see below), Hole U1370F = 0–53.9 mbsf

Lithology: metalliferous zeolitic pelagic clay and metalliferous clay

The overall color of the clay is brown (7.5YR 5/3) (Fig. F9A). Circular and elliptical rings, 1–2 mm thick with diameters between 1 and 3 cm, are very pale brown (10YR 8/4) with occasional black (2.5Y 2.5/1) grains located along the inner and outer rims of the rings. In the intervals with a large number of rings, the overall color is a slightly lighter shade of dark brown (10YR 3/3). The manganese nodule and hardground recovered in Hole U1370D and U1370F, respectively, are black (2.5/N) (Fig. F9B).

Smear slide analyses identify RSO, phillipsite, and clay as the dominant sedimentary components of Subunit IA (Fig. F10A). The lower contact of the subunit is based on a gradational color change that corresponds to modal changes in phillipsite abundance. Average phillipsite abundance is 26% and changes very little throughout the upper 45 m of Subunit IA (Fig. F7). Phillipsite abundance decreases sharply through the lower 8 m of the subunit. Clay occurs in a wide range of abundances, from 13% to 43%, with its highest average concentration in the middle third of Subunit IA. Minerals identified by X-ray diffraction (XRD) analyses are smectite and illite. Other minerals identified by XRD are phillipsite, quartz, cristobalite, tridymite, and plagioclase (Fig. F11A). The cristobalite and tridymite could not be confirmed visually in smear slides and may exist as tiny crystals in the clay. The manganese nodule found in Hole U1370D at 10 mbsf filled the core liner com-

pletely and was apparently trimmed by coring. When sawn in half, the cross-sections showed multiple concentric rings of increasing diameter that coalesced to form the single, large nodule. The exterior surface of the closely spaced manganese-encrusted sediment (i.e., hardground) found at 52.5 mbsf in Hole U1370F contained warty surfaces and a friable exterior rind. The mudline sample from Hole U1370B and two other samples deeper in this unit (Samples 329-U1370B-1H-CC and 2H-CC [residue from catwalk processing]) were scanned for fossils and found to be barren except for rare fish teeth.

Subunit IA sediment changes gradually from very poorly consolidated near the mudline to poorly consolidated at the base of the subunit. The manganese nodule and hardground in Holes U1370D and U1370E, respectively, are well consolidated but brittle.

The structure of Subunit IA is massive with occasional burrows and thin bedding of various thickness (3 mm to 2 cm), color (gray to brown), and sharpness (diffuse to sharp). The majority of the burrows are *Planolites* associated with horizontal traces formed in the seafloor transition layer (5–8 cm; Ekdale et al., 1984). Occasional vertical burrows of unknown ichnofacies association appear in Subunit IA below 4 mbsf. Bedding features are not uniformly distributed. For example, layering is more apparent in the lower subunit intervals. The lower contact with Subunit IB occurs at a core break in Holes U1370D and U1370F. In Hole U1370E, the boundary was likely in the bottom of Core 329-U1370E-6H (Fig. F8); however, the bottom of that core was lost during core recovery. Furthermore, Cores 329-U1370E-7H and 8H consisted of 100% disturbed (fall-in and flow-in) sediment. Thus, the only estimate of the position of the Subunit IA/IB boundary in Hole U1370E that we can make is that it exists below Core 329-U1370E-6H and at a depth of >51.6 mbsf.

Subunit IB

Intervals: 329-U1370D-7H-1, 0 cm, to 7H-6, 88–93 cm; 329-U1370E-6H-CC, 33 cm, to unknown; 329-U1370F-7H-1, 0 cm, to 7H-CC, 23 cm

Depths: Hole U1370D = 53.5–61.9 mbsf, Hole U1370E = >51.6 m to unknown, Hole U1370F = 54.2–62.4 mbsf

Lithology: zeolitic metalliferous pelagic clay

The overall color of the clay is dark brown (7.5YR 3/2), gradually changing to black (7.5YR 2.5/1) in the lower meter of the interval (Fig. F9D). A very small portion of Subunit IB contains elliptical burrow traces with outlines that are very pale brown (10YR 8/4). Claystone pieces and matrix recovered

from interval 329-U1370D-7H-3, 126–128 cm (Fig. F9C), are olive-brown (2.5Y 4/4). In Hole U1370F, the same layer lacks claystone pieces but includes planar burrow traces along its lower contact that are white (10YR 8/1) (Fig. F12). The interval immediately overlying the lower contact (~3 cm thick) is very dark brown (7.5YR 2.5/2).

Smear slide analyses identify RSO, phillipsite, and clay as the dominant sedimentary components of Subunit IB (Fig. F7). Although RSO concentration is sharply lower than that found in the lower 5 m of Subunit IA, the overall abundance increases to 40% (an increase of 16%). Phillipsite abundance varies between 18% and 59% with an average modal concentration of 38%. Throughout the unit, the phillipsite crystals range in size from <10 to 60 μm (Fig. F10B). Clay abundance drops from an average of 30% in Subunit IA to 16% in Subunit IB. XRD analysis of Sample 329-U1370D-7H-2, 143–144 cm, a representative sample from the middle of Subunit IB, shows that clay mineralogy is illite-smectite (Fig. F11A). Several peaks in the diffractogram are unresolved but could result from the very small amounts of plagioclase and quartz noted during petrographic inspection of smear slides or weakly crystalline iron and manganese hydroxides associated with the RSO. The only fossils noted in smear slide analyses of Subunit IB are coccolithophores in the lowermost (3 cm) interval immediately overlying Unit II. Their abundance is roughly 5% of the total sediment volume.

Subunit IB is firm clay. The claystone hardground located just below the interval's midpoint is highly indurated.

Subunit IB is ~8.5 m thick. The upper 1 m is massive with faint mottling. Occasionally isolated burrows (2 cm maximum diameter) are visible in the middle of the very dark brown sediment. The middle of the interval also contains bioturbation that forms 1–3 cm thick brown and dark gray horizontal layers. There are no burrows in the 70 cm overlying Unit II. A claystone hardground 2 cm thick and consisting of small clay pebbles residing in a coarse matrix was observed in intervals 329-U1370D-7H-3, 126–128 cm, and 329-U1370F-7H-3, 79–85 cm (Fig. F9C). Upper and lower contacts of the bed are irregular and bioturbated. In Hole U1370F, the lower contact of the hardground contains thin, white, hexagonal *Paleodictyon* burrow traces (Fig. F12). The lower contact of Subunit IB (with Unit II) has three notable attributes:

- The contact is very sharp and sets zeolitic metalliferous pelagic clay that is lacking any evidence of carbonate, directly upon nannofossil ooze with a very high concentration (>80%) of coccolithophores and foraminifers (see “[Paleontology and biostratigraphy](#)”);

- The contact is inclined by 30° in the core; and
- A ~3 cm thick zone overlies the contact and, although it is zeolitic metalliferous pelagic clay similar to the overlying darker parts of Subunit IB, it is noticeably lighter in color (very dark brown, 7.5YR 2.5/2).

Unit II

Intervals: 329-U1370D-7H-6, 88–93 cm, to 8H-2, 10 cm; Hole U1370E (not recovered/observed; see below); 329-U1370F-7H-6, 80–90 cm, through 7H-6, 115–120 cm

Depths: Hole U1370D = 61.9–64.6 mbsf, Hole U1370E (unit not recovered/observed; see below), Hole U1370F = 62.38–62.47 to 62.73–62.77 mbsf

Lithology: nannofossil ooze

The overall color of the ooze is very pale brown (10YR 8/4) to pale yellow (2.5Y 8/4–8/6) (Fig. F9D). Darker shades of pale brown and pale yellow are associated with vertical burrows that lie in close proximity to the overlying (black) zeolitic metalliferous pelagic clay. Two nearly white (10YR 8/1) sediment layers (6 cm and 1 mm thick) lie 1 m and 1.1 m below the upper unit contact in Hole U1370D (Fig. F9E). One of these layers was observed in photographs of the ends of two sealed whole-round samples taken for microbiology studies in Hole U1370F.

Smear slide analyses show that Unit II is nannofossil ooze (Fig. F10C). The unit matrix is composed of disaggregated coccolithophorid tests. The ooze is nearly pure calcite containing small amounts of phillipsite (3%) and RSO (1%) only where bioturbation has mixed Unit II with Units I and III (Figs. F7, F11B). There are two white intervals that are 100% coccolithophores, coccolithophorid debris, and foraminifers. Micropaleontological analyses of wet-sieved samples show that the sediment fraction >38 μm is composed mainly of planktonic and benthic foraminifers of early Paleocene age (planktonic foraminifer Zone P1). The foraminifers found in Unit II are described fully in “[Paleontology and biostratigraphy](#).”

Unit II sediment is moderately consolidated and was recovered in Holes U1370D and U1370F. The stratigraphically equivalent interval in Hole U1370E recovered only fall-in and flow-in sediment. In Hole U1370D, the unit spans Cores 329-U1370D-7H and 8H. Unit II occupies the lowermost 140 cm of Core 7H (Sections 329-U1370D-7H-6, 7H-7, and 7H-CC). Core 329-U1370D-8H includes 12 cm of undisturbed ooze in Sections 329-U1370D-8H-1 and 8H-2 and 1.4 m of fall-in in the upper part of Section 8H-1. Thus, the true stratigraphic thickness of Unit II is likely 1.52 m, although as much as 2.9 m of Unit II was re-

covered in Hole U1370D. In Hole U1370F, the entire interval was removed by microbiological whole-round sampling. After observing the whole-round ends and photographs of whole-round ends, we conclude that the total thickness of Unit II in Hole U1370F is between 30 and 40 cm. Because cross-sections of the whole-round samples could not be observed, the cause of the observed difference in stratigraphic thickness cannot be ascertained and the description of structure that follows is based exclusively on observations from Hole U1370D.

Unit II is thoroughly bioturbated. *Trichichnus* (vertical) burrows are visible throughout the unit. The maximum burrow width is 6 mm and the length of an individual burrow ranges from 15 cm within the unit to 35–50 cm into the underlying clay (Fig. F9F). Two intervals within Unit II display white horizontal layering with clearly visible, small-scale (1–3 cm) bioturbation effects. The upper layer is 6 cm thick and the lower layer is ~1 mm thick. The lower contact of Unit II contains two tiers of bioturbation. The upper tier comprises 10 cm of mixed ooze and clay that is completely filled with short, overlapping vertical burrows. In the lower tier of burrowing, distinct *Trichichnus* burrows extend as far as 50 cm into the underlying metalliferous clay.

Unit III

Intervals: 329-U1370D-8H-2, 10 cm, to 8H-5, 40 cm; Hole U1370E (not recovered/observed); 329-U1370F-7H-6, 115–120 cm, to 7H-CC, 22 cm

Depths: Hole U1370D = 64.6–69.4 mbsf, Hole U1370E (not recovered/observed), Hole U1370F = 62.73–62.77 to 72.08 mbsf

Lithology: metalliferous clay

The color of the clay is very dark brown (7.5YR 2.5/3) to black (7.5YR 2.5/1) (Fig. F9F). There are no visible color changes.

Smear slide analyses show that RSO and clay are the two principal components of Unit III. RSO is dominant, comprising 88% of the unit (Fig. F10D). Although RSO grains come in a variety of sizes from <10 to 50 μm , most are ~10 μm with relatively few large semiopaque grains. The relative purity of the interval allows XRD results to partially resolve the diffraction pattern created by RSO. As shown in Figure F11B, the broad hump between 20.5° and 22°2 θ is centered on the peak locations for goethite ($\text{Fe}^{+3}\text{O}[\text{OH}]$; ICDD card 00029-0713) and ramsdellite (MnO_2 ; ICDD card 00-042-1316). These results do not, however, mandate the occurrence of goethite and ramsdellite within the RSO component. Rather,

they support previous work that suggests RSO is comprised of iron and manganese oxyhydroxides in poorly crystalline to amorphous solids (Heath and Dymond, 1977; Kastner, 1986).

The clay is uniformly firm. Flow-in occurred in Holes U1370D–U1370F. Flow-in was easily identified because it contained grains and clasts of green altered basalt.

There are no visible structures in any of the recovered portions of Unit III other than the *Trichichnus* burrows described previously. The unit's lower contact was not recovered in any of the holes (i.e., the recovery at the bottom of each hole was flow-in). Although the flow-in contained metalliferous clay from Unit III and basalt fragments from the underlying formation, the actual contact was not recovered.

Interhole correlation

Lithologic units are correlated among holes at Site U1370 to facilitate the integration of physical property, geochemical, and microbiological data. The stratigraphic correlation panel for Site U1370 is presented in Figure F8. Correlations shown in this figure are based on principal characteristics of the sediment, including

- Variable phillipsite and clay abundances that mark the Unit I subunit boundaries are evident in all three holes,
- Dramatic lithologic change from Unit I clay to Unit II ooze appears in Holes U1370D and U1370F,
- Characteristically very high natural gamma ray emanations occur just below the mudline in Holes U1370E and U1370F, and
- Strong magnetic susceptibility responses corresponding to the hardground facies are found in Holes U1370D and U1370F.

Lithostratigraphic correlation shows the strata at Site U1370 are not uniform. The most significant difference among the holes is the thickness of Unit II. Although coring disturbances make correlation difficult, Unit II thickness could differ by as much as 50% between Holes U1370D and U1370F. Lithology of Unit II in Hole U1370F could not be petrographically inspected or analyzed by XRD, but based on visual inspection of the sediment from Hole U1370F through core liner end caps, the unit appears to have similar composition in Holes U1370D and U1370F. Manganese nodules and hardgrounds are also unevenly distributed with depth among the three holes at Site U1370. However, Units I and III appear to be similar in both thickness and composition.

Paleontology and biostratigraphy

A ~70 m thick section of predominantly zeolitic metalliferous pelagic clay was recovered at Site U1370. The section also contained a short interval (30 cm in Hole U1370F to 2.9 m in Hole U1370D) of nannofossil ooze at ~62 mbsf (Fig. F13; see “[Lithostratigraphy](#)”). Site U1370 is on basement located within magnetic polarity Chron 33n, which implies a crustal age between 73.6 and 79.5 Ma (Gradstein et al., 2004). Based on a tectonic reconstruction of the region by Larson et al. (2002), the crust was accreted along the Pacific-Phoenix spreading center at ~75 Ma.

Three samples taken from the distinct layer of nannofossil ooze found in Hole U1370D (see “[Lithostratigraphy](#)”) were examined for paleontological and biostratigraphic purposes. Sample 329-U1370D-7H-6, 97–99 cm, just below the sharp contact with the overlying pelagic clay; Sample 7H-CC, from the middle of the layer; and Sample 8H-1, 147–149 cm, from the base. The samples were wet-sieved using a 38 μm mesh sieve to ensure the capture of smaller size planktonic foraminifers (see “[Paleontology and biostratigraphy](#)” in the “Methods” chapter [Expedition 329 Scientists, 2011a]). The silt- and clay-size fractions (<38 μm) were examined in smear slide samples (see “[Lithostratigraphy](#)”).

The biogenic component of the >38 μm sediment size fraction of the samples taken from the calcareous ooze interval is dominated by planktonic and benthic foraminifers with significantly lesser amounts of ostracods (Tables T2, T3). The <38 μm sediment size fraction is dominated by calcareous nannofossils (see “[Lithostratigraphy](#)”). Planktonic and benthic foraminifers are generally well preserved, although a fraction of the benthic specimens are abraded or show signs of dissolution. Preliminary results from postexpedition studies indicate that dissolution is more pervasive in the pelagic clay below and above the nannofossil ooze. No planktonic foraminifers were found in the pelagic clay immediately above the sharp contact with the underlying ooze, and calcareous benthic foraminifers are quickly replaced uphole by simple agglutinated forms.

Planktonic foraminifers

The overall planktonic foraminiferal assemblage is composed of *Chiloguembelina midwayensis*, *Chiloguembelina morsei*, *Eoglobigerina edita*, *Eoglobigerina eobulloides*, *Guembelitria cretacea*, *Parasubbotina pseudobulloides*, *Parasubbotina* aff. *pseudobulloides*, *Subbotina triloculinoides*, and *Subbotina trivialis*, among

others (Table T2). Planktonic foraminiferal taxonomic concepts follow Olsson et al. (1999).

Because of time limitations for shipboard micropaleontological analyses during Expedition 329, it was possible to produce only a preliminary planktonic foraminifer biostratigraphic control for the calcareous ooze interval recovered at Site U1370. The uppermost Sample 329-U1370D-7H-6, 97–99 cm, was provisionally assigned to lower Paleocene planktonic foraminiferal Zone P1b (~64.3 Ma) based on the presence of *S. triloculinoides* and *P. pseudobulloides* and the absence of distinctive markers of Zone P1c (Olsson et al., 1999; Wade et al., 2011). Basal Sample 8H-1, 147–149 cm, was provisionally assigned to lower Paleocene planktonic foraminiferal Zone P1a (64.97–64.8 Ma) based on the common occurrence of *G. cretacea*, *P.* aff. *Pseudobulloides*, and *C. morsei* and the absence of characteristic Zone P1b markers (Olsson et al., 1999; Wade et al., 2011). More detailed postexpedition shore-based analyses using scanning electron microscopy will be carried out to check the zonal assignments and better characterize the planktonic foraminiferal assemblages.

Calcareous nannofossils

Calcareous nannofossils were examined after the expedition by Dr. John Firth (IODP-Texas A&M University) in a few samples taken just above, below, and within the calcareous sedimentary interval found in Cores 329-U1370D-7H and 8H (lithologic Unit II [nannofossil ooze]; see “[Lithostratigraphy](#)”).

Sample 329-U1370D-7H-6, 75–79 cm, is composed primarily of red clay ~15 cm above the top of the calcareous ooze. This sample contains moderate to poorly preserved rare specimens of *Watzneuria* sp., *Quadrum* cf. *Q. gothicum*, *Prediscosphaera* sp., and *Eiffelithus* sp. These taxa are all Cretaceous taxa and do not range above the Cretaceous/Tertiary boundary. In addition, one specimen of *Discoaster* sp., with six slender rays, rounded tips, and very small knobs on the sides of the rays, occurs in this sample. This form of *Discoaster* only occurs in sediments of Eocene or younger age. Its presence in this sample could either be from contamination of the core surface or it could indicate an Eocene sedimentary age.

Sample 329-U1370D-7H-7, 37–41 cm, is within the calcareous ooze and contains abundant nannofossils. The assemblage is dominated by elliptical, mostly dark-shielded (both in cross-polarized light and in phase contrast) placoliths of small to medium size (3 or 4 μm up to ~10 μm). Many specimens of placoliths show some kind of internal structures either crossing or filling the central area. The preservation of nannofossil in this sample is moderate to

poor, which obscures the central structures in most specimens. Therefore identification of taxa is limited in most cases to the Genus level, or even the Subfamily or Family level. The following species are observed: *Markalius inversus* (rare), *Coccolithus pelagicus* s.l. (common to abundant?, small to medium sized), *Cruciplacolithus edwardsii* (few?), and *Cruciplacolithus* sp. cf. *C. tenuis* (medium sized, very rare?). The following genera are observed: *Thoracosphaera* spp. (rare), *Reinhardtites* sp. (rare to few?), *Eiffellithus* sp. (rare to few?), and *Cruciplacolithus* spp. (common to abundant?). The following Family/Subfamilies are observed: Podorhabdaceae/Podorhabdoideae (few to common?), Podorhabdaceae/Retecapsoideae (few to common?, possibly including the genera *Stradneria* and *Cretarhabdus*). Other than *M. inversus*, no other taxa from the Family Ellipsagelosphaeraceae, such as *Watzneuria*, were observed. This sample, therefore, appears to correspond to the upper part of Martini's (1971) Zone NP1 or possibly the base of Zone NP2, based on the occurrence of *C. edwardsii* and *Cruciplacolithus* cf. *C. tenuis* (one specimen). The occurrence of Cretaceous placoliths along with lower Paleocene placoliths indicates that the former have been reworked.

The assemblage in Samples 329-U1370D-7H-6, 90 and 130 cm, near the top of the calcareous ooze, is similar to that in Sample 7H-7, 37–41 cm, and does not show any taxa of younger age than in Sample 7H-7, 37–41 cm.

Sample 329-U1370D-8H-1, 67–71 cm, near the base of the calcareous ooze, was studied using scanning electron microscopy. The increased image resolution confirmed light microscope observations from the other calcareous ooze samples, specifically that the preservation of nannofossils is poor, with considerable overgrowth and dissolution/breakage of specimens. The assemblage is also similar to that from Samples 329-U1370D-7H-6, 90 and 130 cm, and Sample 7H-7, 37–41 cm. Common *Cruciplacolithus* specimens of early Paleocene age are accompanied by rare to common, poorly preserved specimens of Cretaceous age. In addition to Cretaceous taxa listed above, this sample also contained specimens of *Rhagodiscus* cf. *R. angustus*, *Eiffellithus* cf. *E. eximius*, possible *Teichorhabdus ethmose*, and *Cribrosphaerella* cf. *C. daniae*. Very small (3 μm) specimens of *Biscutum* sp. also occur, which have been recorded in both late Maastrichtian and early Paleocene age sediments elsewhere.

Sample 329-U1370D-8H-5, 18–25 cm, is within the red clay below the calcareous ooze and contains very rare specimens of Cretaceous nannofossils, such as *Watzneuria*.

These results indicate that the calcareous ooze of Core 329-U1370D-7H and 8H is all of early Paleocene age, approximately upper Zone NP1 or basal Zone NP2 (Martini, 1971). Cretaceous taxa within the ooze all have stratigraphic ranges into the Maastrichtian, except for *Eiffellithus* cf. *E. eximius*, which has a highest occurrence in the upper Campanian. However, the red clay above the calcareous ooze (Sample 7H-6, 75–79 cm) contains rare Cretaceous taxa that were not observed within the calcareous ooze. We interpret these specimens to be reworked based on the lower Paleocene nannofossils recovered within the calcareous ooze and based on the single specimen of *Discoaster* in that sample, which may indicate a possible Eocene age.

Benthic foraminifers

Benthic foraminifers are abundant and moderately well preserved throughout the calcareous nannofossil ooze at the base of the Hole U1370D. Benthic foraminiferal assemblages from this interval are dominated by large, heavily calcified Paleocene to Eocene taxa. More than 23 species were identified (Table T3). The most common taxa are *Aragonia ouezzanensis*, *Aragonia velascoensis*, *Dorothia trochoides*, *Nuttalides truempyi*, *Lenticulina* spp., *Oridorsalis umbonatus*, and *Stilostomella* spp. Benthic foraminiferal taxonomic concepts follow Tjalsma and Lohman (1983).

Ostracods

One as yet unidentified ostracod specimen was found in Sample 329-U1370D-7H-CC.

Paleoenvironmental interpretation

The nannofossil ooze found at Site U1370 was deposited during lower Paleocene foraminiferal Zone P1. The ooze's occurrence in this deep-sea clay sequence is attributed to deepening of the calcite compensation depth and lysocline during the interval of decreased planktonic carbonate precipitation that followed the end-Cretaceous mass extinction (D'Hondt, 2005).

Physical properties

At Site U1370, physical properties measurements were made to provide basic information characterizing lithologic units. After sediment cores reached thermal equilibrium with ambient temperature at $\sim 20^{\circ}\text{C}$, gamma ray attenuation (GRA) density, magnetic susceptibility, and *P*-wave velocity were measured with the Whole-Round Multisensor Logger (WRMSL) on whole-round core sections. After

WRMSL scanning, the whole-round sections were logged for natural gamma radiation (NGR). Thermal conductivity was measured using the full-space method on sediment cores. Discrete *P*-wave measurements were made on split sediment cores using the Section Half Measurement Gantry. Moisture and density (MAD) were measured on discrete subsamples collected from the working halves of the split sediment cores. Additional discrete measurements of electrical resistivity were made on the split sediment sections to calculate formation factor. The Section Half Imaging Logger was used to collect images of the split surfaces of the archive-half cores, and a color spectrophotometer was used to measure color reflectance on the Section Half Multisensor Logger (SHMSL). Three holes targeted the sedimentary cover, Holes U1370D–U1370F. The most complete hole for logging physical properties was Hole U1370D. The sediment recovered from different holes has not been correlated and offsets exist.

Density and porosity

Bulk density values at Site U1370 were determined from both GRA measurements on whole cores and mass/volume measurements on discrete samples from Hole U1370D from the working halves of split cores (see “[Physical properties](#)” in the “Methods” chapter [Expedition 329 Scientists, 2011a]). A total of 44 discrete samples were analyzed for MAD.

Bulk density values in Hole U1370D increase slightly with depth throughout lithologic Unit I (Fig. [F14A](#)). In lithologic Unit II (nannofossil ooze), density is greater than in Units I and III (metalliferous clay). The average density of Units I and III is 1.32 g/cm³, and the average density of Unit II is 1.49 g/cm³. Bulk density discrete values generally agree with GRA values of bulk density above ~30 mbsf, but beneath this depth the discrete values are significantly lower than GRA values. GRA density calibrations were checked, but the source of this offset is not known. Grain densities have a mean value of 2.38 g/cm³, with some values approaching 3 g/cm³ (Fig. [F14B](#)). Porosity generally decreases with depth and varies between ~87% and 71% (Fig. [F14C](#)).

The mean value of bulk density in Hole U1370B is 1.3 g/cm³ and is slightly higher in lithologic Unit II than in Unit I. The scattered values in Hole U1370B deeper than 15.5 mbsf likely reflect core disturbance. Gaps and scatter in bulk density values for Holes U1370C and U1370E are due to whole rounds being taken for geochemical and microbiological sampling prior to WRMSL measurements.

Bulk densities for Holes U1370D, U1370E, and U1370F are shown in Figure [F15](#). Bulk density values

in Holes U1370E and U1370F are in good agreement with those in Hole U1370D, suggesting that the offset between GRA and MAD values shown in Figure [F14](#) are more likely due to the MAD values than the GRA values.

Magnetic susceptibility

Volumetric magnetic susceptibilities were measured using the WRMSL, and point measurements were made on the SHMSL in all recovered cores from Site U1370. Uncorrected values of magnetic susceptibility are presented for Holes U1370D–U1370F (Fig. [F16](#)). Point measurements from archive halves are much more scattered than whole-core measurements, and peak-to-peak variability is greatly subdued in the point measurements. Notably, point measurements of magnetic susceptibility in areas of core disturbance show the largest scatter, with means that are either high or low relative to the bulk of the data. The spatial resolution of the WRMSL magnetic susceptibility loop is ~5 cm, and the observed ringing in Holes U1370C and U1370E is due to edge effects.

Magnetic susceptibility generally increases with depth through lithologic Unit I with a peak ~5 m above the Unit I/II contact. Magnetic susceptibility values within Unit II (Holes U1370D and U1370F) are low, although about half of the core material in this unit is disturbed (i.e., Section 329-U1370D-8H-1; see “[Lithostratigraphy](#)”). Magnetic susceptibility in Unit III reaches a maximum just below the Unit II/III contact and then decreases with depth. The high magnetic susceptibility in Units I and III is likely due to the RSO content of the clay (see “[Lithostratigraphy](#)”).

Natural gamma radiation

NGR results are reported in counts per second (Fig. [F17](#)). NGR counting intervals were ~60 min per whole-core interval for Hole U1370D and decreased to 30 min per whole-core interval for Holes U1370E and U1370F. NGR counts are considered reliable. NGR at the tops of Holes U1370E and U1370F are high, indicating that the sediment/water interface was sampled.

In general, NGR counts increase with depth through lithologic Unit I, are low in Unit II, and decrease with depth through Unit III (Fig. [F17](#)). These patterns are similar to those observed in the magnetic susceptibility data (Fig. [F16](#)). Ringing is more prevalent in cores from Holes U1370E and U1370F because only short core pieces remained after whole-round sampling prior to NGR measurements.

P-wave velocity

P-wave velocity at Site U1370 was determined from measurements on whole-round sediment cores (Fig. F18) and on discrete samples from the working halves of sediment split cores (see “Physical properties” in the “Methods” chapter [Expedition 329 Scientists, 2011a]). Only six discrete measurements of P-wave velocity were measured. These discrete values are somewhat higher than measurements made on whole rounds, which may be due to drying of core material. The mean value of all whole-core measurements is ~1510 m/s (Fig. F18B). In Hole U1370B, compressional wave velocities are relatively uniform except in the upper portion of lithologic Unit III, where it is <1500 m/s.

Formation factor

Electrical conductivity was measured on working halves of the split sediment cores from Hole U1370B. Measurements in Hole U1370B were made at a nominal interval of 10 cm. For each measurement, the temperature of the section was also noted. Surface seawater was used as a standard and measured at least twice per section (Table T4), normally prior to making measurements for that section and again around the 75 cm offset of each section. These measurements were used to compute the drift for this set of measurements (Fig. F19). Near measurement 400, the drift changed substantially, likely caused by wearing away of platinum on the electrodes. For this set of measurements, we used two linear trends to describe the drift. The temperature dependence of electrical conductivity was corrected and all reported measurements correspond to a temperature of 20°C. Electrical conductivity measurements were transformed to a dimensionless formation factor by dividing the measurements for the drift (Table T5).

In general, the formation factor in lithologic Unit I increases with depth and varies between ~1.4 and ~2.5 (Fig. F20). The formation factor in Unit II is scattered between 2 and 2.5. Within Unit III values decrease from about 2.2 to 1.6. This pattern correlates with porosity (Fig. F14C).

Thermal conductivity

Thermal conductivity measurements were conducted on sediment whole-round cores using the needle-probe method and on basement split cores using the half-space method (see “Physical properties” in the “Methods” chapter [Expedition 329 Scientists, 2011a]). In general, measurements appear reliable, although values <0.6 W/(m·K) were culled from the analysis. Values <0.6 W/(m·K) are attributed to either poor contact between the probe and the

sediment or convection that leads to unreasonably low estimates of thermal conductivity by causing the thermal response to heating to depart from the theoretical prediction. Values are relatively constant with depth through lithologic Unit I and appear to decrease with depth through Unit III. The mean thermal conductivity is 0.7 W/(m·K) (Fig. F21A). In the uppermost 3 m or so, thermal conductivities collected during the KNOX-02RR site survey cruise (R. Harris, unpubl. data) are somewhat higher than the values reported but also have a mean of 0.7 W/(m·K).

Downhole temperature

Downhole temperature was measured using the APCT-3. In total, four measurements were attempted between 25.2 and 53.7 mbsf in Holes U1370D and U1370E (Table T6). All measurements were made in lithologic Unit I.

All temperature-time series were recorded with a sample interval of 1 s. The temperature tool was stopped at the mudline for up to 10 min prior to the first measurement and then for a period of 5 min thereafter. The average bottom water temperature is 1.24°C (Table T6). All measurements were made in a relatively extreme sea state (~5 m swell), and each temperature-time series suffers to some extent from the ship’s heave (Fig. F22). Significant frictional heating occurred on all penetrations of the APCT-3, with the temperature-time records exhibiting characteristic probe penetration and subsequent decay. Tool movement was observed in all temperature records as sudden shifts in temperature both before and after the usable section of the temperature-time series. Tool movement is attributed to the ship’s heave. The effective origin time of the frictional heat pulse was estimated by varying the assumed origin time until the thermal decay pulse best fit a theoretical curve. As a result of tool movement, delay times are large and fits to the equilibrium curve are short (Table T4). Nevertheless, all measurements appear to be reliable. Equilibrium temperatures plotted as a function of depth are relatively linear; coupled with the average bottom water temperature, they give a least-squares gradient of 93.0°C/km (Fig. F21B).

Heat flow

Because thermal conductivity appears relatively constant in lithologic Unit I and the thermal gradient is linear, heat flow is computed as the product of the thermal conductivity and thermal gradient. Using the average thermal conductivity of 0.7 W/(m·K) and thermal gradient of 3.0°C/km yields a heat flow value of 65 mW/m². This value is consistent with conductive cooling models for crust of this age.

Color spectrometry

Spectral reflectance was measured on split archive-half sections from Holes U1370D–U1370F. Measurements from Hole U1370D are shown in Figure F23. All parameters generally decrease with depth. Values for L^* are generally <50 but are >50 in lithologic Unit II (nannofossil ooze). Values for a^* and b^* are between 10 and 0 and 30 and 0, respectively, with maximum values in Unit II. Values for a^* and b^* appear modestly correlated.

Paleomagnetism

At Site U1370, we measured natural remanent magnetization of all archive-half sections for Holes U1370B and U1370D–U1370F using the three-axis cryogenic magnetometer at 2.5 cm intervals before and after alternating-field demagnetization. The archive-half sections were demagnetized by alternating fields of 10 and 20 mT. The present-day normal field in this region, as expected from the geocentric axial dipole model at Site U1370, has a negative inclination (approximately -60.8°), so positive remanence inclinations indicate reversed polarity. Data from Holes U1370E and U1370F provide only a partial record because whole-round core samples were taken from these holes for geochemical and microbiological analyses. The primary objective of the shipboard measurements for Site U1370 was to provide chronostratigraphic constraint by determining magnetic polarity stratigraphy. During coring operations at Site U1370, both nonmagnetic core barrels and the Flexit core orientation tool were used (see “[Operations](#)”).

Results

Paleomagnetic data for Holes U1370B and U1370D–U1370F are presented in Figures F24, F25, F26, and F27, together with the whole-core susceptibility data measured on the WRMSL (see “[Physical properties](#)”). The lithology at Site U1370 changed from zeolitic metalliferous pelagic clay (Unit I) at the top to nannofossil ooze in Unit II and metalliferous clay in Unit III, immediately above the basaltic basement (see “[Lithostratigraphy](#)”).

Using magnetic susceptibility data, it was possible to correlate between Holes U1370B and U1370D (Fig. F28). For the upper sediment column, this correlation was applied to the magnetic intensity data and to the inclination and declination data. The correlation between Holes U1370B and U1370D clearly shows that changes in magnetic polarity are consistent between the two holes in the uppermost ~ 10 mbsf. Reversals are seen in inclination and declina-

tion data throughout most of the ~ 70 m of Holes U1370D–U1370F. Correlation between Holes U1370D–U1370F for the entire ~ 70 m section using magnetic susceptibility and magnetic intensity is shown in Figure F29. This correlation was applied to the inclination and declination data (Fig. F30), showing that some reversals are consistent between the three holes in the deeper part of the section.

According to the shipboard interpretation of planktonic foraminiferal assemblages found in the nannofossil ooze in Unit II in Hole U1370D (at ~ 64 mbsf), the sedimentary record at Site U1370 has been assigned an estimated age of early Paleocene (~ 64.9 Ma) (see “[Paleontology and biostratigraphy](#)”). However, it is not possible to make any interpretation of the magnetic polarity stratigraphy at Site U1370. Given the difficulty in determining the age of the sediment section by shipboard paleomagnetic studies, chronostratigraphy for Site U1370 must be determined by postexpedition studies, including further magnetic cleaning by increased alternating-field demagnetization and use of other chronostratigraphic tools.

Biogeochemistry

Site U1370 sediment comprises 60–70 m of mostly zeolitic metalliferous pelagic clay and metalliferous pelagic clay (see “[Lithostratigraphy](#)”) deposited on 74 to 80 Ma basement at the southern edge of the oligotrophic South Pacific Gyre. Extensive sampling and analyses were performed to address

- How biogeochemical parameters in the sediment and interstitial water vary with oceanographic factors, such as ocean productivity and sedimentation rate, from gyre center (Site U1368) to the southern gyre edge (Site U1370);
- The extent to which the microbial community within the sediments may be supplied with electron donors by water radiolysis; and
- How sediment-basement exchange and potential activities in the basaltic basement vary with basement age and hydrologic regime from ridge crest to abyssal plain.

Given its relatively thick sedimentary sequence, Site U1370 also presented an opportunity to obtain interstitial water profiles for study of deepwater nutrient and oxygen variations subsequent to the Last Glacial Maximum.

Oxygen concentrations were profiled on complete sections from Holes U1370B (a mudline core; see “[Operations](#)”) and U1370D and from intact section intervals that remained after biogeochemical and microbiological sampling on Holes U1370E and

U1370F. Samples for methane (both safety and refined; see “**Biogeochemistry**” in the “Methods” chapter [Expedition 329 Scientists, 2011a]) were obtained during catwalk sampling on core ends from Holes U1370B and U1370D. Interstitial water samples were obtained through squeezing (54 samples) and Rhizon sampling (70 samples) on sediment intervals from Holes U1370B (Rhizon only), U1370E, and U1370F. With the exception of six interstitial water intervals from Core 329-U1370E-1H cut in the Hold Deck core refrigerator, all of the interstitial water whole-round cores were taken on the catwalk after core recovery and delivered to the Geochemistry Laboratory for interstitial water squeezing.

Interstitial water was extracted by Rhizon sampling after oxygen measurements on Core 329-U1370B-1H in the Geochemistry/Microbiology Laboratory cold room. Otherwise, Rhizon sampling took place in the ship’s core refrigerator on the Hold Deck. Because of the low permeability of the samples from Site U1370, extraction using the Rhizon samplers often continued for up to 12 h and recovery was sometimes as low as 4 mL (see Fig. F11 in the “Methods” chapter [Expedition 329 Scientists, 2011a]). Syringe sampling for dissolved hydrogen analysis was coupled to interstitial water whole-round sampling. Separate interstitial water samples for He and ^{14}C -dissolved inorganic carbon were also cut on the catwalk and delivered directly to the container laboratory on the deck above the bridge for immediate squeezing and sampling. These samples never entered the interior of the ship. Poor recovery during coring operations in Hole U1370E necessitated the addition of samples from Hole U1370F. For analysis of solid-phase carbon and nitrogen concentrations, 44 samples from Holes U1370E and U1370F were obtained. An additional 8 samples from Hole U1370D were analyzed to characterize lithologic Unit II (nannofossil ooze) and the clay that lay immediately above and below it.

Dissolved oxygen

Dissolved oxygen (O_2) was measured using optodes and electrodes on intact 1.5 m core sections from Holes U1370B and U1370D after delivery from the catwalk to the Geochemistry/Microbiology Laboratory cold room. Additionally, dissolved oxygen was determined using both optode and electrode measurements on intact core section intervals remaining after biogeochemistry and microbiological sampling (Hole U1370E) had taken place in the Hold Deck’s core refrigerator. Electrode measurements in Holes U1370B and U1370D were performed at 20–30 cm intervals (Table T7) and optode measurements were performed at 10–50 cm depth intervals (Table T8) for

the uppermost 3 mbsf. At greater depths, measurements were performed at 20 (electrode) and 50 cm (optode) intervals. Electrode measurements in Holes U1370E and U1369F were performed at 20–50 cm intervals in the remaining whole rounds (Table T7).

Dissolved oxygen concentration profiles obtained with both optode and electrode methods show that the dissolved oxygen profile at Site U1370 is strikingly different from the previous sites. The dynamic range of oxygen concentration measurements captures both oxygen consumption in the sediment and deep fluxes of oxygen toward the basaltic crust. Oxygen concentrations in Holes U1370B and U1370D range from 122.4 to 149.7 μM in sediment from surface to 0.2 mbsf. Oxygen concentrations decrease to 80.9 μM at 7.8 mbsf (Hole U1370B electrode) (Table T7; Fig. F31B) and 88.3 μM at 7.6 mbsf (Hole U1370B optode) (Table T8; Fig. F31A). Explanation of the decrease in the uppermost 5–10 m of sediment as caused by organic oxidation is consistent with steep increases in phosphate and nitrate concentrations through these depths. Below 10 mbsf, oxygen concentrations continue to decrease with a gradual concave-upward pattern to 20 mbsf (except for data from a disturbed core of U1370B [18–22 mbsf]). Between 20 and 30 mbsf, the dissolved oxygen profile exhibits a deep zone where concave-upward curvature of the profile is at a maximum in subsurface depths. Processes controlling the oxygen profile above 40 mbsf are attributed to oxygen consumption by aerobic respiration of sedimentary microbes.

Below 40 mbsf, dissolved oxygen measurements decrease monotonically from $\sim 10 \mu\text{M}$ to a few micromolar at the sediment/basalt interface ($\sim 6 \mu\text{M}$ from 67 to 68 mbsf, as measured by optode [Table T8; Fig. F31C]; $\sim 1 \mu\text{M}$ from 64 to 68 mbsf, as measured by electrode [Table T7; Fig. F31D]). The relatively high oxygen concentrations below 69.3 mbsf (Fig. F31D) are consistent with visual evidence of flow-in (see “**Lithostratigraphy**”). Since the sediment/basement interface in Hole U1370D was tagged by the drill bit at 78.2 mbsf (see “**Operations**”), the total sediment column thickness slightly exceeds the apparent depth of the hole. This excess is consistent with flow-in of sediment in the deepest core.

The very slight offset between optode and electrode measurements may be attributed to the challenges of measuring extremely small concentrations of oxygen with microsensors in these sediments. Most important is that both methods show that oxygen concentrations monotonically decrease with the same gradient toward the basement. This suggests that oxygen concentration in the lower sediment column is controlled by a continued flux toward the underlying basalt crust.

Dissolved hydrogen and methane

Dissolved hydrogen (H_2) concentration was quantified for 45 samples collected from Hole U1370E and 13 samples from Hole U1370F (Fig. F32; Table T9). The depths analyzed ranged from 0.4 to 65.0 mbsf. Five samples were taken during subsampling in the core refrigerator on the Hold Deck, whereas the remaining samples were collected on the catwalk immediately after core recovery. After describing the split core, Core 329-U1370E-8H was determined to be disturbed; consequently, H_2 concentrations in samples taken from this core cannot be interpreted as in situ. Based on the average of 13 blanks, the detection limit at this site is 2.3 nM. The concentration of hydrogen in all but one sample (329-U1370E-9H-1, 135–140 cm) is below the detection limit. The H_2 concentration in this sample at 63.5 mbsf is 2.7 nM.

Methane concentrations are below the detection limit ($<0.98 \mu\text{M}$) in all eight samples from Hole U1370B (one sample) and Hole U1370D (seven samples), both for the IODP standard safety protocol and the refined protocol. The detection limit is defined here as three times the standard deviation of the blank (ambient air).

Interstitial water samples

A total of 70 Rhizon samples for dissolved nitrate analyses were obtained from Holes U1370B, U1370E, and U1370F (Table T10). Profiles of dissolved nitrate concentration are well correlated between these holes (Fig. F33A). Nitrate concentration near the seafloor (Section 329-U1370B-1H-1; 0.45 mbsf) is $33.86 \mu\text{M}$ but sharply increases to $41.5 \mu\text{M}$ at 1 mbsf (Section 1H-1; 0.95 mbsf) and then gradually increases to $51 \mu\text{M}$ at 20 mbsf (Sample 329-U1370E-3H-3, 60–70 cm). The increase from surface sediment to 20 mbsf is greater than at previous Expedition 329 sites (U1365–U1369), consistent with the organic nitrogen flux to the sediment being greater at this site, which is located at the more productive margin of the gyre. The increase in nitrate exhibits Redfield stoichiometry with the decrease in oxygen concentration. Between 20 and 40 mbsf, nitrate concentration remains relatively constant but decreases with increasing depth to $45 \mu\text{M}$ at 64.85 mbsf (Sample 329-U1370E-9H-2, 120–130 cm). The pooled relative standard deviation (1σ) on random duplicate runs is 1.3%.

Phosphate was measured on 53 interstitial water samples obtained through squeezing from Holes U1370E and U1370F. The pooled standard deviation (1σ) on triplicate measurements of the phosphate concentration is $0.10 \mu\text{M}$. Similar to the previous Site U1369 on the southern transect of Expedition

329, phosphate concentrations exhibit a subsurface peak before declining with depth (Table T11; Fig. F33B). At Site U1370, phosphate concentrations increase from a near-surface concentration of $1.94 \mu\text{M}$ at 0.05 mbsf to $2.88 \mu\text{M}$ at 4.4 mbsf (Sample 329-U1370E-1H-3, 40–50 cm). The surface increase in phosphate has a Redfield stoichiometry with nitrate (16N:1P), suggesting that the release is due to the degradation of marine organic matter. Below this peak, phosphate concentrations decrease with a concave-upward profile to slightly less than $1 \mu\text{M}$ below 35 mbsf. Phosphate concentrations scatter between 0.5 and $1 \mu\text{M}$ from 35 mbsf to basement. A slight decrease in phosphate with depth is apparent below 35 mbsf.

The concentration of dissolved silica near the seafloor is $205 \mu\text{M}$ (Sample 329-U1370E-1H-1, 5–15 cm) (Table T11; Fig. F33C). Dissolved silica concentration in Hole U1370E varies in the uppermost three sections of Core 1H, from 205 to $288 \mu\text{M}$ (Sample 329-U1370E-1H-1, 90–100 cm). However, the samples that exhibit relatively high dissolved silica concentrations are from the six interstitial water whole-round intervals that were not cut on the catwalk but in the ship's core refrigerator on the Hold Deck (Samples 329-U1370E-1H-1, 43–53 cm; 1H-1, 90–100 cm; 1H-2, 40–50 cm; 1H-2, 90–100 cm; 1H-3, 40–50 cm; and 1H-3, 90–100 cm). Otherwise, dissolved silica concentrations show a general increase to $240 \mu\text{M}$ at 10 mbsf. Below 20 mbsf, dissolved silica decreases slightly to concentrations generally close to $170 \mu\text{M}$ at 60 mbsf. A slight increase may be observed in the dissolved silica concentrations to $228 \mu\text{M}$ near basement at 65 mbsf (Sample 329-U1370E-9H-2, 140–150 cm). Pooled standard deviation for duplicate measurements is $4 \mu\text{M}$.

Alkalinity and dissolved inorganic carbon (DIC) in interstitial water behave similarly with depth (Table T11; Figs. F33D, F33E). Alkalinity increases from 2.2 mM in the 0–0.1 mbsf interval to 2.6 mM at ~15 mbsf and then gradually decreases to 2.15 mM between 15 and 65 mbsf. No difference in alkalinity was observed between the interstitial samples cut in the ship's Hold Deck core storage and the samples squeezed immediately after delivery from the catwalk. Standard deviation and error of alkalinity measurements on standard seawater CRM94 are 0.019 and 0.005 mM ($N = 16$), respectively.

DIC varies around 2.45 mM in the uppermost 6 mbsf and then increases toward a maximum of 2.56 mM at 14.88 mbsf (Table T11; Fig. F33E). Below this maximum, values decrease downhole, reaching 2.17 mM at 63.15 mbsf (Sample 329-U1370F-7H-6, 140–150 cm). The pattern and values of DIC at Site U1370 are very similar to those observed at Site U1365. The

range in DIC values is 0.49 mM. Average standard deviation of triplicate injection of the samples is 0.023 mM. Values from catwalk samples fall within the values of samples stored longer.

Chloride was determined from the squeezed interstitial water samples (Table T11; Fig. F33F). The chloride concentration near the seafloor is indistinguishable from inferred local bottom water (Talley, 2007) but monotonically increases by ~12 mM to 2 mbsf. This 2% increase may be due to relict higher salinity seawater from the Last Glacial Maximum. Below this depth, there is no significant gradient.

Sulfate was determined in the squeezed interstitial water samples. Sulfate concentrations begin at the surface sediment at 28.32 mM (Fig. F33G), which is close to the inferred 28.6 mM concentration of sulfate in local bottom water. Sulfate concentrations exhibit a slight decline in concentration deeper than 20 mbsf. The sulfate anomaly (Fig. F33H; see “**Biogeochemistry**” in the “Methods” chapter [Expedition 329 Scientists, 2011a]) decreases from -1.26% near the surface to -6.15% at 63.15 mbsf. Loss of sulfate may reflect the downward flux of sulfate to the underlying basalt due to removal of sulfate into authigenic minerals during basalt weathering. Local excursions in the sulfate anomaly to values of -9% are attributed to coring and sampling artifacts.

As at previous sites, cations were measured at Site U1370 by both inductively coupled plasma-atomic emission spectroscopy (ICP-AES) and ion chromatography. The precision of cation measurements by ICP-AES was, as quantified by multiple triplicate and quadruplicate analyses of International Association for the Physical Sciences of the Oceans (IAPSO) standard seawater and internal matrix matched standards,

Ca = 1.0% of the measured value,
Mg = 0.7% of the measured value,
Na = 1.5% of the measured value,
K = 3.0% of the measured value,
Fe = 7% of the measured value,
Mn = 2% of the measured value,
B = 2.0% of the measured value, and
Sr = 0.6% of the measured value.

Accuracy of the ICP-AES results, as quantified by comparison to multiple replicate analyses of IAPSO standard seawater not included in the calibration, was within precision of the measurement. For the ion chromatography analyses, precision (pooled standard deviation, 1σ) was

Ca = 0.6%,
Mg = 0.3%,
Na = 0.3%, and
K = 0.2%.

The shapes of the concentration profiles determined by ICP-AES and ion chromatography agree very well with no appreciable offsets between the two data sets (Table T11; Figs. F33I, F33J, F33K–F33O, F33P). The ion chromatography profiles, because of their greater precision, tend to be smoother, but the results track together well through local minima and maxima for those species measured by both techniques.

The profiles of dissolved Ca show a consistent and linear increase with depth of ~1.5 mM (Fig. F33I). Concentrations of Mg are either constant or appear to very slightly increase from the surface to ~55 mbsf, below which depth they decrease by ~3 mM to the basement (Fig. F33J). Sr shows no change with depth (Fig. F33P), whereas K shows a marked decrease of ~2 mM from the surface to the basement (Fig. F33L). The constancy of Sr indicates that there is no appreciable ongoing carbonate recrystallization, which is not surprising considering the very low CaCO₃ values (see below) at this site. Because there is no carbonate recrystallization, the general Ca increase with depth likely reflects release of Ca from basement during alteration. The general decrease in K with depth (Fig. F33L) is also consistent with basement alteration. The Na concentration profile did not change significantly with increasing depth (Fig. F33K). Boron concentrations are greater than in typical seawater (Fig. F33M) and may also decrease through the deepest 5 m of sediment closest to the basalt.

Concentrations of dissolved Fe and Mn are above their detection limits (both ~2 μM) and are reproducible (Figs. F33N, F33O). Because it is difficult to explain the presence of appreciable amounts of dissolved Fe and Mn in oxygenated pore water, the Fe and Mn may be recording a very fine particulate phase that is an artifact of the squeezing process. However, the Mn concentration profile does exhibit a slight convex-upward increase over the uppermost 10 m of sediment, coinciding with the enhanced organic carbon mineralization observed at the same depths.

At Site U1370, only six interstitial water samples were processed through the Hold Deck’s core refrigerator (see “**Biogeochemistry**” in the “Methods” chapter [Expedition 329 Scientists, 2011a]). Nonetheless, comparison of the catwalk samples (squeezed immediately upon core recovery) to those samples stored in the Hold Deck’s core refrigerator shows no offset between the data sets for any cation.

Solid-phase carbon and nitrogen

Concentrations of total carbon, total organic carbon (TOC), total inorganic carbon (TIC), and total nitro-

gen were determined for 44 samples from Holes U1370E and U1370F (Fig. F34; Table T12). In addition, 8 samples from Hole U1370D were analyzed to characterize lithologic Unit II (i.e., the nannofossil ooze).

Total nitrogen shows a rapid decrease from 0.079 wt% at 0.06 mbsf to 0.055 wt% at 0.91 mbsf. It then remains relatively stable to 2.95 mbsf (0.052 wt%), where a second more gentle decrease occurs until 17.15 mbsf (0.014 wt%). From 17.15 mbsf to the basement, total nitrogen shows a very slight decrease with depth, reaching 0.002 wt% at 65.05 mbsf (Fig. F34A). TOC shows similar features, with a rapid decrease from 0.25 wt% at 0.06 mbsf to 0.12 wt% at 0.91 mbsf, followed by little change to 2.95 mbsf (0.10 wt%) and gently decreasing thereafter to 0.02 wt% at 65.05 mbsf (Fig. F34B). Total carbon also shows similar features, decreasing from 0.30 wt% at 0.06 mbsf to 0.13 wt% at 0.91 mbsf and then remaining stable until 2.95 mbsf (0.11 wt%), finally decreasing downcore to 0.02 wt% at 50.65 mbsf. However, total carbon concentrations slightly increase from 55 to 65 mbsf, reaching a maximum of 0.07 wt%. In addition, one data point from Hole U1370F shows a high value of 0.33 wt% at 63.15 mbsf, possibly resulting from mixing with the nannofossil ooze that was only successfully recovered in Hole U1370D.

TIC and CaCO₃ values obtained by coulometry follow a different pattern from the total carbon content obtained from the CHNS elemental analyzer. CaCO₃ (TIC) content shows a very slight increase downcore, varying around 0.04 wt% in the uppermost 15 mbsf and then around 0.10 wt% to 50 mbsf. Below 50 mbsf, the TIC and CaCO₃ values mimic the total carbon values obtained by coulometry. In particular, the anomalous sample from Hole U1370F records a CaCO₃ content of 3.52 wt% at 63.15 mbsf (Fig. F34C). The nannofossil ooze recovered from Hole U1370D contains up to 90.8 wt% CaCO₃. One white-colored interval shows slightly lower values (86.3 wt% CaCO₃ at 63.97 mbsf).

Microbiology

Sediment samples for microbiological studies were obtained by APC coring, primarily from Holes U1370E and U1370F. PFT was continuously injected into drilling fluid for quantification of sample contamination with gas chromatography. Samples for cell and virus-like particle (VLP) abundance were taken from the cut cores facing interstitial water whole-round samples and preserved for subsequent microscopic studies. After core recovery, core sections were immediately transferred to the core refrig-

erator on the Hold Deck where microbiological whole-round cores were sampled. The temperature of the core refrigerator during subsampling ranged from 7°–10°C. Microbiological whole-round cores were taken at a high depth resolution from the first core (1H) as well as the penultimate core (7H) because the bottom core (8H), which contained the sediment/basalt interface, was highly disturbed. All the whole-round cores for cultivation from Cores 329-U1370F-4H through 8H were immediately transferred into N₂-flushed foil packs to prevent excess oxidation of fresh microbiological samples from the air and stored at 4°C before subsampling.

Cell abundance

Microbial cells were enumerated by direct counting using epifluorescence microscopy (see “Microbiology” in the “Methods” chapter [Expedition 329 Scientists, 2011a]). Sediment subcores (2 cm³) were taken using tip-cut syringes from Holes U1370E and U1370F for shipboard analysis. For shore-based analysis, 10 cm whole-round cores were taken from Hole U1370F and frozen at –80°C. Fifty-nine 2 cm³ syringe samples (Table T13) and 11 whole-round cores were taken at Site U1370.

Two blanks were prepared and counted during processing of the samples from Site U1370. As at the previous site, a slurry of heat-sterilized (4 h at 450°C) sediment was used as a blank instead of Tris-EDTA buffer. The mean blank value of the heat sterilized blanks was 1×10^3 cells/cm³ with a standard deviation of 2.7×10^2 cells/cm³, resulting in a minimum detection limit (MDL; blank plus three times standard deviation) of 1.8×10^3 cells/cm³. As the blanks showed little variation between sites, they were pooled from all sites. At the end of the expedition, a single MDL for all sites (1.4×10^3 cells/cm³) was calculated based on the extended database.

Cell abundance in the uppermost sample (329-U1370E-1H-1, 35–43 cm) is $\sim 3 \times 10^4$ cells/cm³. With one exception at 7.55 mbsf (Sample 2H-1, 135–140 cm), cell abundances were above the detection limit to 36 mbsf, which is much deeper than most of the previous sites drilled during this expedition. Below this depth, cell abundances were below the MDL (with a few below the blank) (Fig. F35).

Six samples were recounted by another shipboard microbiologist for cross-comparison. These counts were generally in good agreement with the original counts, suggesting that differences in cell recognition among observers are very small (Table T13). Cell counts on samples without cell extraction steps were made on three samples (329-U1370E-1H-1, 135–140 cm; 1H-2, 135–140 cm; and 1H-3, 135–140 cm).

Cells in the topmost sample were above the nonextracted detection limit, ranging from 9×10^4 to 2×10^5 cells/cm³, slightly higher than in the extracted samples. In the two deeper samples, nonextracted counts were below the blank.

The sediment/basalt interface sample was collected in the core catcher from Core 329-U1370E-9H, which included a relatively large piece of basalt. Microbial cell abundance on the basaltic rock sample was directly counted without cell separation. Before counting, the basalt sample was processed by washing and flaming, and then ground into powder (see “Microbiology” in the “Methods” chapter [Expedition 329 Scientists, 2011a]). No cells were observed in 300 fields of microscopic view.

Virus abundance

Sixty three samples for VLP enumeration were taken at a high depth resolution from Holes U1370E and U1370F (Table T14). All samples from Site U1370 were preserved at -80°C for shore-based analyses.

Cultivation

Sediment samples

Sediment whole-round cores were subsampled aseptically with sterile tip-cut syringes to make slurries for inoculation of a variety of media. Subsamples from Cores 329-U1370F-4H through 8H were taken under anoxic conditions in the anaerobic chamber deployed in the core refrigerator on the Hold Deck (Table T15). Hydrogen was added as a reductant to remove oxygen in the anaerobic chamber, H₂ concentration was maintained at 2%–3%. Oxygen concentration was consistently 0 ppm. After inoculation, vial headspace for heterotrophic anaerobic cultivation was flushed with N₂, if necessary, to remove hydrogen in the headspace. Additional samples (referred to as SLURRY in Table T15) were stored in N₂-flushed serum bottles or in syringes packed in sterile foil packs and stored at 4°C for shore-based cultivation experiments.

Seawater control sample

A surface seawater sample was collected from Site U1370 with a sterile 500 mL glass bottle immediately after the R/V *JOIDES Resolution* arrived at the site. Aerobic heterotrophic bacteria were cultured on marine agar and marine R2A plates (Table T8 in the “Methods” chapter [Expedition 329 Scientists, 2011a]) at 25°C for 5 days. The abundances of cultivable aerobic heterotrophic bacteria on marine agar and R2A plates were ~ 39 and ~ 22 colony-forming units (cfu)/mL, respectively.

Bottom seawater was collected from the mudline of Core 1H of Holes U1370A–U1370F, placed in a sterile plastic bag, and stored at 4°C. The water was filtered through 0.2 μm pore size polycarbonate filters into sterile 50 mL serum bottles and sparged with N₂ for 5 min. The bottles were capped with rubber stoppers and aluminum crimp caps and stored at 4°C for future preparation of liquid media on shore. Aerobic heterotrophic bacteria were cultured from the unfiltered sample at 25°C for 3 days. The abundances of cultivable aerobic heterotrophic bacteria on marine agar and R2A plates were $\sim 5.7 \times 10^3$ and $\sim 4.0 \times 10^3$ cfu/mL, respectively, which are in marked contrast to numbers obtained from surface seawater as described above. The estimated abundance of *Vibrio*-like species, based on selective enrichment for this genus on thiosulfate citrate bile salts sucrose agar, was ~ 2.5 cfu/mL. Contrary to the seawater samples, we rarely observed colony formation from sediment slurries prepared from Site U1370; only for Core 329-U1370-3H did we observe heterotrophic growth of colonies on marine agar and R2A plates (137 and 112 cfu/cm³, respectively). It is not clear if the colonies were derived from an indigenous microbial community in the sediment or from contamination. This will be addressed by both PFT analysis and postcruise 16S rRNA sequence analysis of the 19 isolates from the core.

Molecular analyses

Sediment samples

Nine 10 cm whole-round cores were taken throughout the entire sediment column (Sections 329-U1370E-CC and 329-U1370F-1H-3, 2H-3, 3H-5, 4H-5, 5H-5, 6H-5, 7H-4, and 7H-5) as routine microbiology samples (curatorial code MBIO) and transferred to -80°C freezers for storage. These samples will be used for shore-based molecular studies (See “Microbiology” in the “Methods” chapter [Expedition 329 Scientists, 2011a]).

Deep seawater control sample

Bottom seawater overlaying the seafloor was collected from the top part of mudline cores (1H) in Holes U1370A–U1370F for shore-based molecular studies. Approximately 300 mL seawater was collected in a sterile plastic bag and stored at 4°C in the Microbiology Laboratory until further processing. The sample was then filtered through 0.2 μm polycarbonate membrane filters under aseptic conditions and stored at -80°C .

Basalt samples

Sediment and basalt samples at the sediment/basalt interface were collected from Section 329-U1370E-

9H-CC on the catwalk immediately after core recovery. The basalt piece was separated from surrounding soft materials, washed three times with 3% NaCl solution, briefly flamed, and crushed into powder (see “**Microbiology**” in the “Methods” chapter [Expedition 329 Scientists, 2011a]). The samples were stored at -80°C for shore-based microbiological and (bio)mineralogical analyses.

Fluorescence in situ hybridization analysis

Duplicate 10 cm³ subcores of sediment from Sections 329-U1370F-1H-1 through 1H-3, 3H-2, 4H-3, 5H-2, 7H-2, 7H-4 through 7H-6, and 8H-1 were collected using sterile tip-cut syringes and fixed as described in “**Microbiology**” in the “Methods” chapter (Expedition 329 Scientists, 2011a) for shore-based fluorescence in situ hybridization analyses.

Radioactive and stable isotope tracer incubation experiments

Stable isotope (¹³C and ¹⁵N) experiments to measure carbon and nitrogen uptake activities were initiated on board in the Isotope Isolation Van. Sediment subcores (15 cm³) were taken from the inner part of 20 cm whole-round cores, placed in a sterile glass vials, flushed with N₂, sealed with a rubber stopper, and stored until processing in the core refrigerator on the Hold Deck (see “**Microbiology**” in the “Methods” chapter [Expedition 329 Scientists, 2011a]). Six whole-round cores from Sections 329-U1370F-1H-2, 2H-3, 4H-3, 6H-3, 7H-5, and 7H-6 were processed for stable isotope tracer incubation experiments as described in “**Microbiology**” in the “Site U1365” chapter (Expedition 329 Scientists, 2011b). Subcore samples (15 cm³) were taken from the inner part of sedimentary whole-round cores.

Whole-round interval 329-U1370C-1H-2, 120–130 cm (2.7 mbsf), from Site U1370 was used for slurry experiments on metabolic activities using radioactive and stable isotopes. The whole-round core section had been stored in the Hold Deck core refrigerator until processing in the Microbiology/Chemistry Laboratory cold room. Samples from Sites U1369 and U1370 were processed together on board. Incubation experiments were prepared to test for autotrophic and heterotrophic activities using radio and stable isotope or a combination thereof according to the methods described in “**Microbiology**” in the “Methods” chapter (Expedition 329 Scientists, 2011a).

For sulfate reduction rate measurements, 13 whole-round cores were collected from Hole U1370E (Samples 329-U1370E-1H-2, 10–20 cm; 1H-4, 50–60 cm; 2H-2, 50–60 cm; 2H-5, 50–60 cm; 3H-2, 50–60 cm; 3H-5, 50–60 cm; 4H-2, 50–60 cm; 4H-5, 50–60 cm;

5H-2, 50–60 cm; 5H-5, 50–60 cm; 6H-2, 30–40 cm; 6H-5, 40–50 cm; and 9H-2, 50–60 cm). Five to seven subsamples (~2.5 cm³) were collected directly from each whole-round core for the shore-based distillation analysis of ³⁵S-labeled reduced sulfur compounds (see “**Microbiology**” in the “Methods” chapter [Expedition 329 Scientists, 2011a]).

Contamination assessment

Perfluorocarbon tracer

We used perfluoromethylcyclohexane as PFT to monitor the level of drilling fluid contamination in sediment cores. PFT was continuously injected into drilling fluids during APC coring in Holes U1370C and U1370E. Sediment subcores (3 cm³) were taken from core sections on the catwalk and stored in vials with 2 mL of water for postexpedition gas chromatography measurement (see “**Microbiology**” in the “Methods” chapter [Expedition 329 Scientists, 2011a]).

References

- D'Hondt, S., 2005. Consequences of the Cretaceous/Paleogene mass extinction for marine ecosystems. *Annu. Rev. Ecol. Evol. Syst.*, 36(1):295–317. doi:10.1146/annurev.ecolsys.35.021103.105715
- D'Hondt, S., Abrams, L.J., Anderson, R., Dorrance, J., Durbin, A., Ellett, L., Ferdelman, T., Fischer, J., Forschner, S., Fuldauer, R., Goldstein, H., Graham, D., Griffith, W., Halm, H., Harris, R., Harrison, B., Hasiuk, F., Horn, G., Kallmeyer, J., Lever, M., Meyer, J., Morse, L., Moser, C., Murphy, B., Nordhausen, A., Parry, L., Pockalny, R., Puschell, A., Rogers, J., Schrum, H., Smith, D.C., Soffientino, B., Spivack, A.J., Stancin, A., Steinman, M., and Walczak, P., 2011. KNOX-02RR: drilling site survey—life in subseafloor sediments of the South Pacific Gyre. In D'Hondt, S., Inagaki, F., Alvarez Zarikian, C.A., and the Expedition 329 Scientists, *Proc. IODP, 329*: Tokyo (Integrated Ocean Drilling Program Management International, Inc.). doi:10.2204/iodp.proc.329.112.2011
- D'Hondt, S., Inagaki, F., and Alvarez Zarikian, C., 2010. South Pacific Gyre Microbiology. *IODP Sci. Prosp.*, 329. doi:10.2204/iodp.sp.329.2010
- D'Hondt, S., Spivack, A.J., Pockalny, R., Ferdelman, T.G., Fischer, J.P., Kallmeyer, J., Abrams, L.J., Smith, D.C., Graham, D., Hasiuk, F., Schrum, H., and Stancin, A.M., 2009. Subseafloor sedimentary life in the South Pacific Gyre. *Proc. Natl. Acad. Sci. U. S. A.*, 106(28):11651–11656. doi:10.1073/pnas.0811793106
- Ekdale, A.A., Bromley, R.G., and Pemberton, S.G. (Eds.), 1984. *Ichnology: The Use of Trace Fossils in Sedimentology and Stratigraphy*. SEPM Short Course, 15.
- Expedition 329 Scientists, 2011a. Methods. In D'Hondt, S., Inagaki, F., Alvarez Zarikian, C.A., and the Expedition 329 Scientists, *Proc. IODP, 329*: Tokyo (Integrated Ocean

- Drilling Program Management International, Inc.).
doi:10.2204/iodp.proc.329.102.2011
- Expedition 329 Scientists, 2011b. Site U1365. In D'Hondt, S., Inagaki, F., Alvarez Zarkian, C.A., and the Expedition 329 Scientists, *Proc. IODP*, 329: Tokyo (Integrated Ocean Drilling Program Management International, Inc.).
doi:10.2204/iodp.proc.329.103.2011
- Fischer, J.P., Ferdelman, T.G., D'Hondt, S., Røy, H., and Wenzhöfer, F., 2009. Oxygen penetration deep into the sediment of the South Pacific gyre. *Biogeosciences*, 6:1467–1478. <http://www.biogeosciences.net/6/1467/2009/bg-6-1467-2009.pdf>
- Gradstein, F.M., Ogg, J.G., and Smith, A. (Eds.), 2004. *A Geologic Time Scale 2004*: Cambridge (Cambridge Univ. Press). <http://cambridge.org/uk/catalogue/catalogue.asp?isbn=9780521781428>
- Heath, G.R., and Dymond, J., 1977. Genesis and transformation of metalliferous sediments from the East Pacific Rise, Bauer Deep, and Central Basin, Northwest Nazca Plate. *Geol. Soc. Am. Bull.*, 88(5):723–733. doi:10.1130/0016-7606(1977)88<723:GATOMS>2.0.CO;2
- Kastner, M., 1986. Mineralogy and diagenesis of sediments at Site 597: preliminary results. In Leinen, M., Rea, D.K., et al., *Init. Repts. DSDP*, 92: Washington, DC (U.S. Govt. Printing Office), 345–349. doi:10.2973/iodp.proc.92.116.1986
- Larson, R.L., Pockalny, R.A., Viso, R.F., Erba, E., Abrams, L.J., Luyendyk, B.P., Stock, J.M., and Clayton, R.W., 2002. Mid-Cretaceous tectonic evolution of the Tonga-reva triple junction in the southwestern Pacific Basin. *Geology*, 30(1):67–70. doi:10.1130/0091-7613(2002)030<0067:MCTEOT>2.0.CO;2
- Martini, E., 1971. Standard Tertiary and Quaternary calcareous nannoplankton zonation. *Proc. Int. Conf. Planktonic Microfossils*, 2:739–785.
- Olsson, R.K., Hemleben, C., Berggren, W.A., and Huber, B.T. (Eds.), 1999. *Atlas of Paleocene Planktonic Foraminifera*. Smithsonian. Contrib. Paleobiol., 85.
- Seilacher, A., 1977. Use of trace fossil for recognizing depositional environments. In Basan, P.B. (Ed.), *Trace Fossil Concepts*. SEPM Short Course, 5:185–200.
- Talley, L.D., 2007. *Hydrographic Atlas of the World Ocean Circulation Experiment (WOCE) (Vol. 2): Pacific Ocean*. Sparrow, M., Chapman, P., and Gould, J. (Eds.): Southampton, U.K. (International WOCE Project Office). http://www-pord.ucsd.edu/whp_atlas/pacific_index.html
- Tjalsma, R.C., and Lohmann, G.P., 1983. Paleocene–Eocene bathyal and abyssal benthic foraminifera from the Atlantic Ocean. *Micropaleontology, Spec. Publ.*, 4.
- Wade, B.S., Pearson, P.N., Berggren, W.A., and Pälike, H., 2011. Review and revision of Cenozoic tropical planktonic foraminiferal biostratigraphy and calibration to the geomagnetic polarity and astronomical time scale. *Earth-Sci. Rev.*, 104(1–3):111–142. doi:10.1016/j.earsci-rev.2010.09.003

Publication: 13 December 2011
MS 329-108

Figure F1. Multibeam bathymetry of the Site U1370 survey area with the KNOX-02RR survey track overlain.

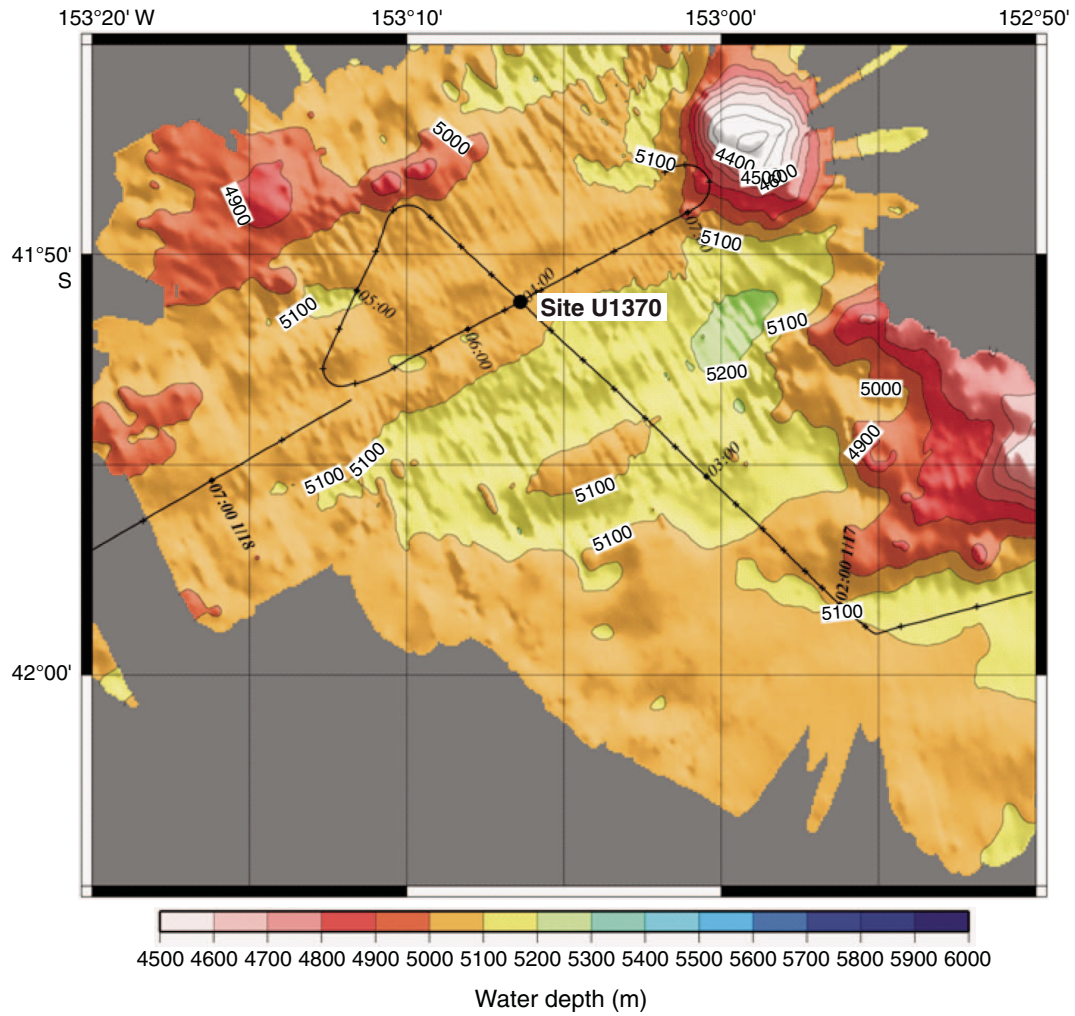


Figure F2. KNOX-02RR seismic survey track, Site U1370. sol = start of seismic line, eol = end of seismic line, z = time (Greenwich Mean Time), sp = shotpoint.

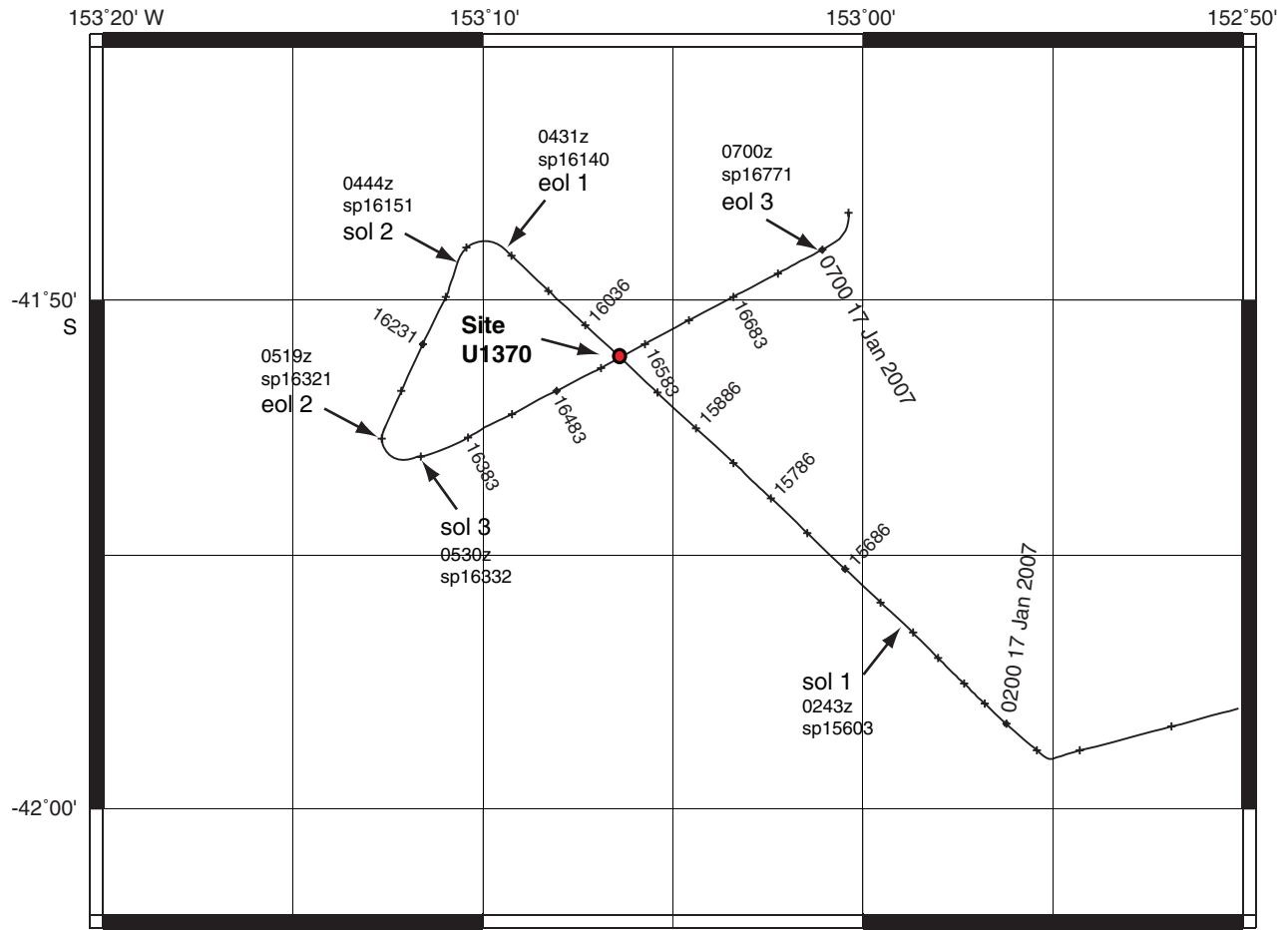




Figure F3. KNOX-02RR Channel 48 of MCS Line 1 across Site U1370. z = time (Greenwich Mean Time), SP = shotpoint, MORB = mid-ocean-ridge basalt, WD = water depth, SCS = single-channel seismic, BP = band-pass, AGC = automatic gain control, VE = vertical exaggeration.

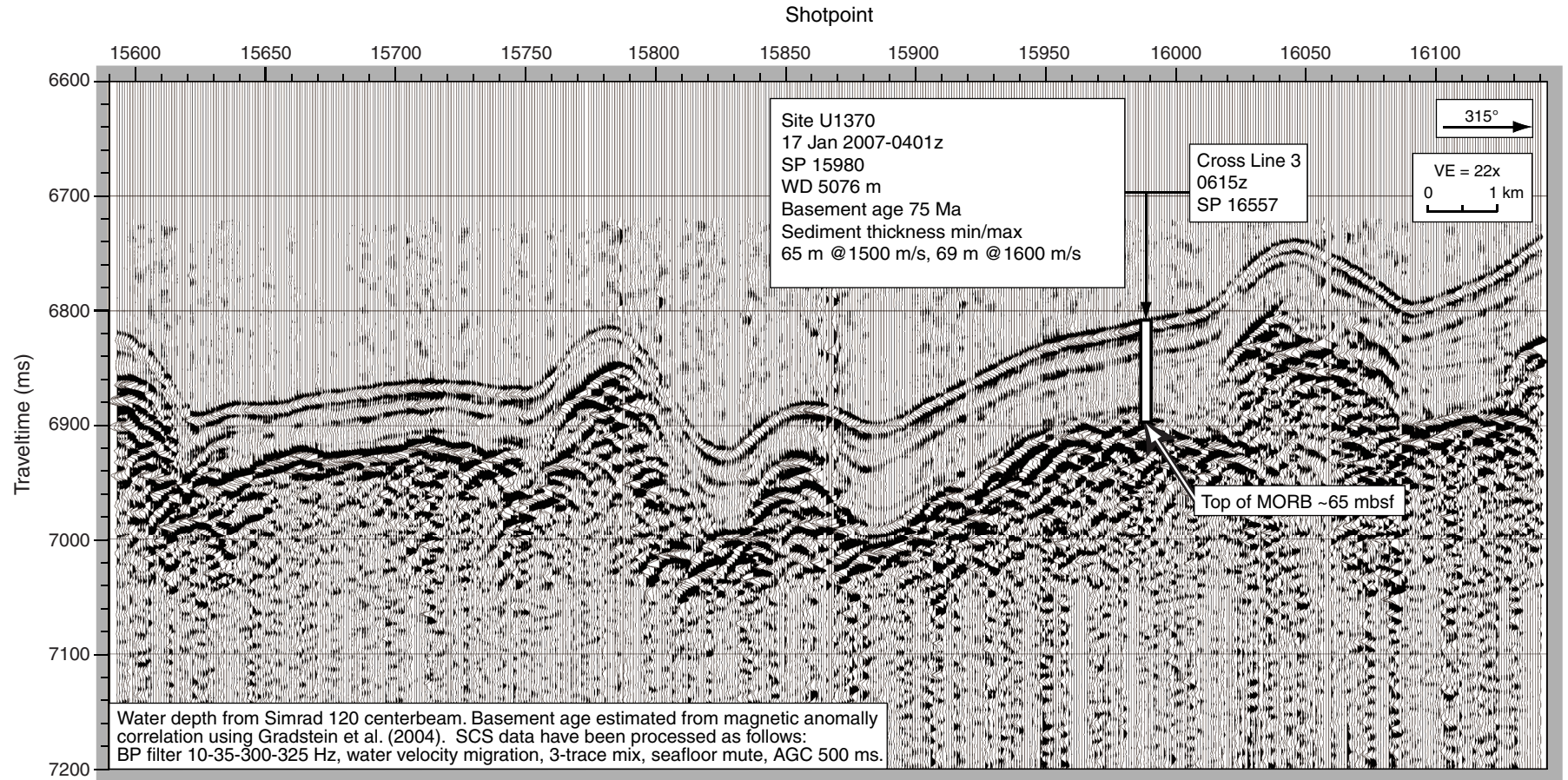




Figure F4. Portion of KNOX-02RR Channel 48 of MCS Line 1 crossing MCS Line 3, northeast of Site U1370. z = time (Greenwich Mean Time), SP = shotpoint, MORB = mid-ocean-ridge basalt, WD = water depth, SCS = single-channel seismic, BP = band-pass, AGC = automatic gain control, VE = vertical exaggeration.

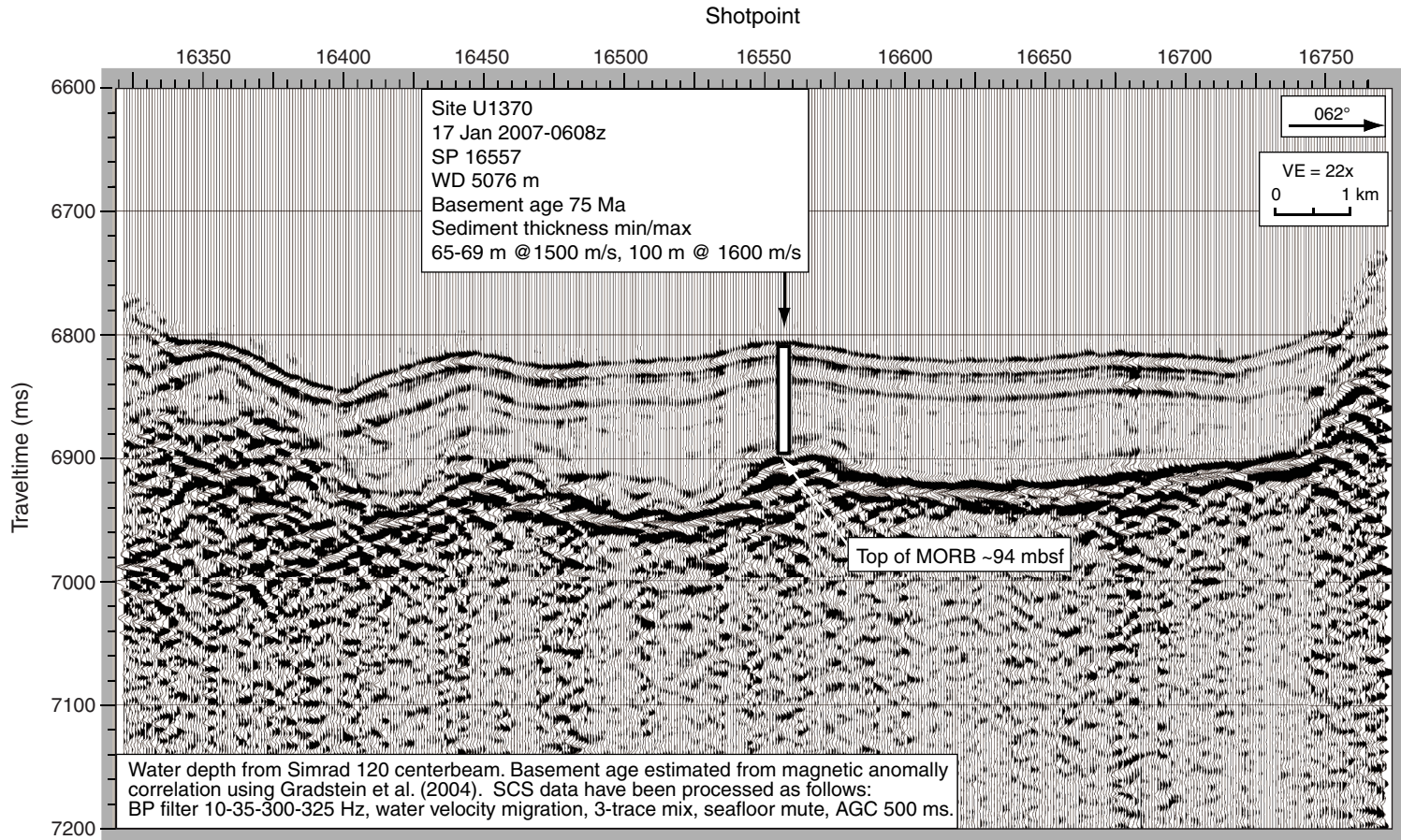


Figure F5. Portion of KNOX-02RR 3.5 kHz seismic Line 1 across Site U1370. CPA = closest point of approach, MORB = mid-ocean-ridge basalt.

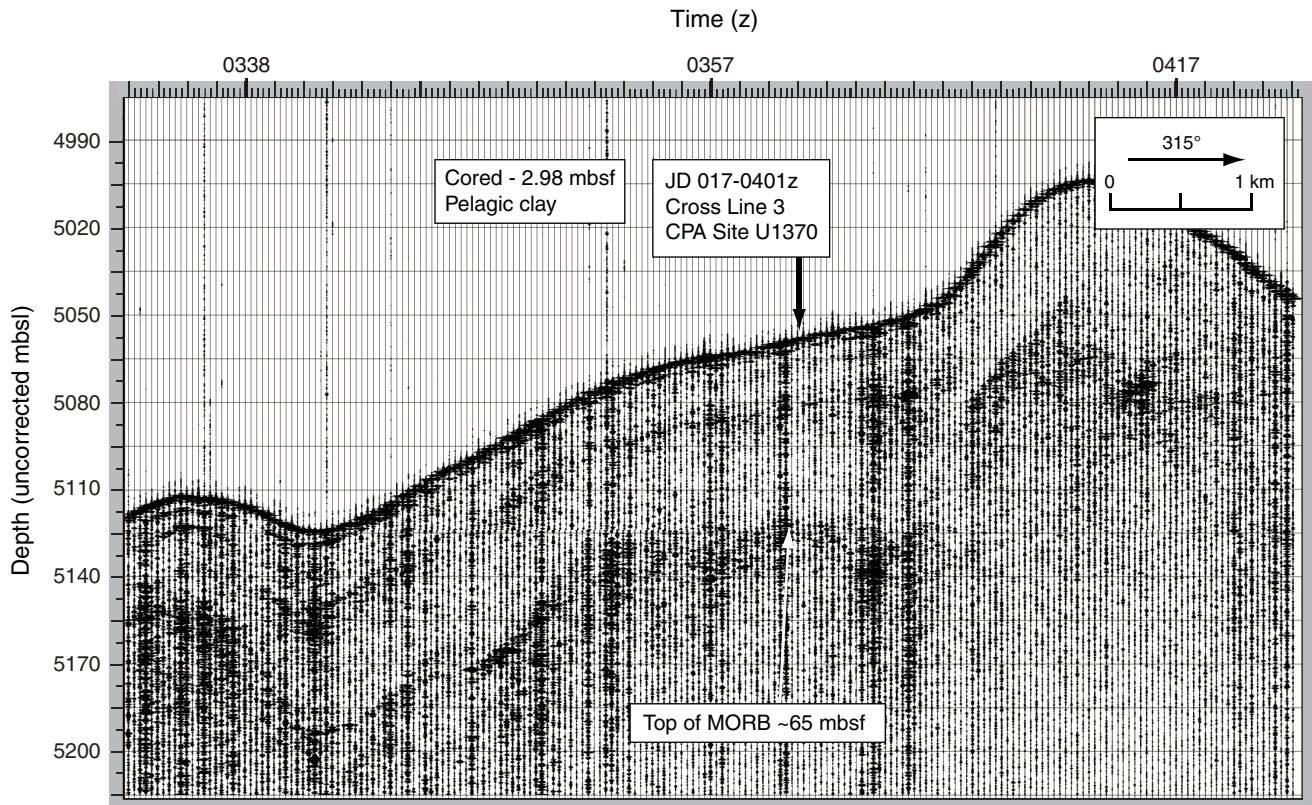


Figure F6. Portion of KNOX-02RR 3.5 kHz seismic Line 3 across Site U1370. MORB = mid-ocean-ridge basalt, SCS = single-channel seismic.

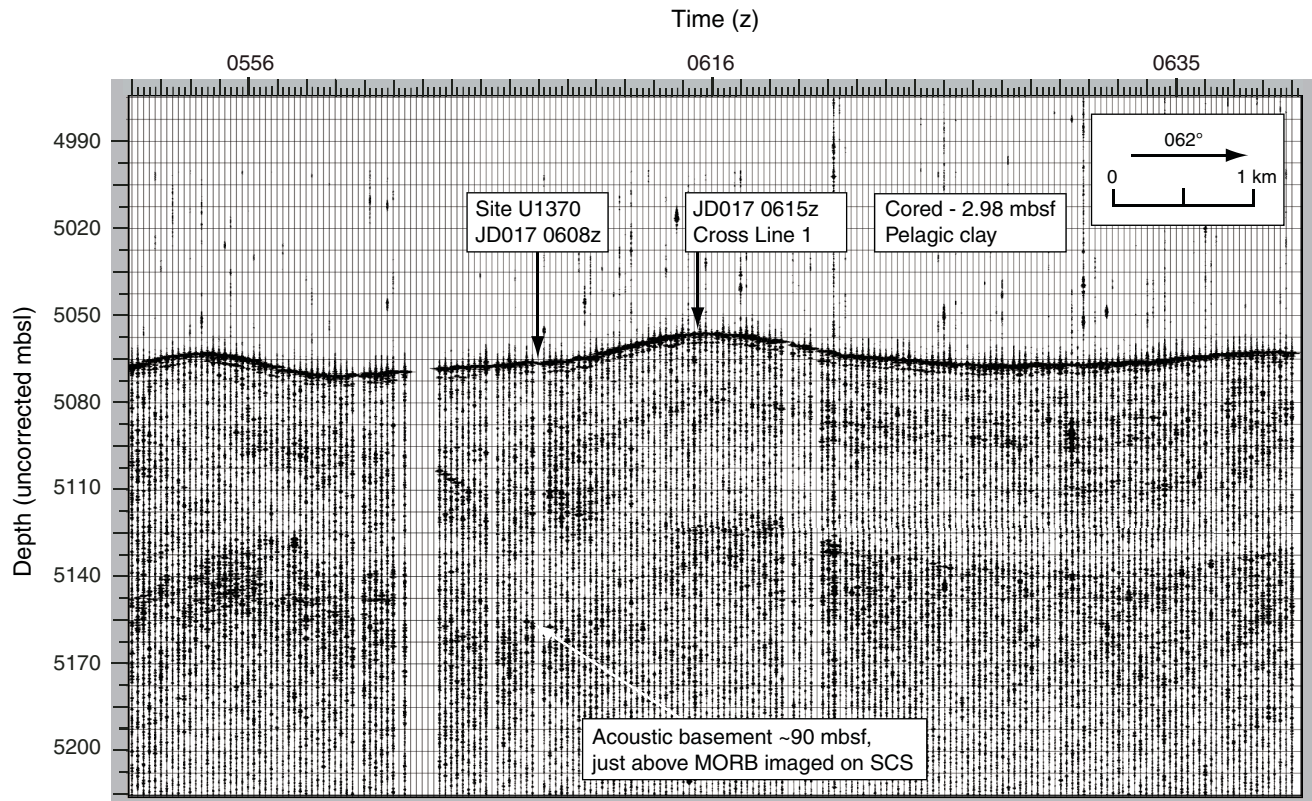


Figure F7. Summary of lithology and physical property data, Hole U1370D. MS = magnetic susceptibility, GRA = gamma ray attenuation, K = potassium composition based on spectral natural gamma ray analyses, NGR = natural gamma radiation, RSO = red-brown to yellow-brown semiopaque oxide.

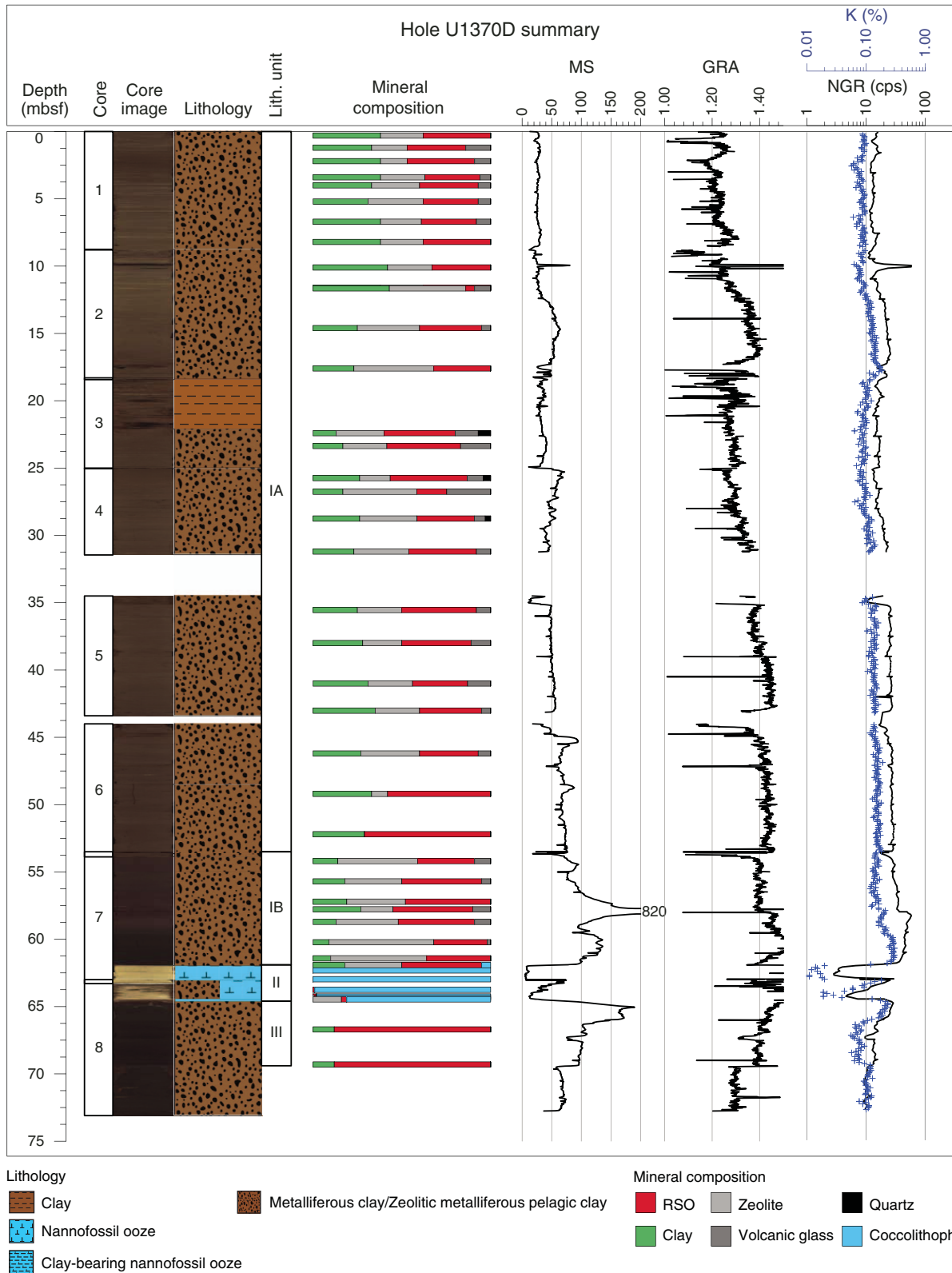


Figure F8. Lithostratigraphic correlations of holes at Site U1370.

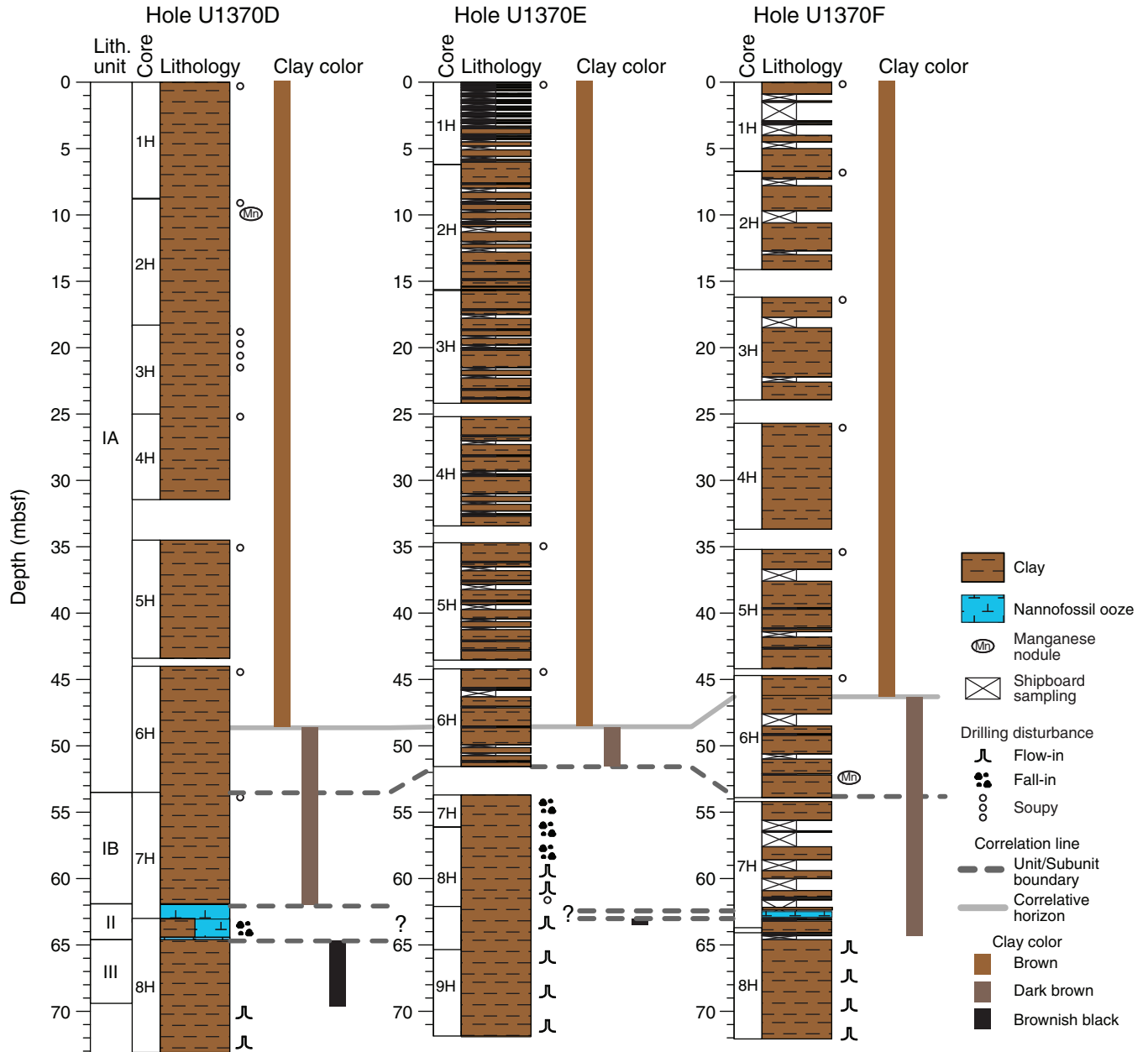




Figure F9. Representative core photographs of sediment, Site U1370. **A.** Brown zeolitic metalliferous pelagic clay containing burrows in Subunit IA (interval 329-U1370D-1H-1, 90–130 cm). **B.** Manganese nodule in Subunit IA (interval 329-U1370D-2H-2, 40–80 cm). **C.** Dark brown zeolitic metalliferous pelagic clay in Subunit IB. The olive-brown interval between 125 and 129 cm is a hardground (interval 329-U1370D-7H-3, 110–150 cm). **D.** Boundary between black zeolitic metalliferous pelagic clay in Subunit IB and very pale brown nannofossil ooze in Unit II (interval 329-U1370D-7H-6, 70–110 cm). **E.** Very pale brown nannofossil ooze containing white nannofossil ooze layer in Unit II (interval 329-U1370D-7H-7, 10–50 cm). **F.** Abundant burrows in uppermost part of Unit III (interval 329-U1370D-8H-2, 5–45 cm).

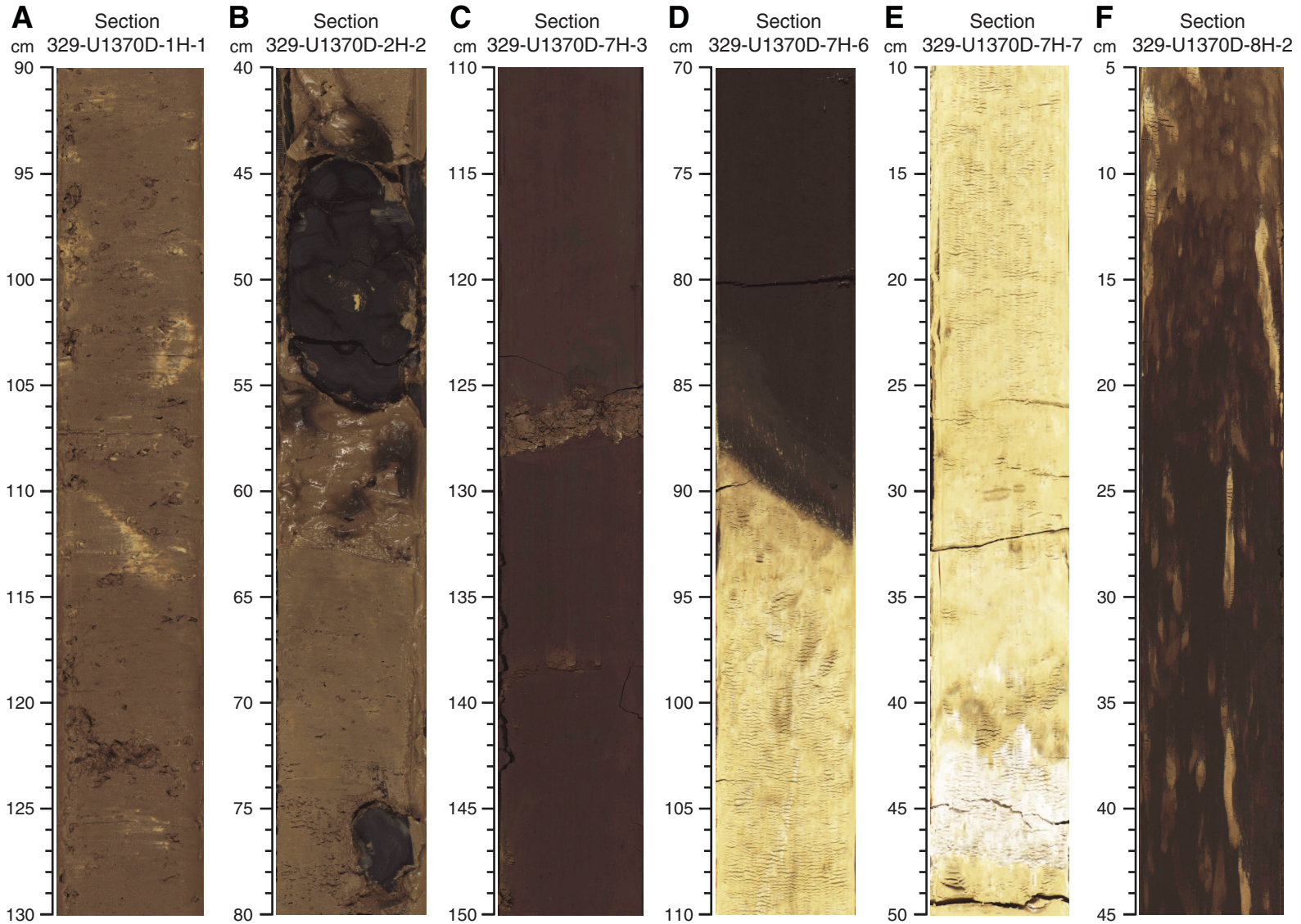




Figure F10. Selected smear slide photomicrographs of clay and ooze sediments, Site U1370. **A.** Zeolitic metalliferous pelagic clay in Subunit IA (Sample 329-U1370B-1H-3, 100 cm). **B.** Zeolitic metalliferous pelagic clay in Subunit IB (Sample 329-U1370B-7H-1, 70 cm). **C.** Nannofossil ooze in Unit II (Sample 329-U1370B-7H-6, 130 cm). **D.** Metalliferous clay in Unit III (Sample 329-U1370B-8H-3, 70 cm).

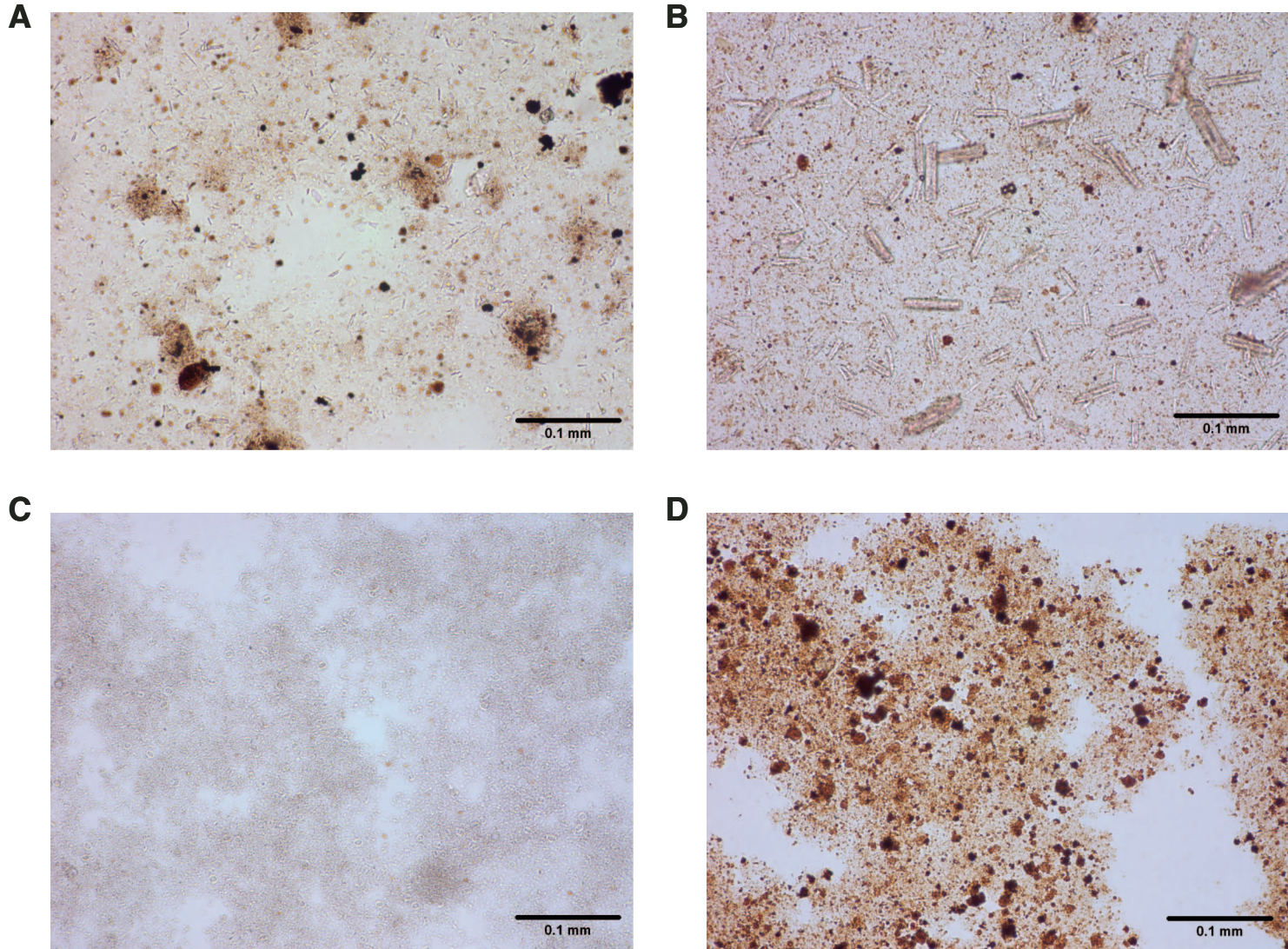


Figure F11. X-ray diffractograms of selected sediment, Site U1370. **A.** Subunits IA (red) and IB (black). Although quartz (Q) is in small abundance in Subunit IA, the intensity of its peak far exceeds those formed by other minerals including phillipsite (P), illite (I), smectite (S), cristobalite-tridymite (CT), and plagioclase (Plag). Only maximum intensity peaks for each of these minerals are plotted. For Subunit IB, smectite peak intensity is enhanced, whereas quartz and illite peak intensities are reduced. **B.** Units II (black) and III (green). Unit II has an abundance of calcite in the nannofossil ooze. Unit III is nearly amorphous with small peaks for smectite, goethite (G), ramsdellite (R), and possibly barite (B).

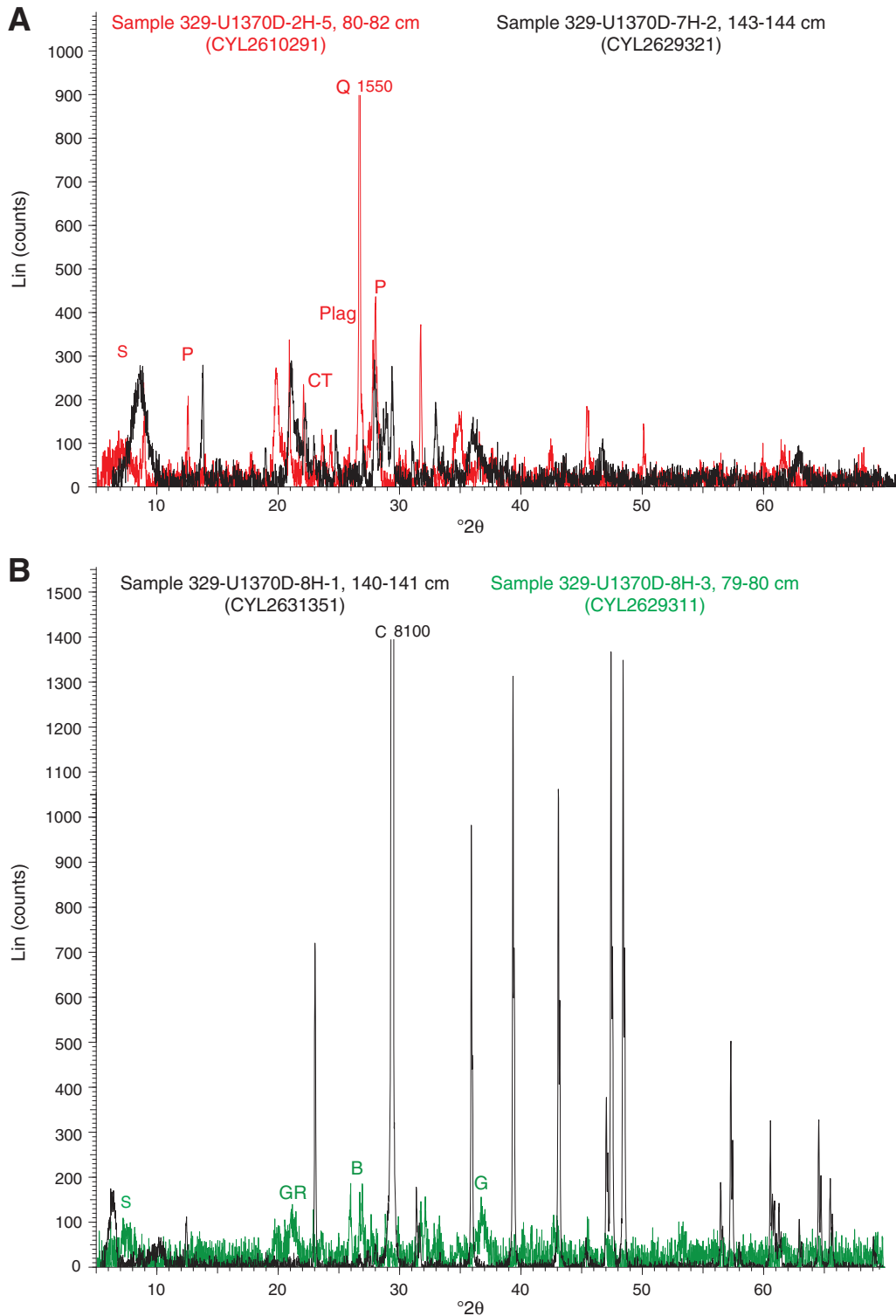


Figure F12. Core image of *Paleodictyon* burrows underlining an indurated claystone in Subunit IB (interval 329-U1370F-7H-3, 40–45 cm). The underside of the claystone is facing up, dislodged from the section half during splitting operations. The two brown tones in the image resulted from drying of the specimen following splitting and preceding close-up photography. The thin, white, hexagonal burrows resulted from horizontal feeding behaviors of organisms of the *Nereites* association in abyssal environments (Seilacher, 1977).

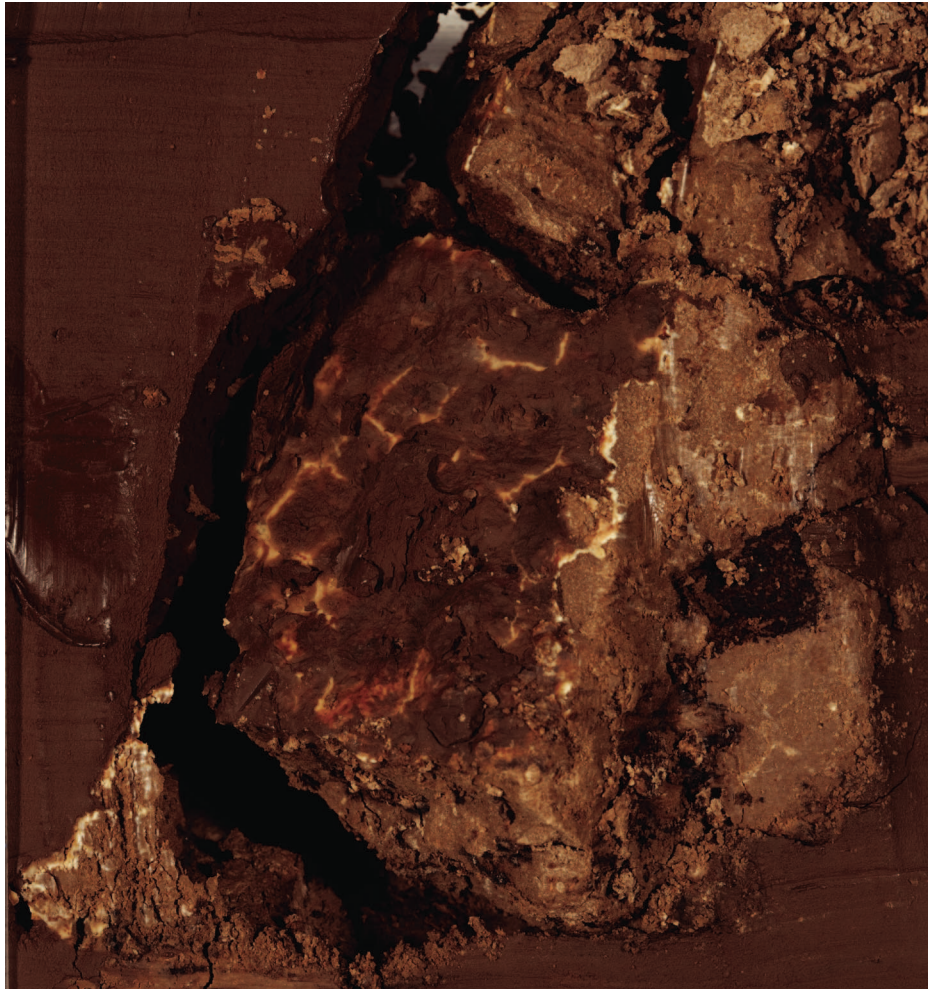


Figure F13. Lithology summary and preliminary biostratigraphy of Site U1370. The main lithology is metalliferous pelagic clay, but a short (2.7 m) interval of calcareous nannofossil ooze was observed in Hole U1370D (61.9–64.6 mbsf; see “[Lithostratigraphy](#)”). Close-ups of selected section intervals from the calcareous nannofossil ooze show the location where the three shipboard samples were taken and examined. Ages of foraminiferal zones are based on Olsson et al. (1999) and Wade et al. (2011).

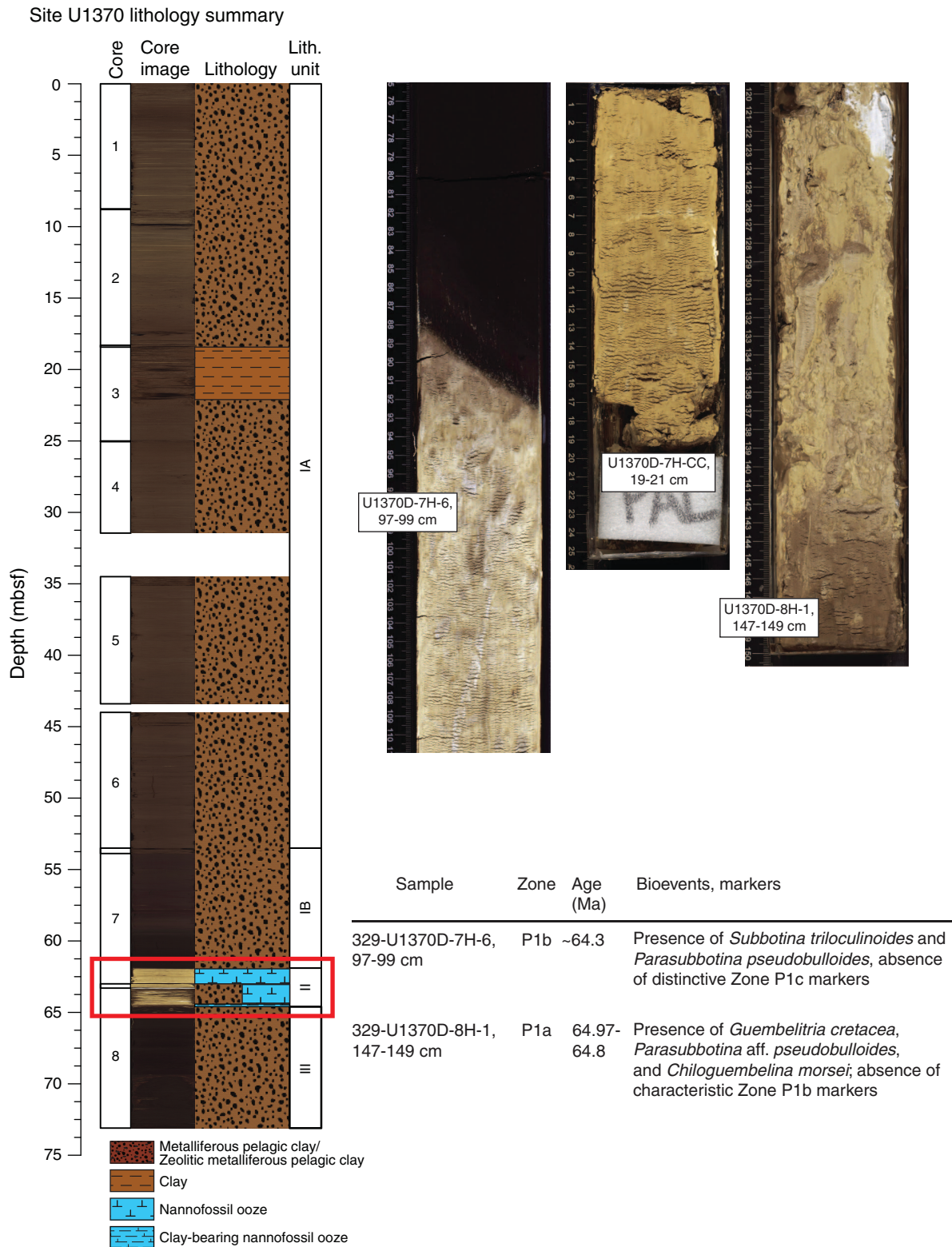


Figure F14. Plots of moisture and density (MAD) measurements, Hole U1370D. Shaded regions denote areas of disturbed core. A. Bulk density. Red = bulk density derived from MAD Method C, blue = bulk density derived from GRA. B. Grain density. C. Porosity.

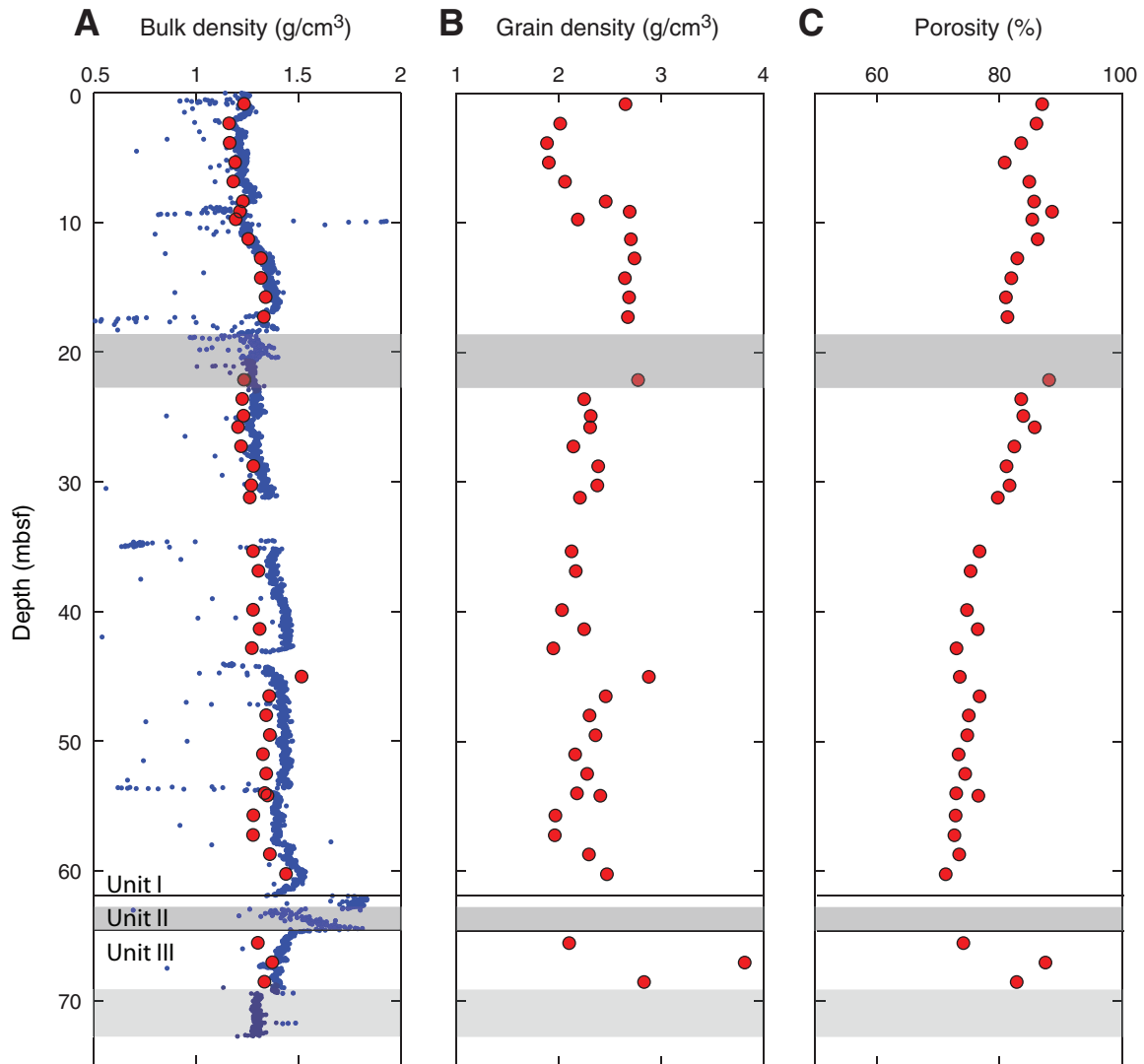


Figure F15. Plots of bulk density values determined by GRA, Site U1370. Shaded regions denote areas of disturbed core.

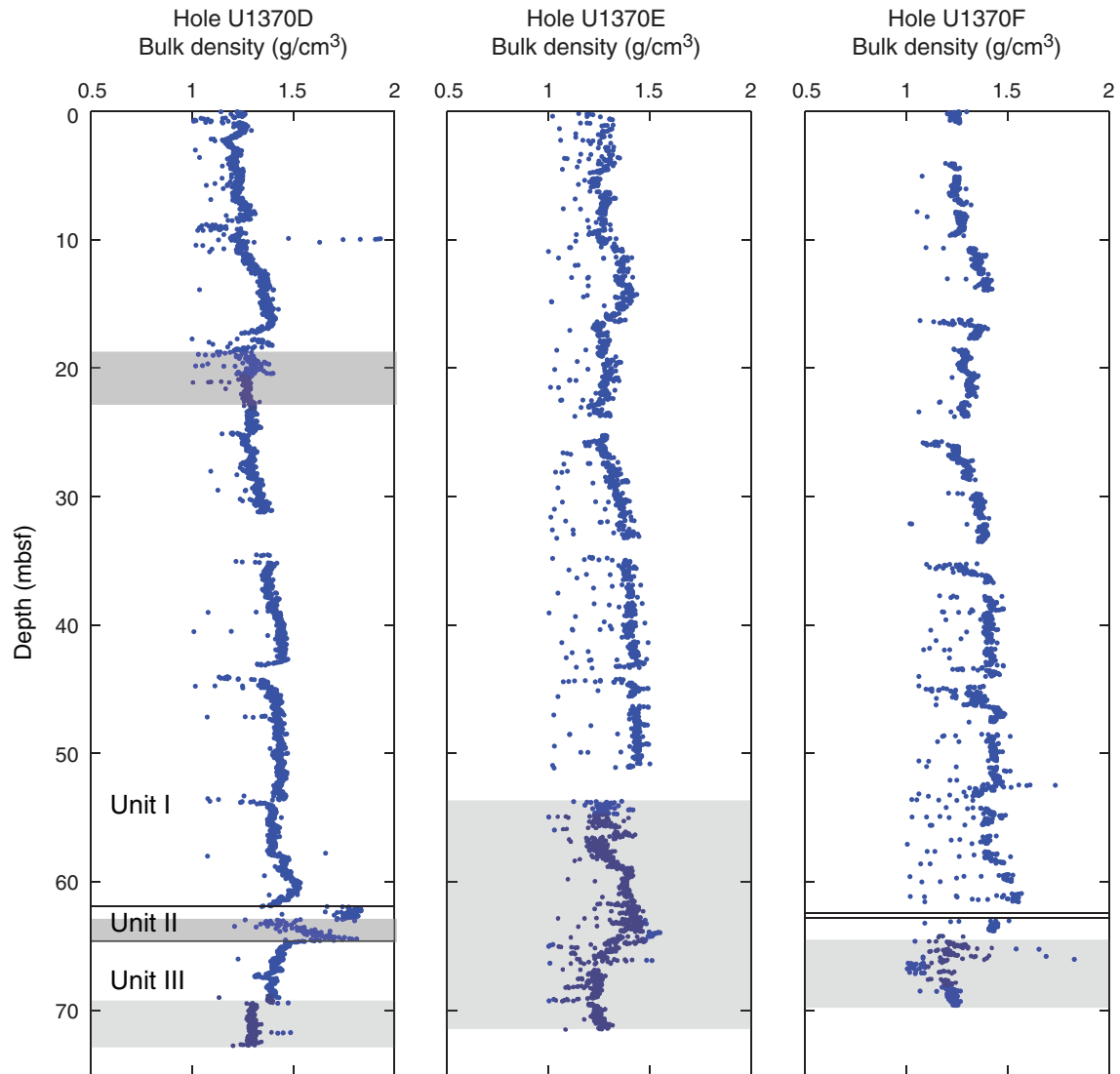


Figure F16. Plots of (A–C) magnetic susceptibility measurements made on the Whole-Core Multisensor Logger and (D–F) point magnetic susceptibility measurements made on the Section Half Multisensor Logger. Shaded regions denote areas of disturbed core.

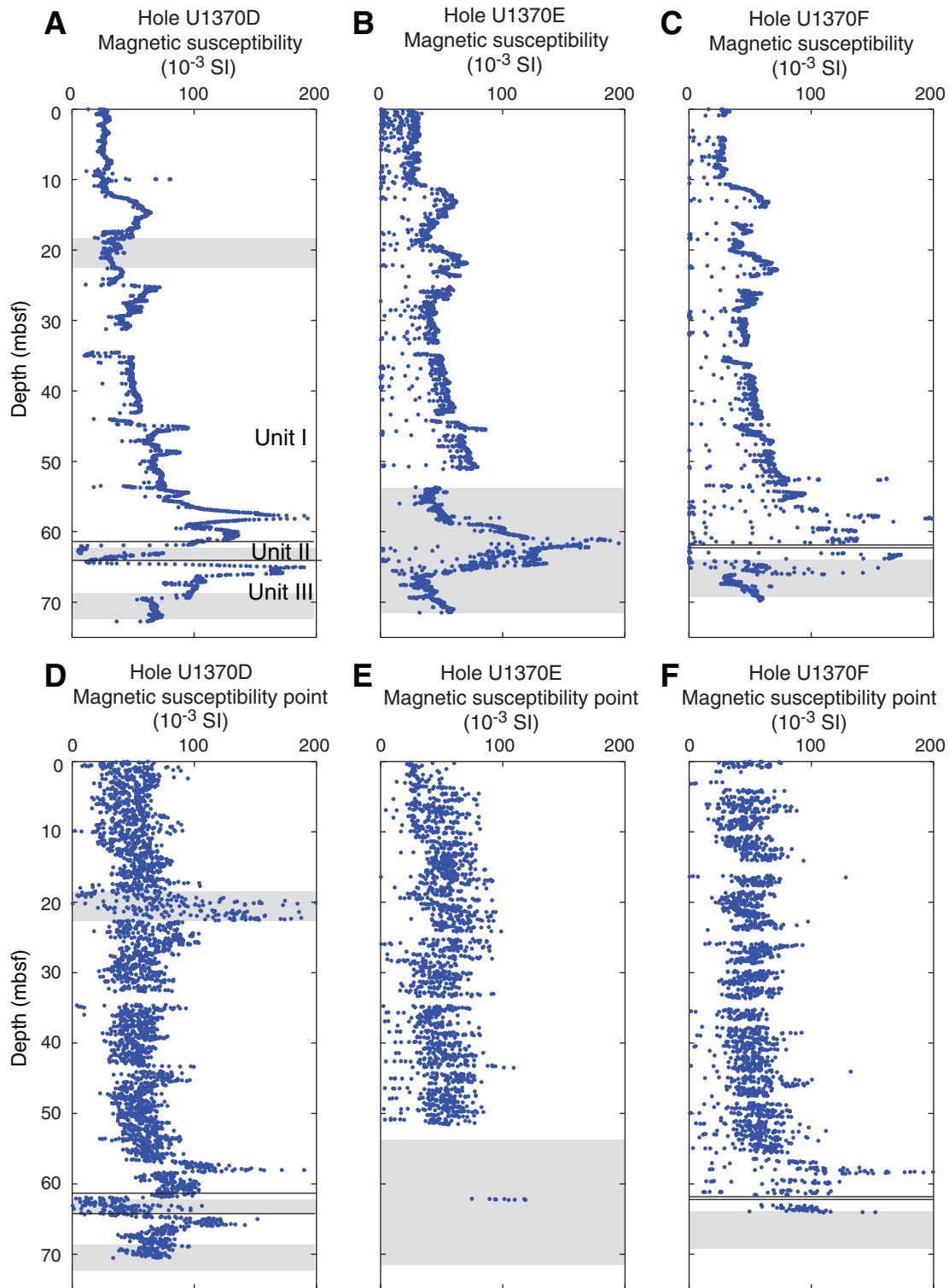


Figure F17. Plots of natural gamma radiation (NGR) as a function of depth, Site U1370. Shaded regions denote areas of disturbed core.

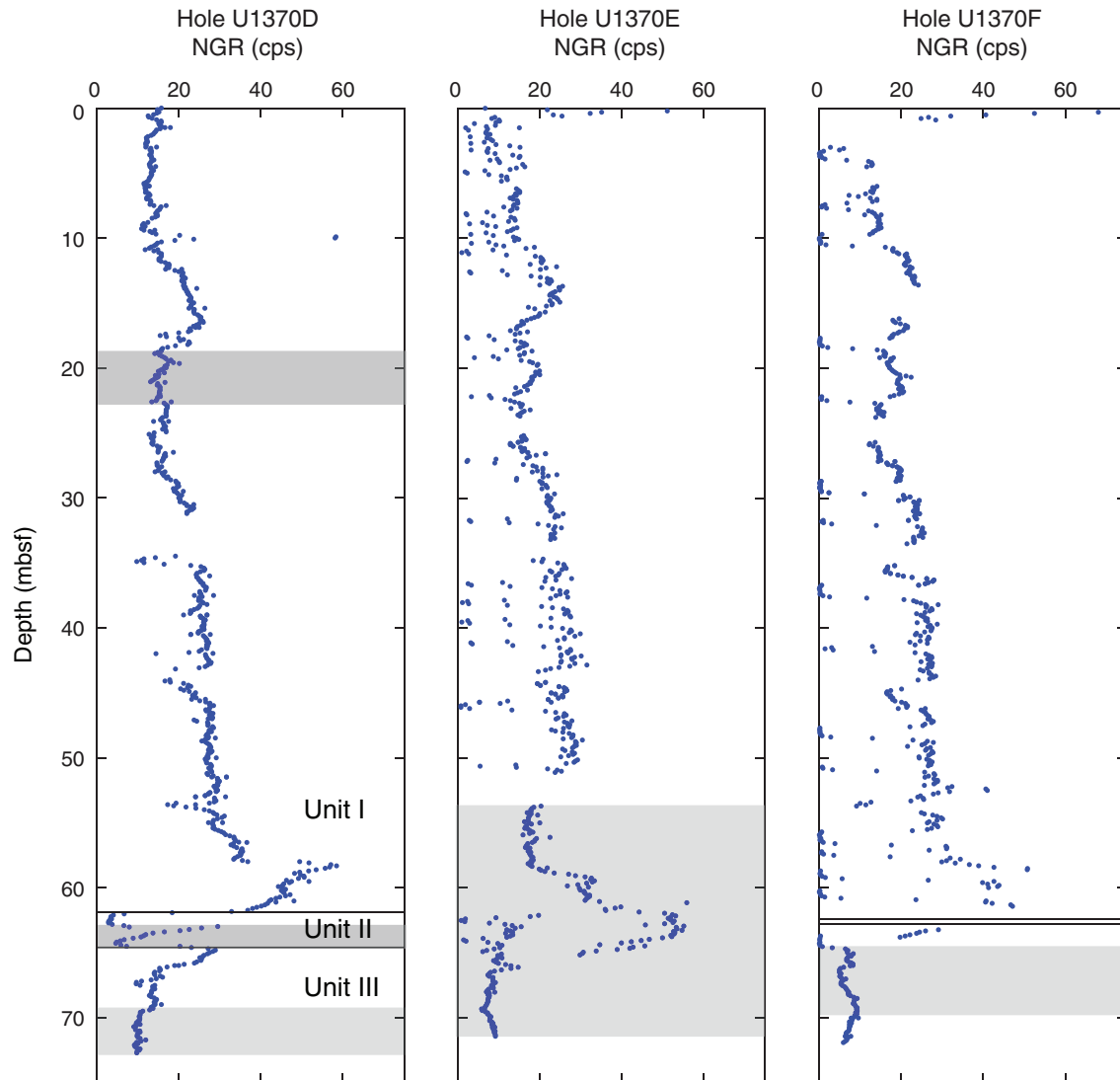


Figure F18. A. Plots of compressional wave velocity measured on Whole-Round Multisensor Logger (WRMSL). Red = discrete measurements. Shaded regions denote areas of disturbed core. **B.** Histogram of WRMSL *P*-wave velocity from all holes.

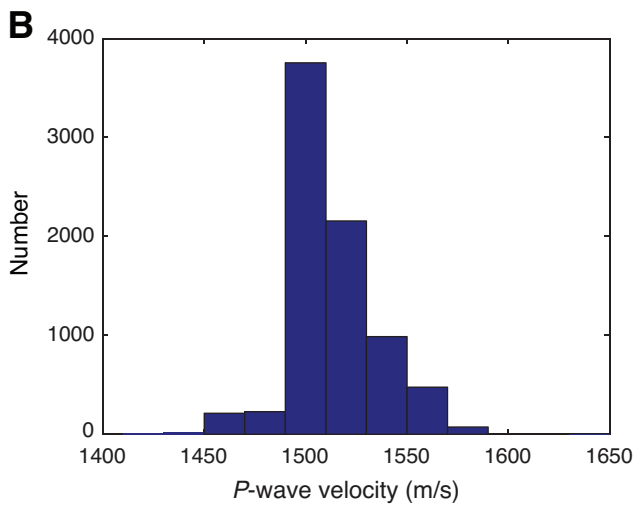
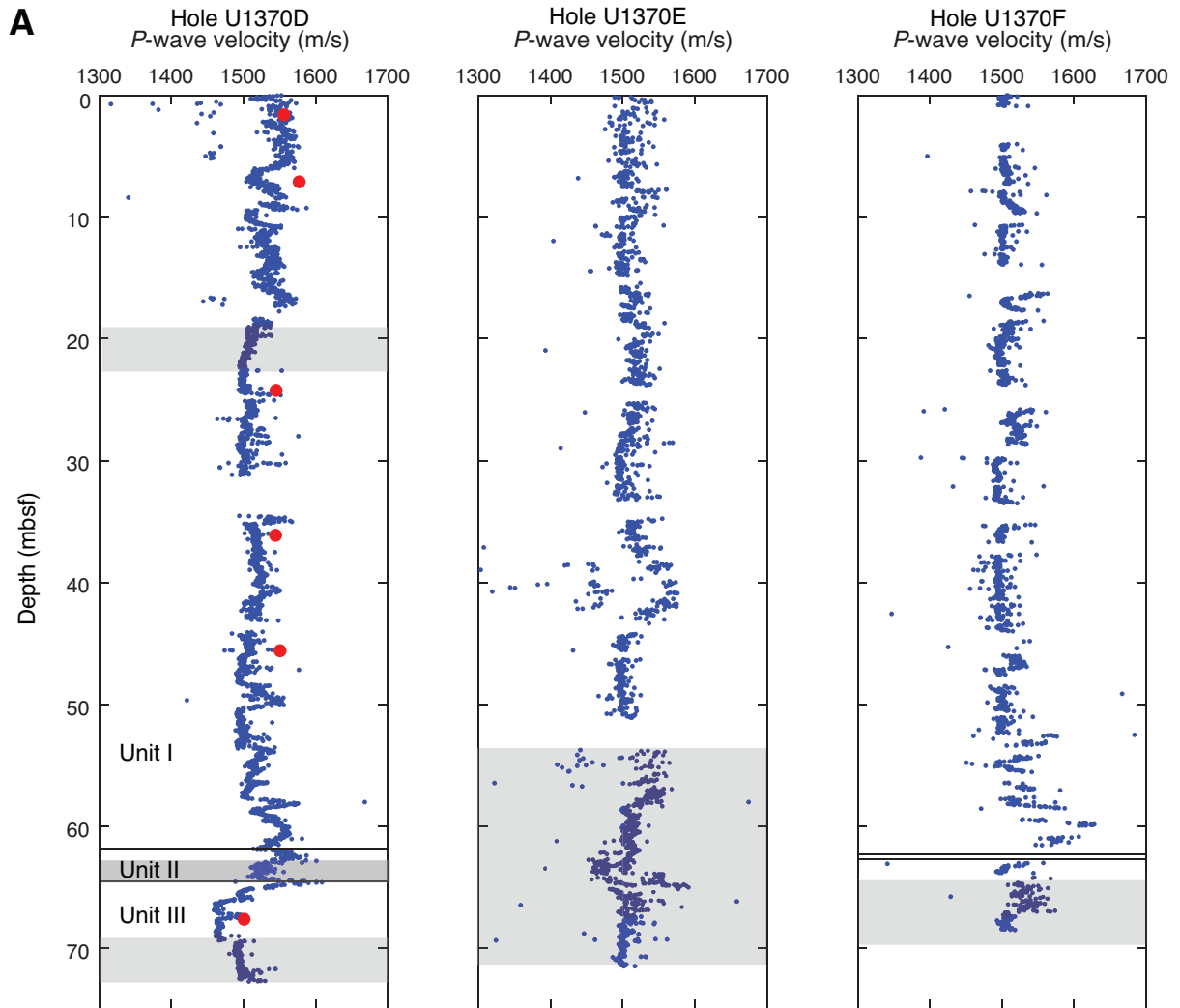


Figure F19. Plot of electrical conductivity measured on surface seawater standard. Lines show best linear fit to data. Best-fitting slope and y -intercept to measurements <400 are -2.8×10^{-5} mS/m/measurement number and 49.44 mS/m, respectively. Best fitting slope and y -intercept to measurements >400 are -9.5×10^{-3} mS/m/measurement number and 53.16 mS/m, respectively.

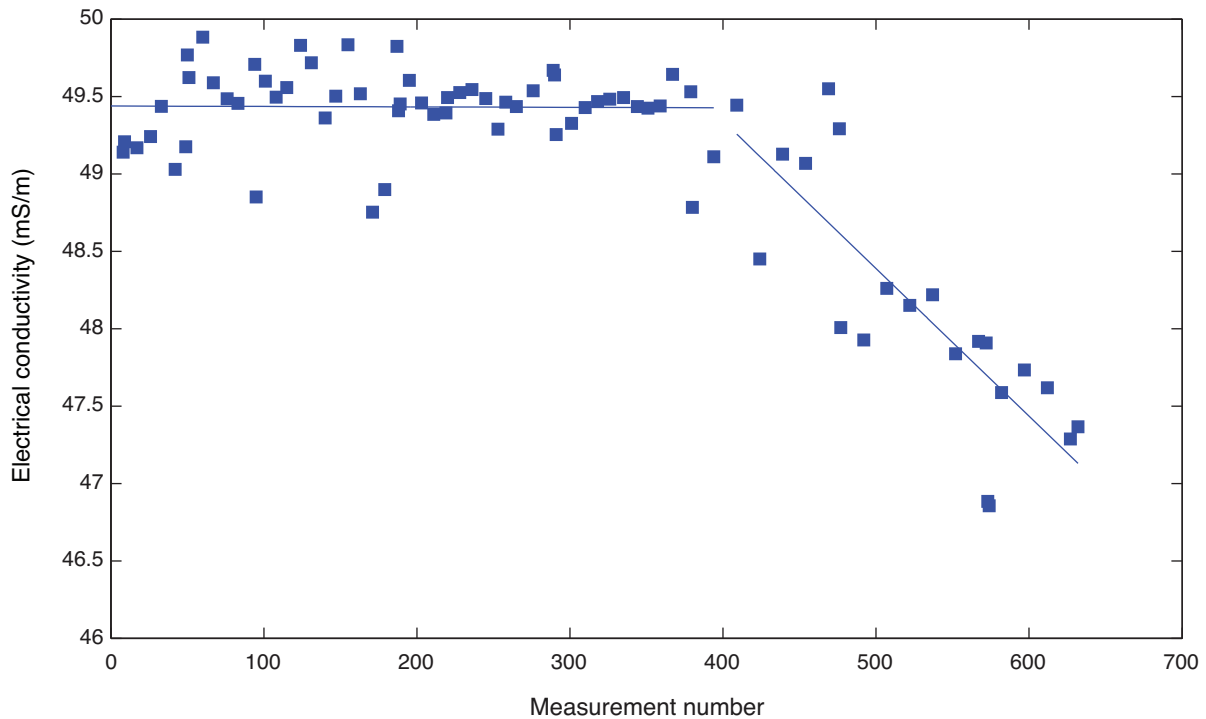


Figure F20. Plot of formation factor as a function of depth, Hole U1370D. Shaded regions denote areas of disturbed core.

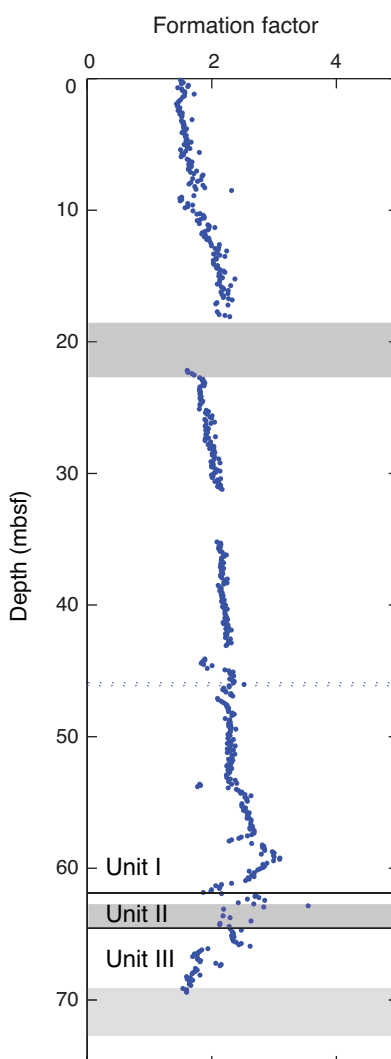


Figure F21. Plots of thermal data, Site U1370. **A.** Thermal conductivity values. Blue circles indicate full-space measurements from Expedition 329, black triangles indicate measurements from KNOX-02RR site survey cruise (R. Harris, unpubl. data). Shaded regions denote areas of disturbed core. **B.** Equilibrium temperatures. Best-fitting linear gradient to the equilibrium temperatures is $93.0^{\circ}\text{C}/\text{km}$.

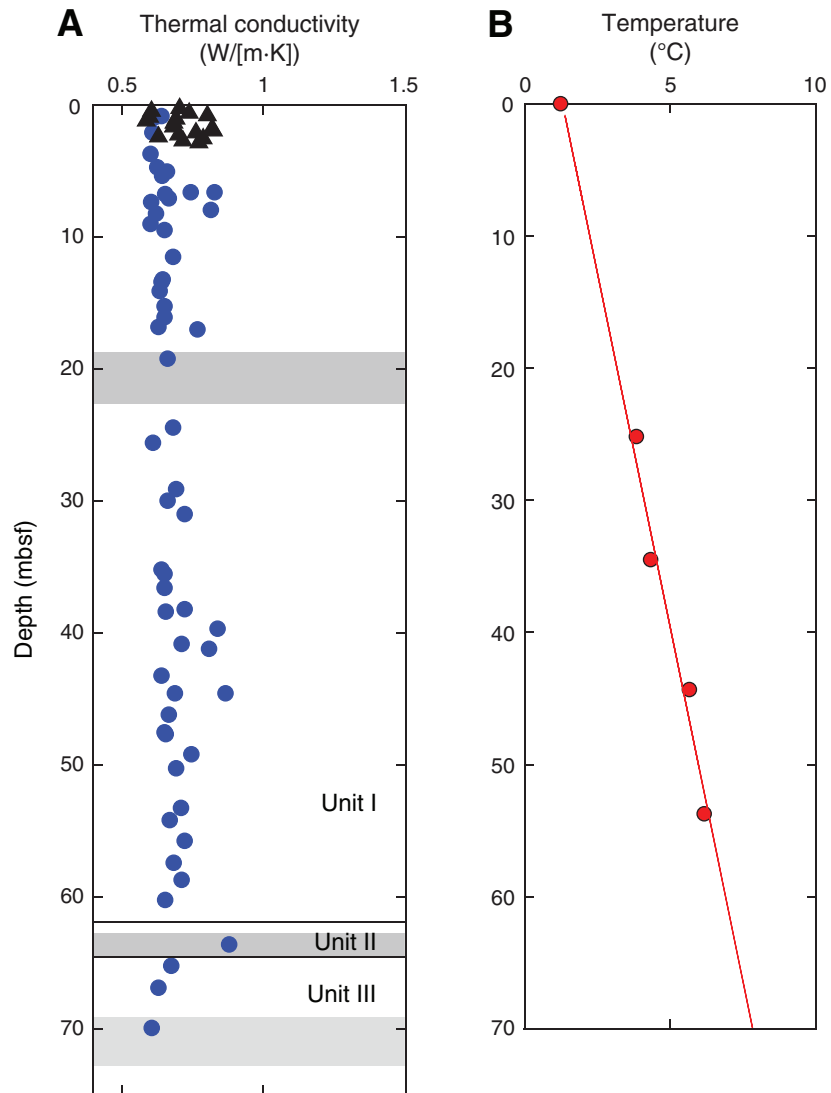


Figure F22. APCT-3 temperature-time series, Site U1370. Unshaded area indicates data used for equilibrium temperature fit, red line indicates theoretical equilibrium curve, triangle shows beginning of fit, inverted triangle shows end of fit. Dashed red line with circles shows estimate of equilibrium temperature.

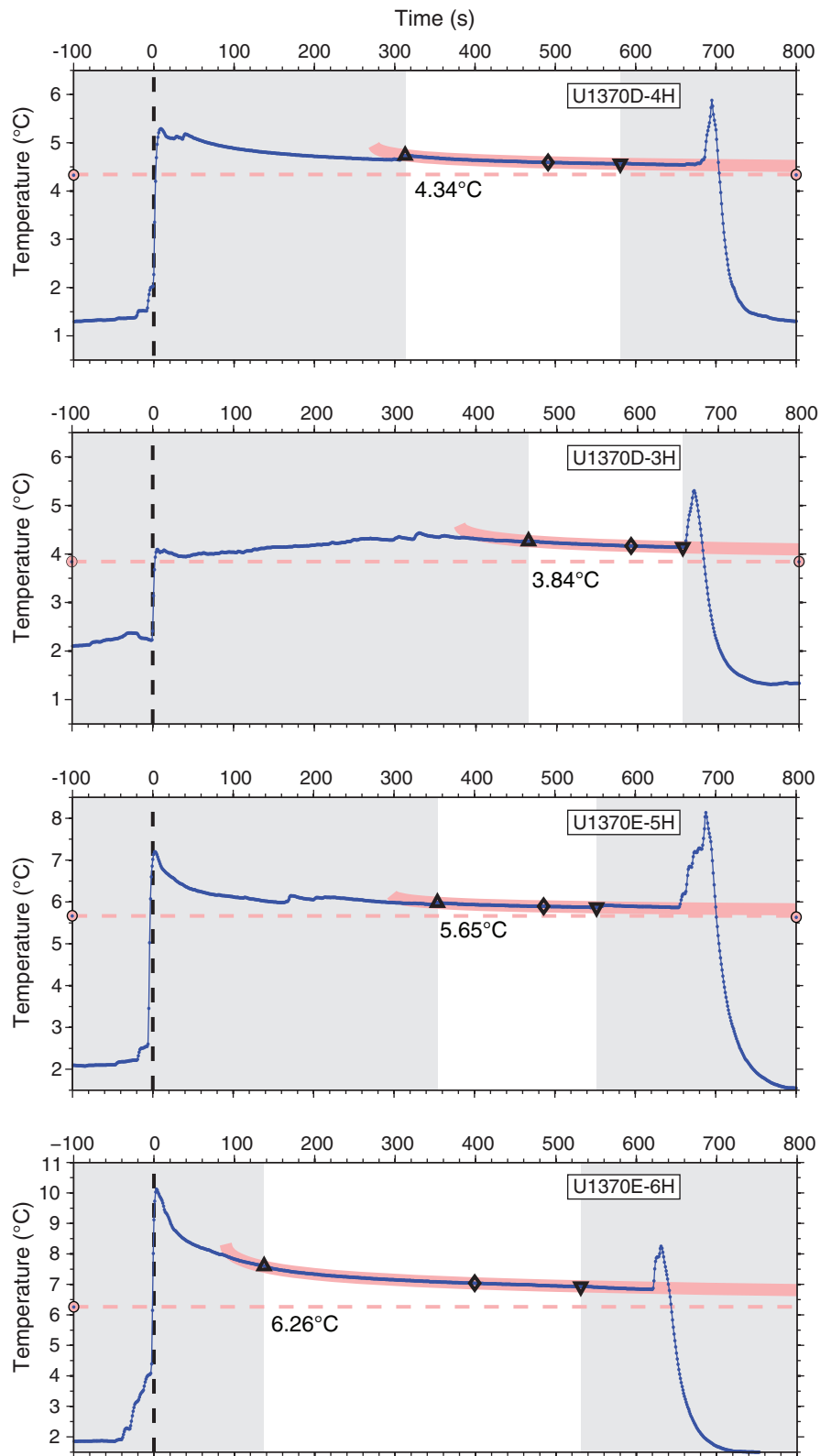


Figure F23. Plots of color spectrometry values, Hole U1370D. Shaded regions denote areas of disturbed core.

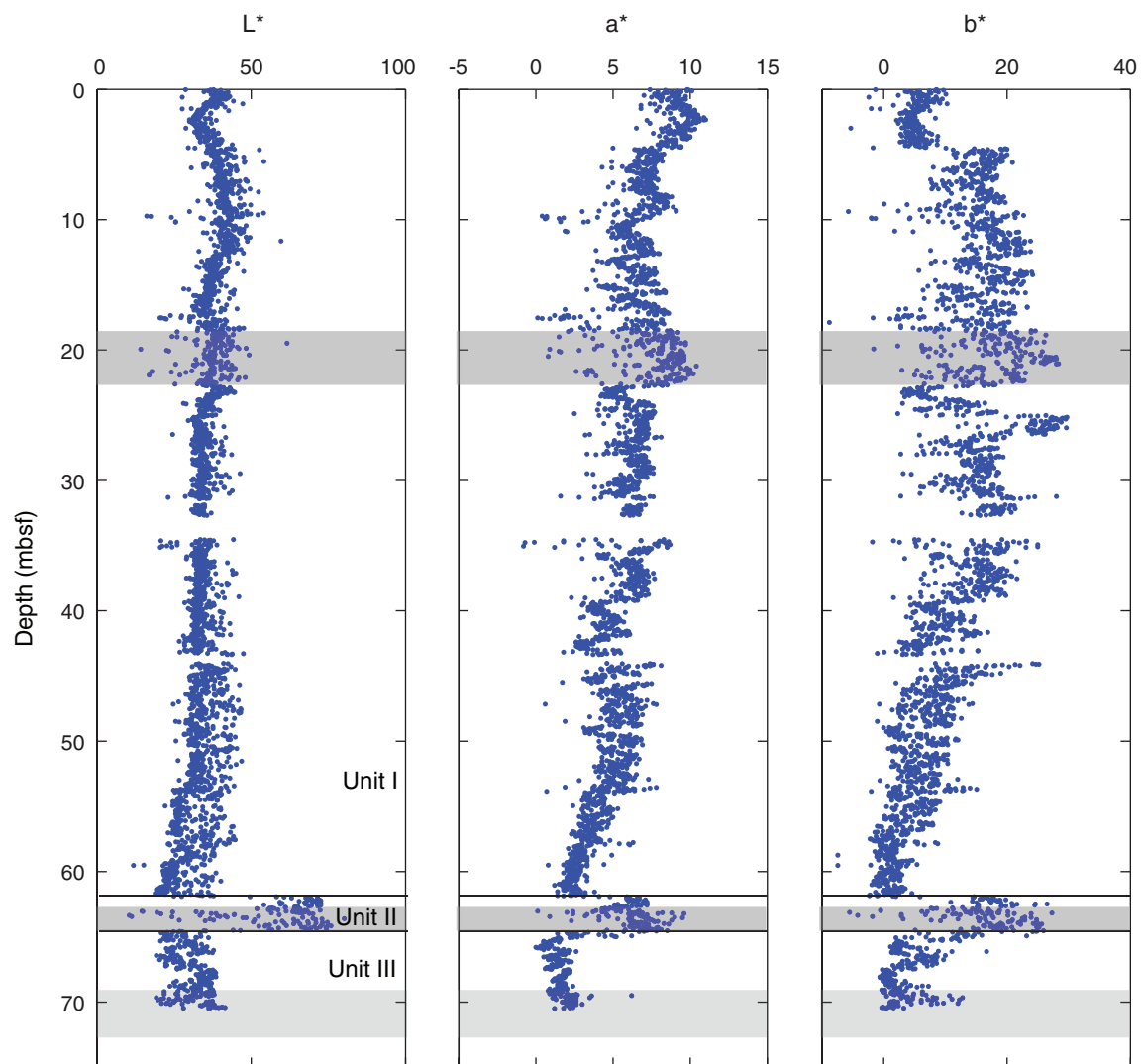


Figure F24. Summary of magnetic susceptibility and paleomagnetic intensity, Hole U1370B. Gray = measurement before demagnetization, red = measurement after 20 mT AF demagnetization step (inclination and intensity), blue = declination measurements, green = magnetic susceptibility data.

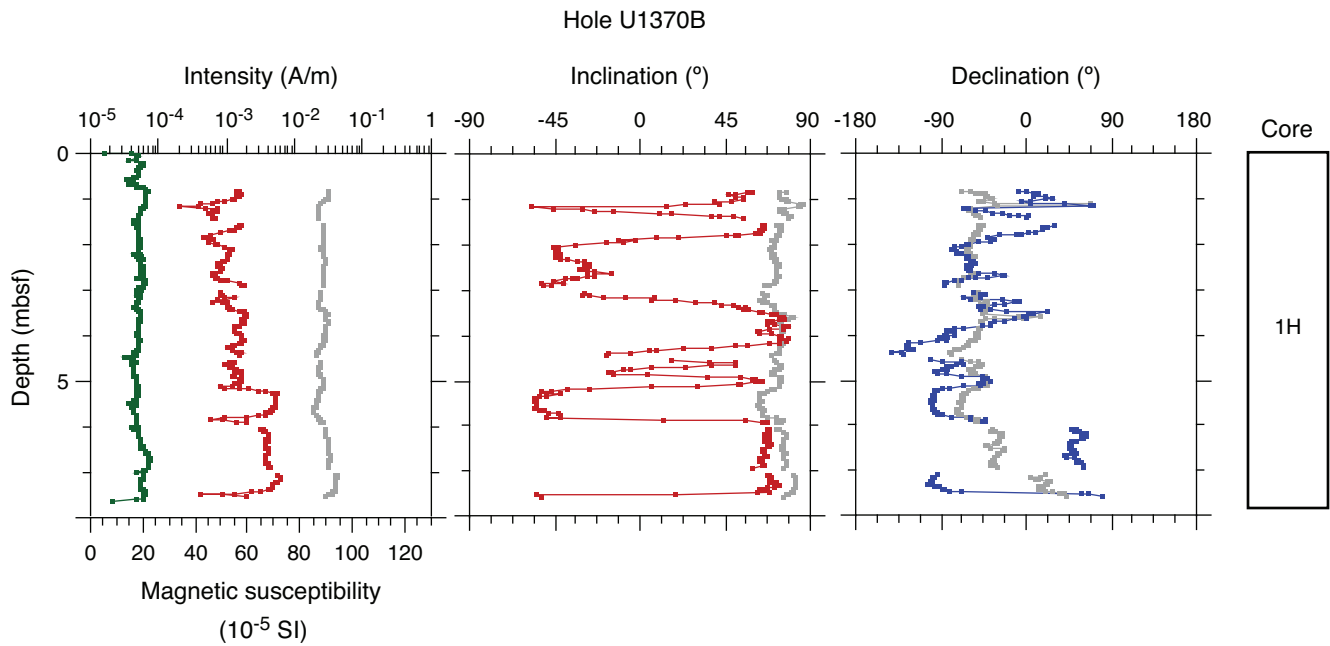


Figure F25. Summary of magnetic susceptibility and paleomagnetic results, Hole U1370D. Gray = measurement before demagnetization, red = measurement after 20 mT AF demagnetization step (inclination and intensity), blue = declination measurements, green = magnetic susceptibility data. Declinations are raw data before orientation using the Flexitool.

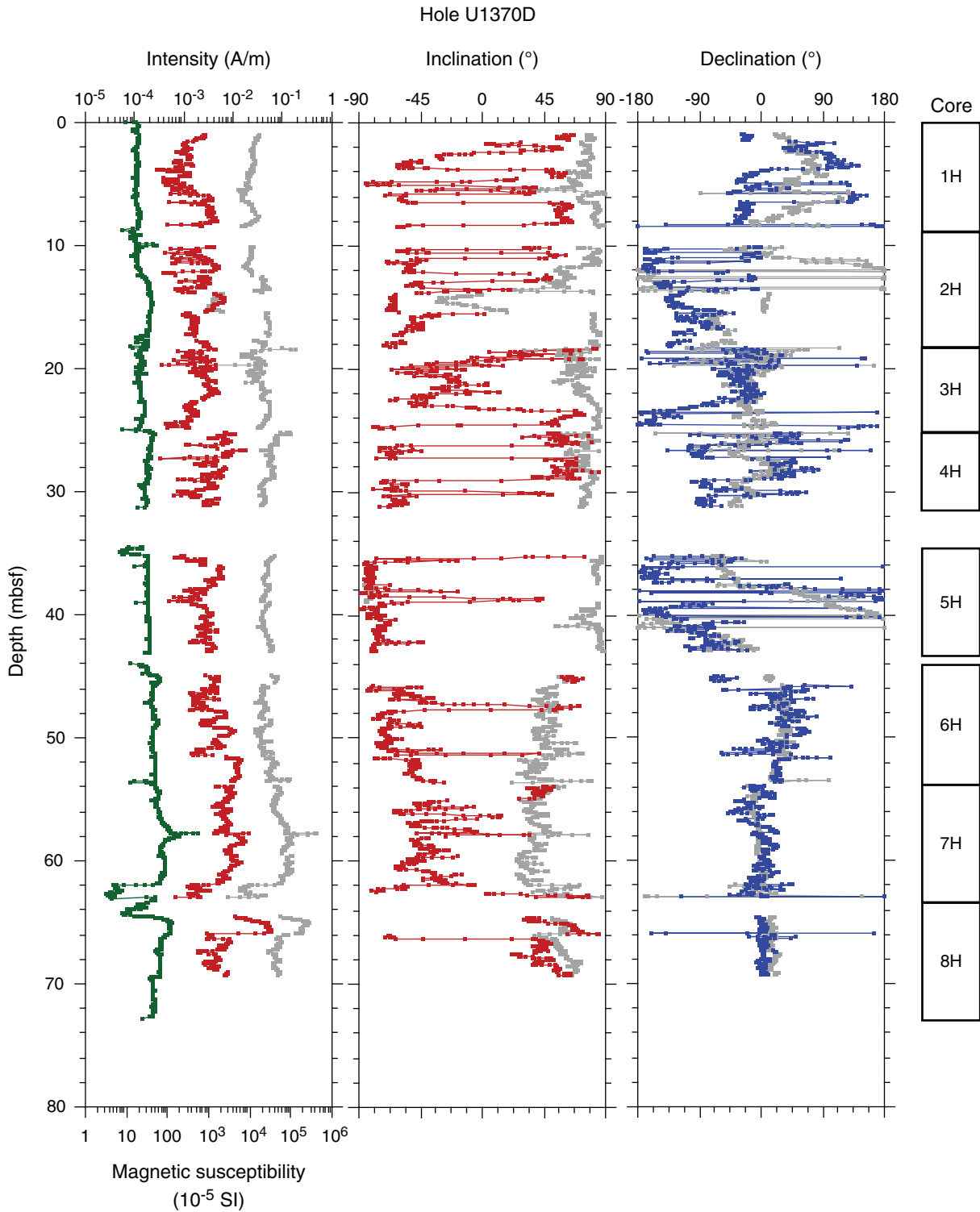


Figure F26. Summary of magnetic susceptibility and paleomagnetic results, Hole U1370E. Gray = measurement before demagnetization, red = measurement after 20 mT AF demagnetization step (inclination and intensity), blue = declination measurements, green = magnetic susceptibility data.

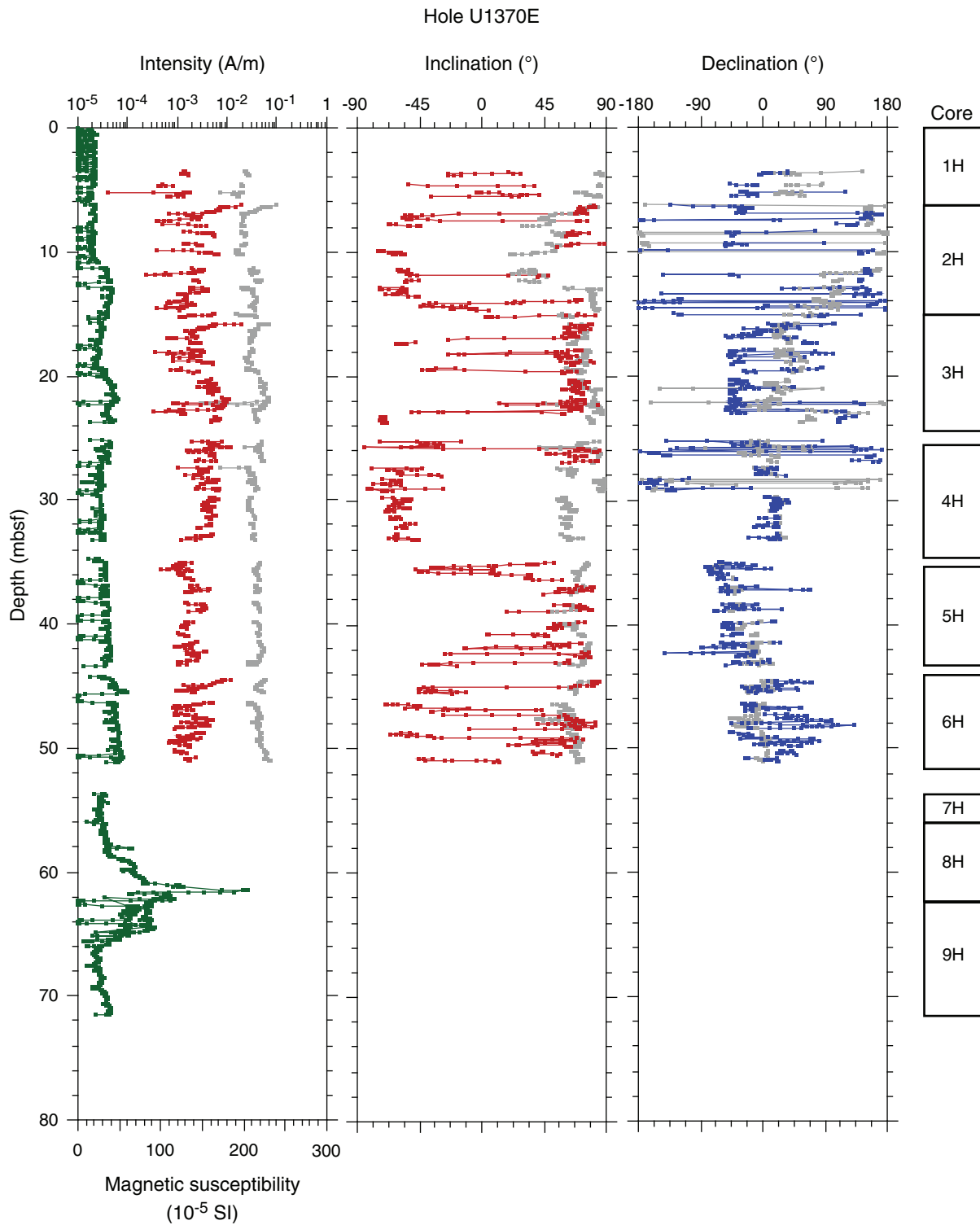


Figure F27. Summary of magnetic susceptibility and paleomagnetic results, Hole U1370F. Gray = measurements before demagnetization, red = data after 20 mT AF demagnetization step (inclination and intensity), blue = declination data, green = magnetic susceptibility data.

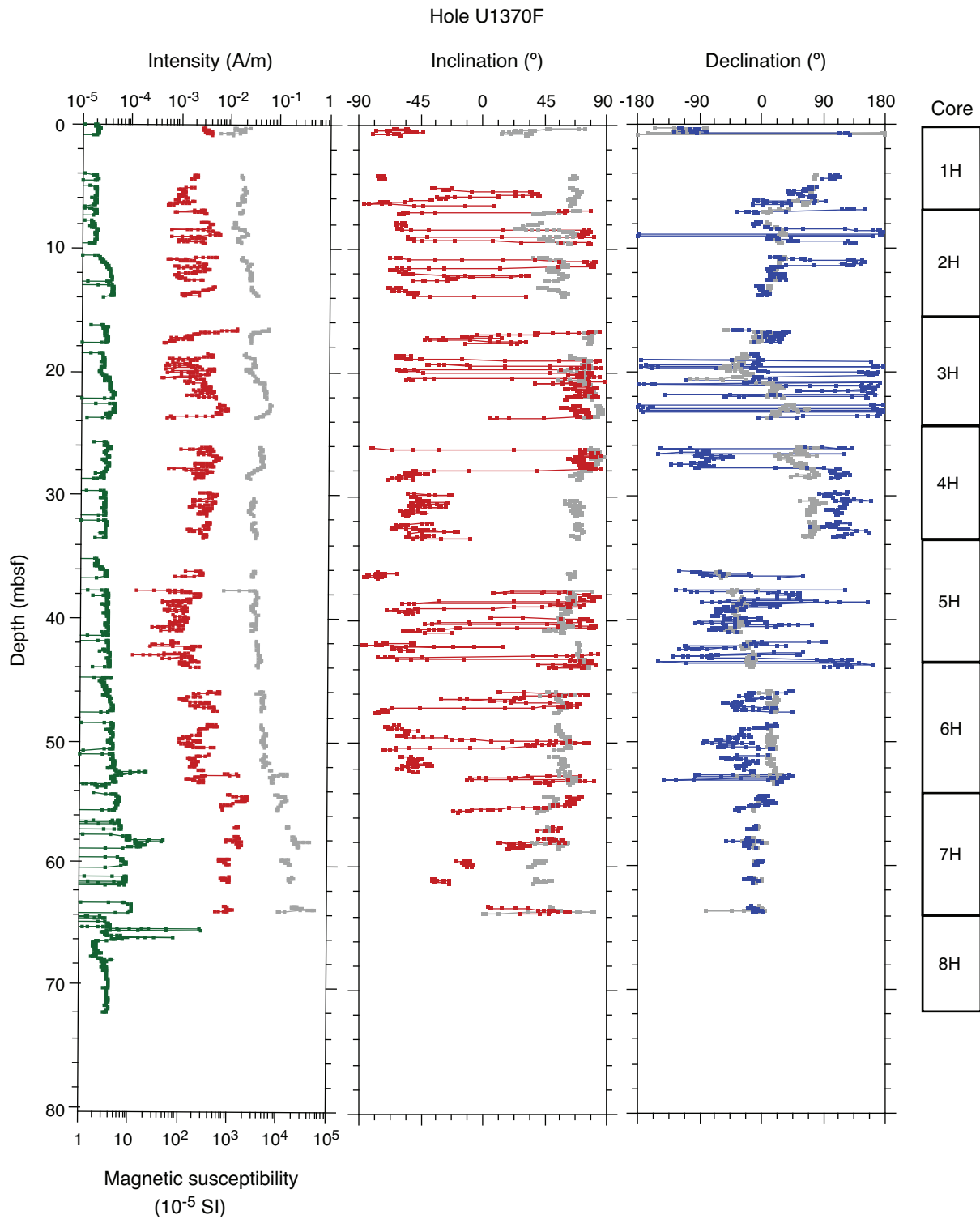




Figure F28. Results of hole-to-hole correlation using magnetic susceptibility (green) and magnetic intensity (red) data from Holes U1370B and U1370D. Black lines indicate correlation points between holes. Paleomagnetic data are also shown after application of the correlation. Gray = measurement before demagnetization, red = inclination after 20 mT AF demagnetization step, blue = declination after 20 mT demagnetization. Declinations are raw data before orientation using the Flexit tool.

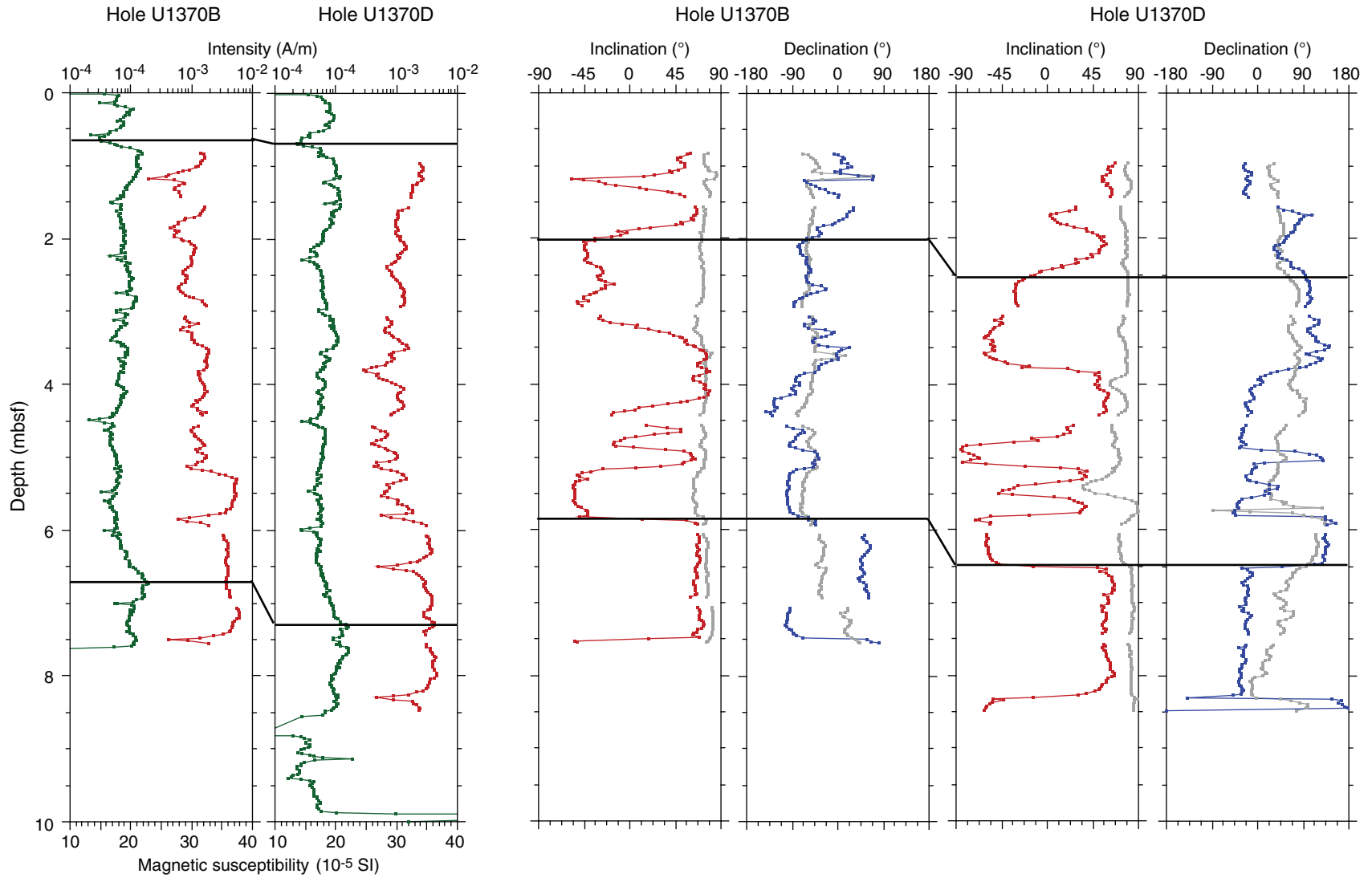




Figure F29. Results of hole-to-hole correlation using magnetic susceptibility (green) and magnetic intensity data (red) from Holes U1370D and U1370E. Black lines indicate correlation points between holes. Gray = measurements before demagnetization.

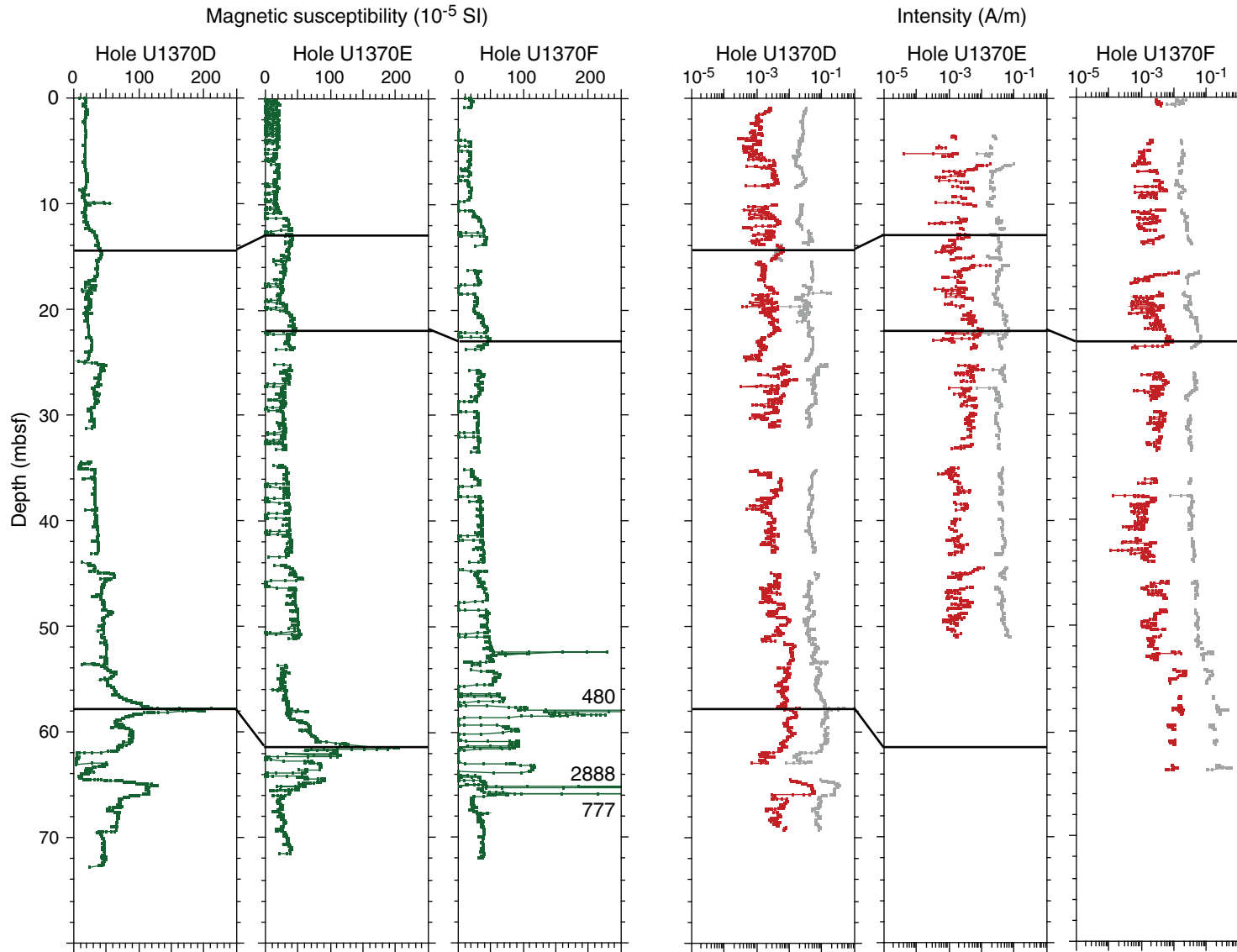




Figure F30. Correlation of the polarity records between Holes U1370D–U1370F. Inclination (red) and declination (blue) data are after the 20 mT AF demagnetization step. Black lines indicate correlation points between holes. Gray = measurements before demagnetization. Declinations are raw data before orientation using the Flexit tool.

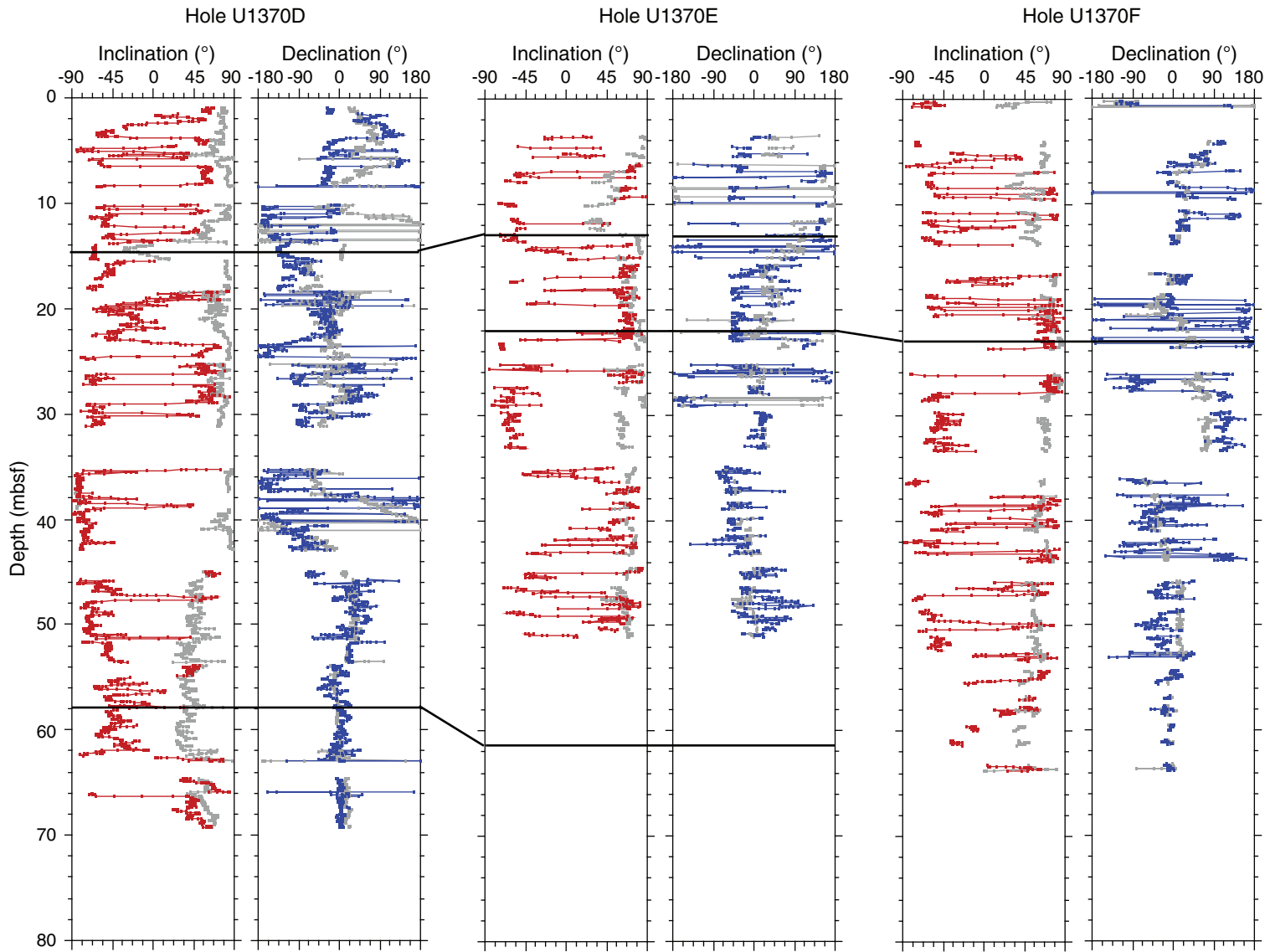


Figure F31. Plots of dissolved oxygen concentrations, Site U1370. **A.** Optode measurements. **B.** Electrode measurements. **C.** Optode measurements in the lowermost 35 m of sediment. **D.** Electrodes measurements in the lowermost 35 m of sediment.

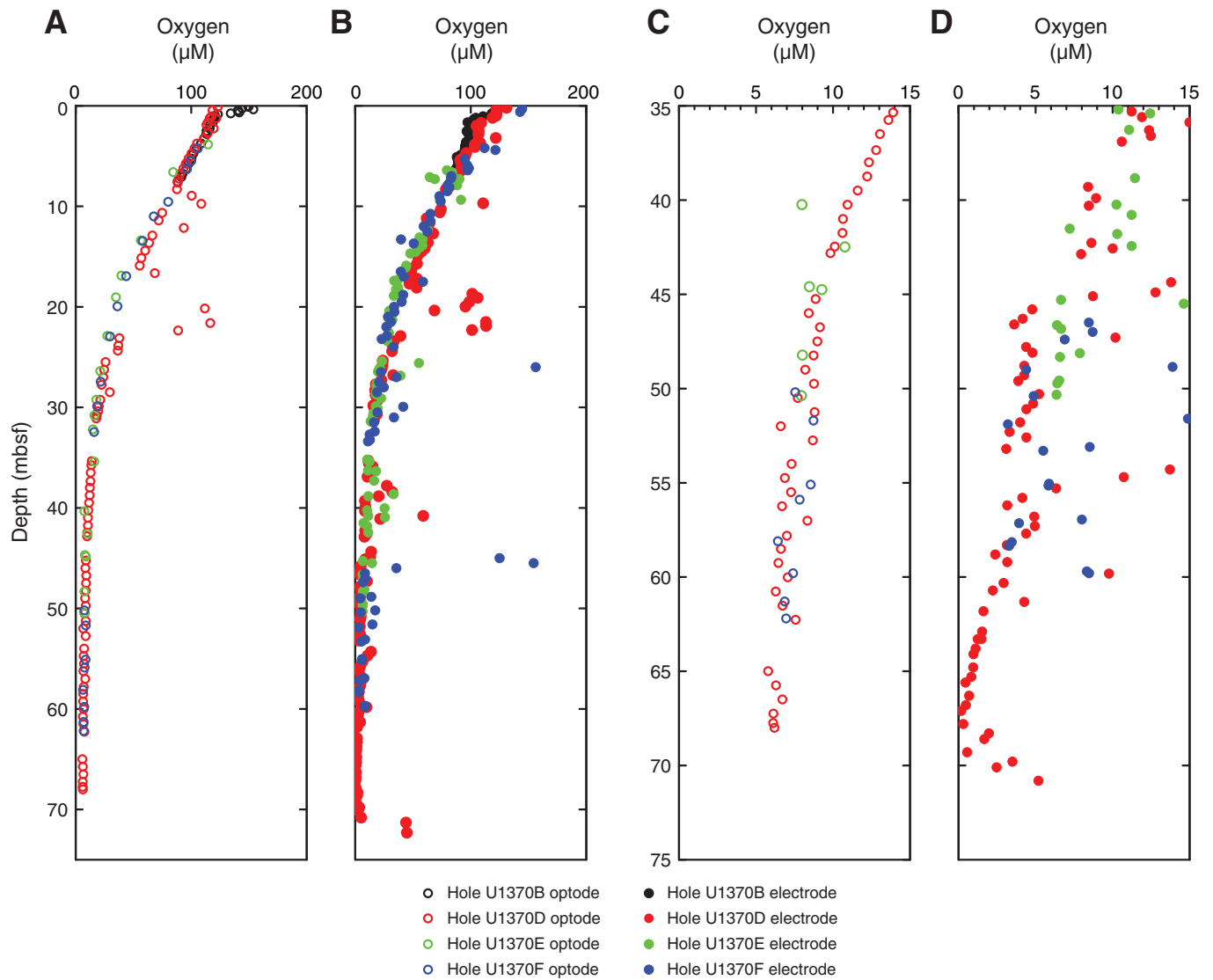


Figure F32. Plot of dissolved hydrogen concentrations, Hole U1369C. Concentrations above detection limit derive from Core 329-U1370E-8H that was subsequently assessed to have flow-in of near-basement sediments.

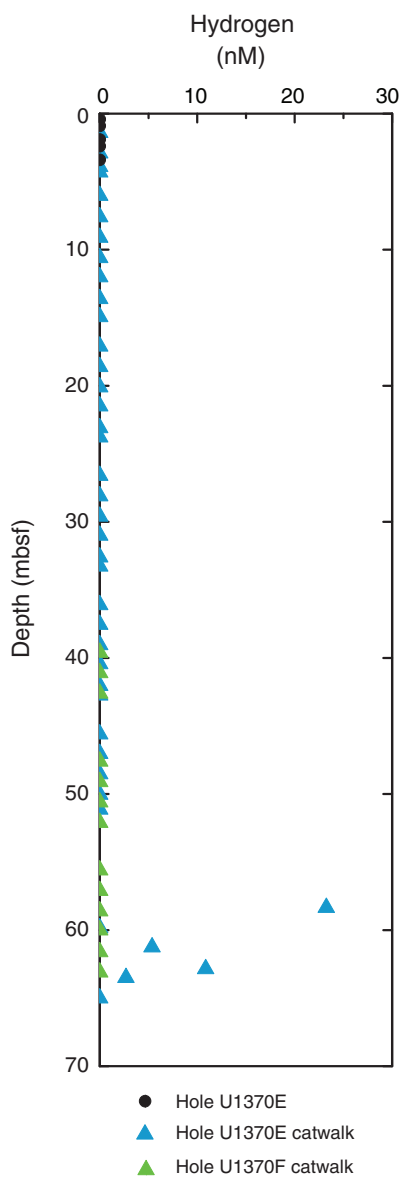




Figure F33. Plots of dissolved interstitial water constituents, Site U1370. IC = ion chromatography, ICP = inductively coupled plasma–atomic emission spectroscopy. **A.** Nitrate. **B.** Phosphate. **C.** Silicate. **D.** Alkalinity. **E.** Dissolved inorganic carbon (DIC). (Continued on next three pages.)

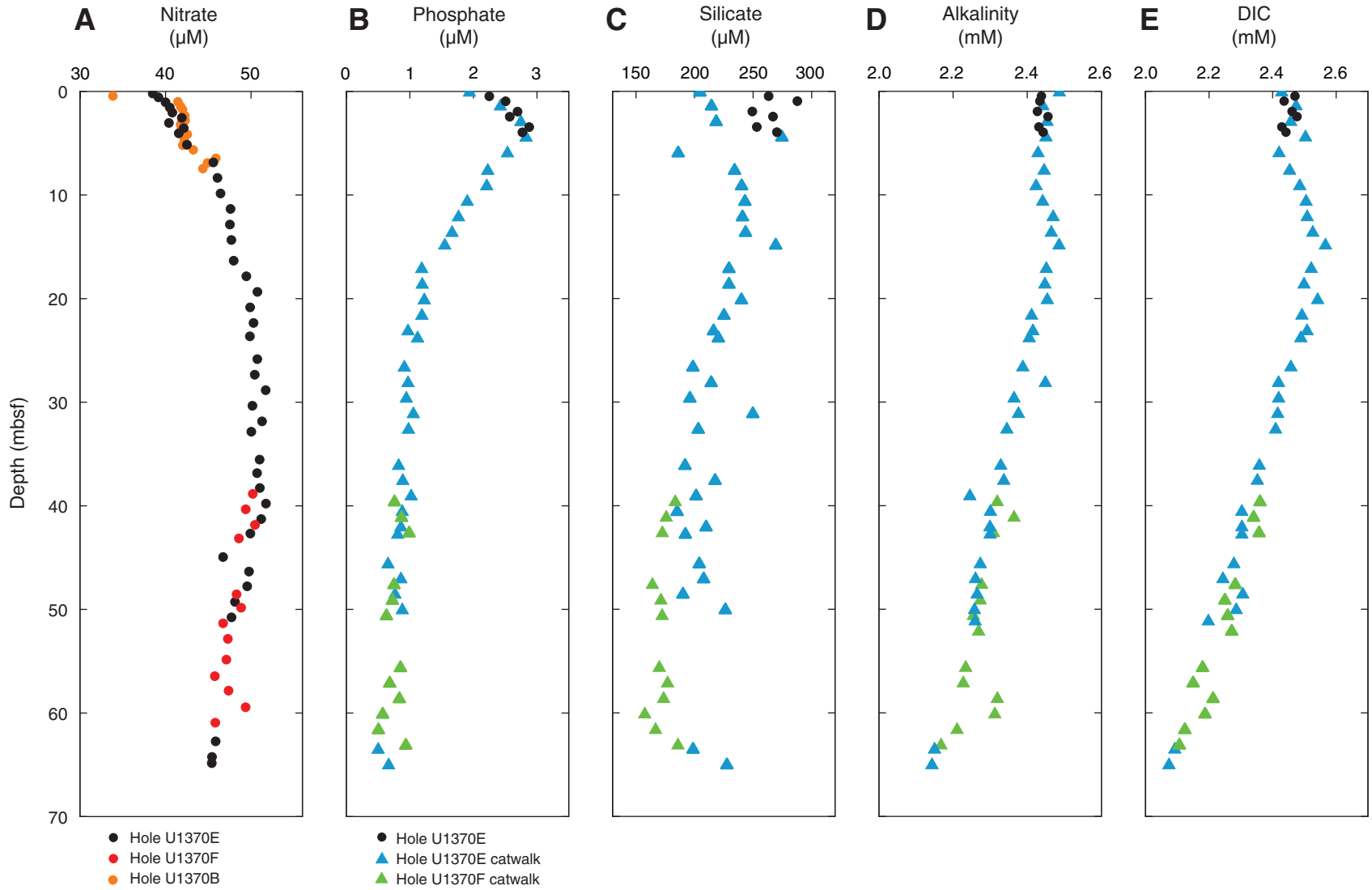




Figure F33 (continued). F. Chloride. G. Sulfate. H. Sulfate anomaly. I. Calcium. J. Magnesium. (Continued on next page.)

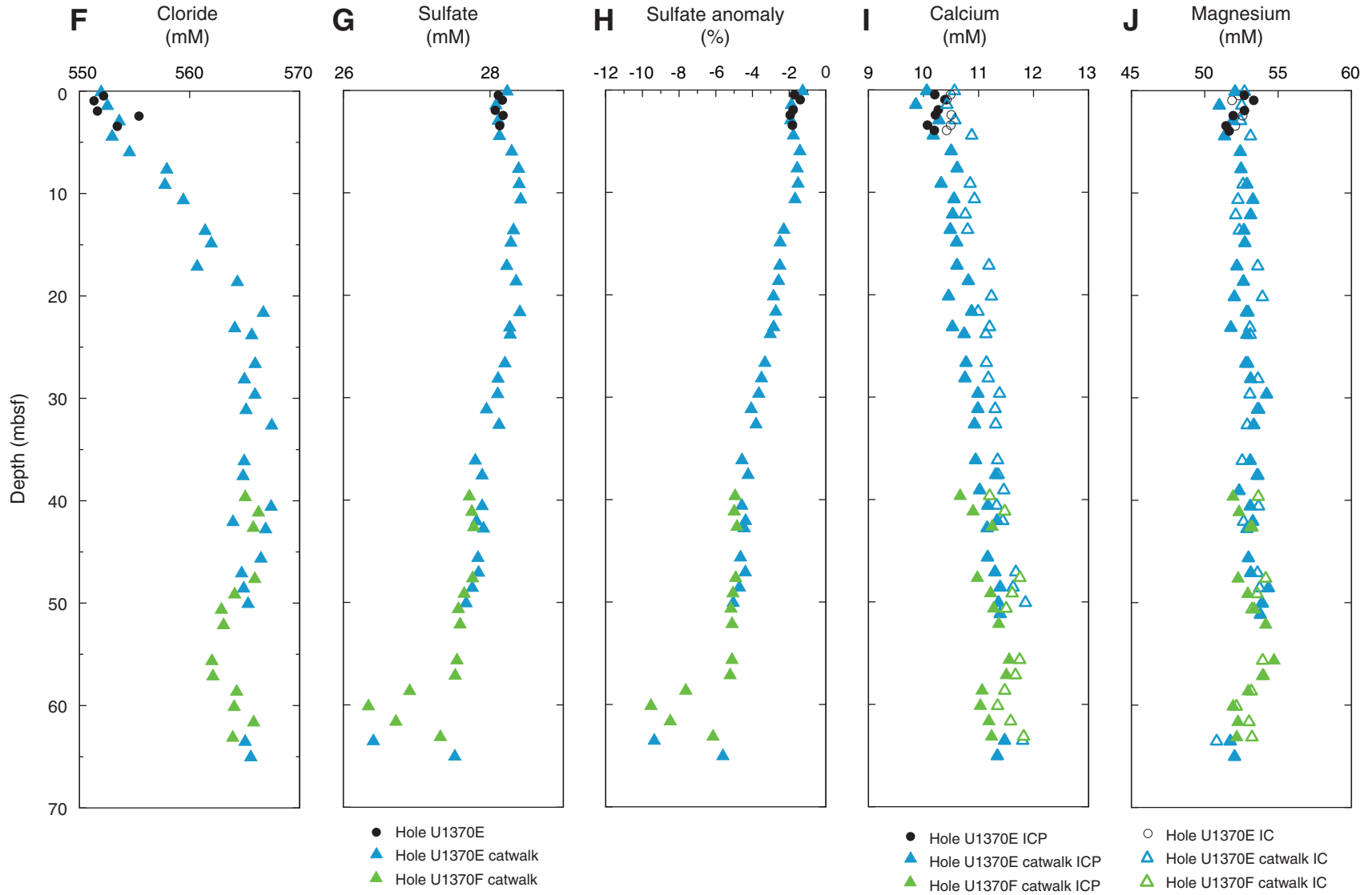




Figure F33 (continued). K. Sodium. L. Potassium. M. Boron. N. Iron. O. Manganese. (Continued on next page.)

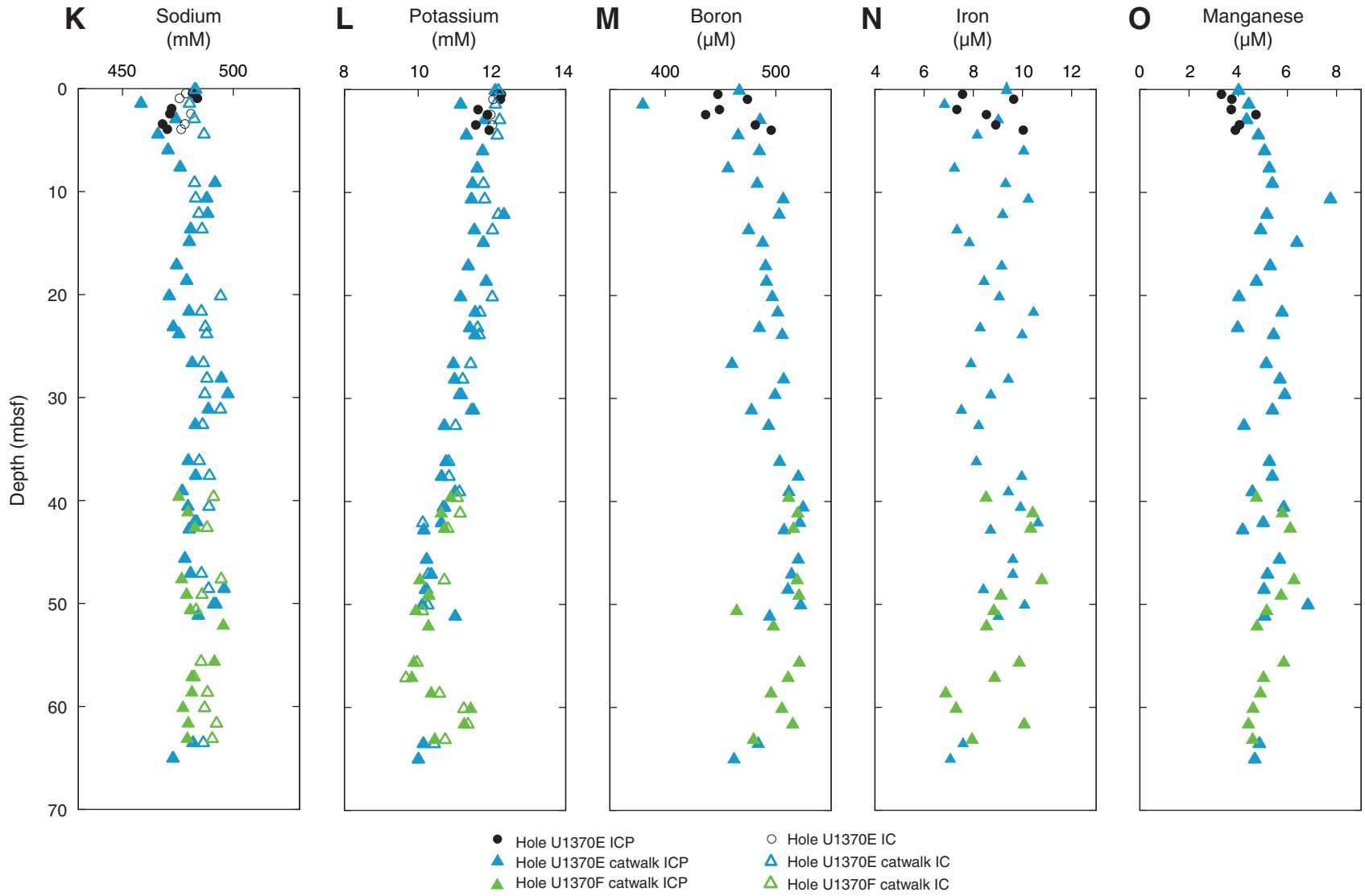




Figure F33 (continued). P. Strontium.

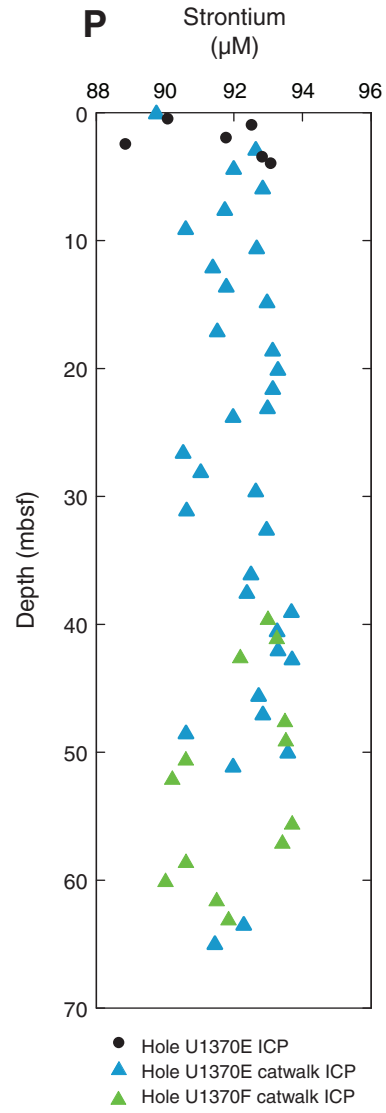


Figure F34. Solid-phase nitrogen and carbon content, Holes U1370D and U1370F. **A.** Total nitrogen (TN). **B.** Total organic carbon (TOC). **C.** Total carbonate (CaCO₃).

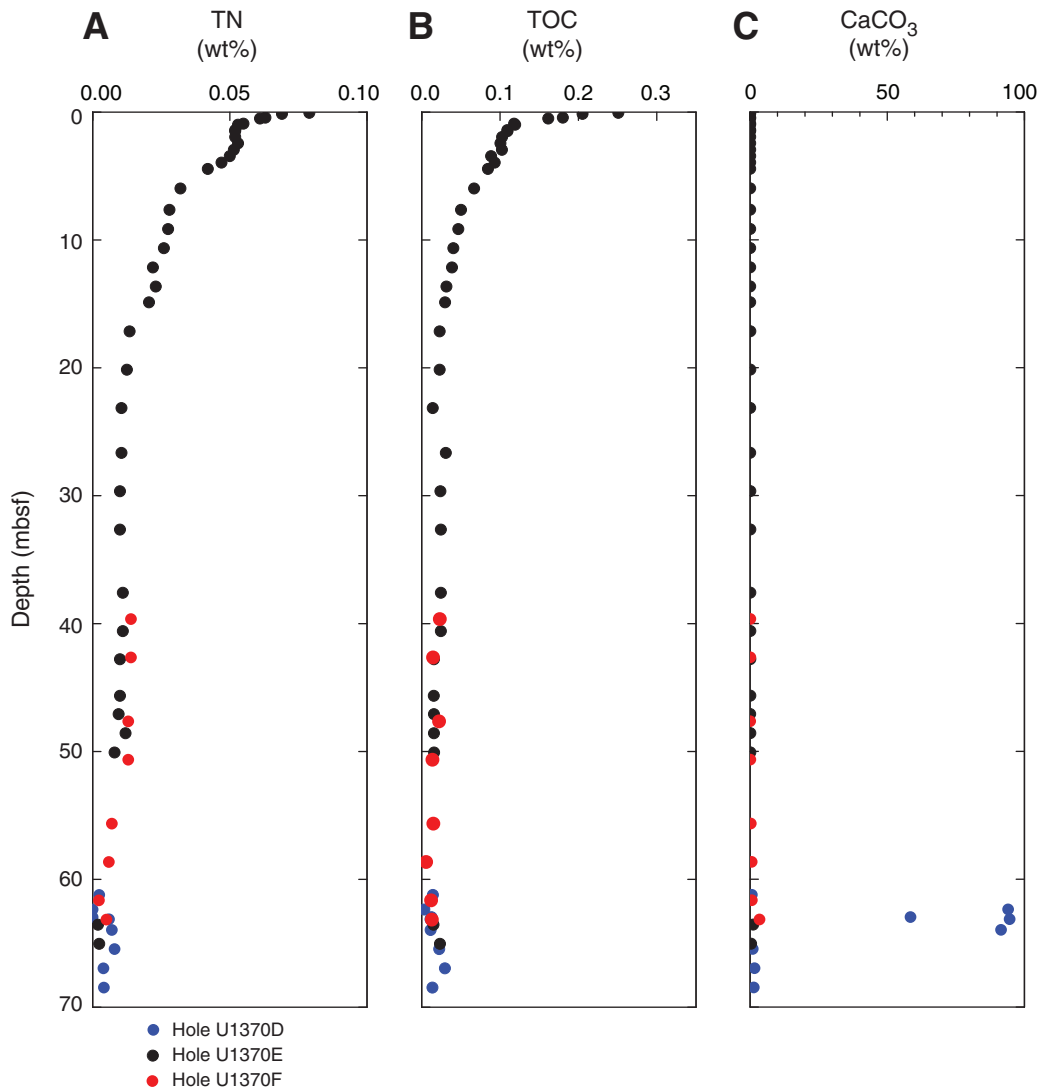


Figure F35. Plot of abundance of microbial cells in Site U1370 sediment as determined by epifluorescence microscopy. Counts below the blank are shown as 10^2 cells/cm³ in order to present them in the graph. See “**Microbiology**” in the “Methods” chapter (Expedition 329 Scientists, 2011a) for a detailed description of the blank and minimum detection limit (MDL) calculation. Red line = MDL for cell counts from extracts, blue line = MDL for nonextracted samples, solid red circles = abundances above MDL, open red circles = direct counts below MDL, solid blue diamonds = nonextracted direct counts above MDL, open blue diamonds = nonextracted direct counts below MDL.

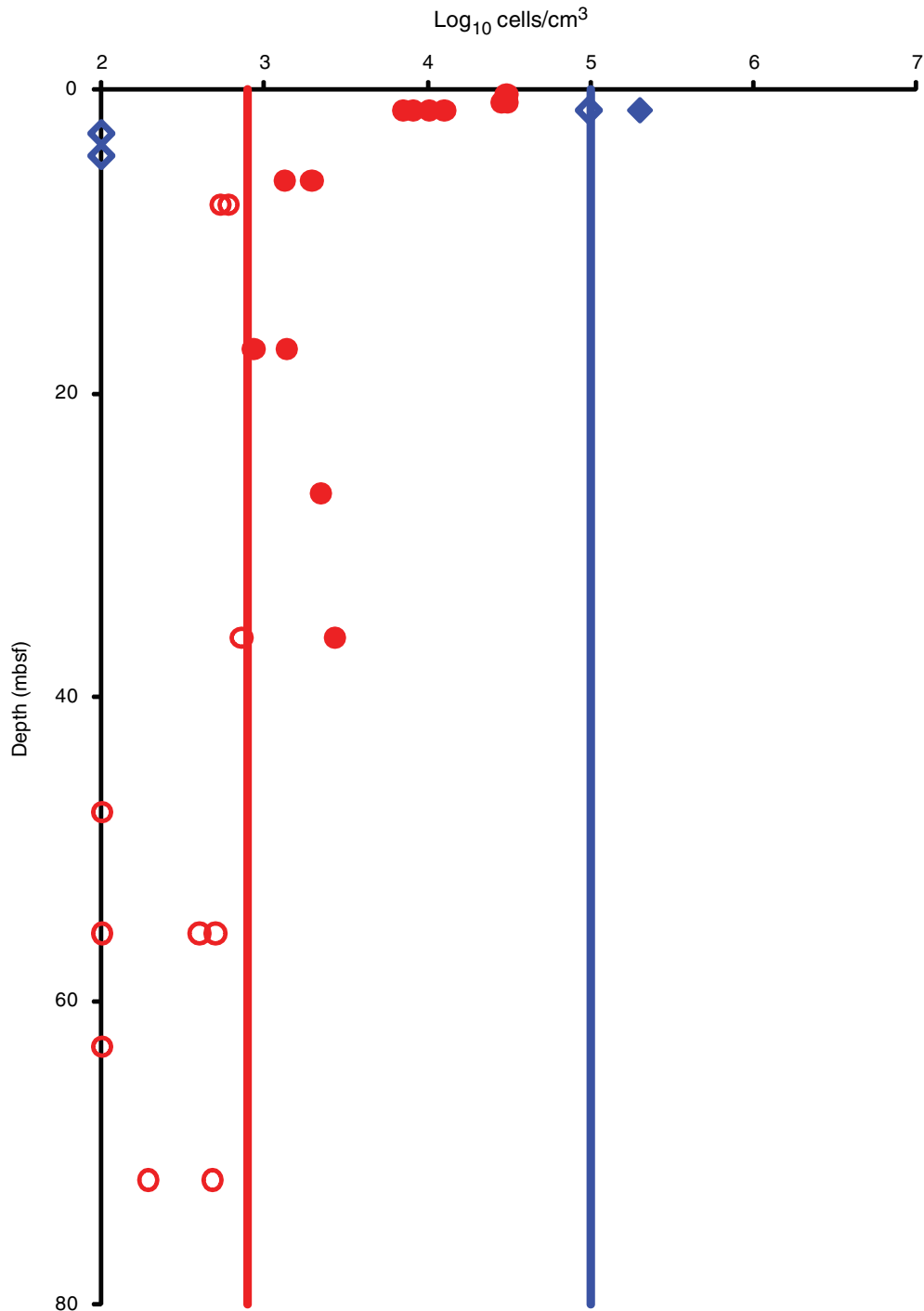




Table T1. Operations summary, Site U1370. (Continued on next two pages.)

Hole U1370A

Latitude: 41°51.1289'S
 Longitude: 153°6.3799'W
 Time on hole (h): 14.25
 Seafloor (drill pipe measurement below rig floor, m DRF): 5085.7
 Distance between rig floor and sea level (m): 11.2
 Water depth (drill pipe measurement from sea level, mbsl): 5074.6 (offset depth from Hole U1370B)
 Total penetration (drilling depth below seafloor, m DSF): 66.7
 Total length of cored section (m): washdown to basement; basement contact established at 5150.4 mbrf; drilled 2 m into basement for verification
 Total core recovered (m): NA
 Core recovery (%): NA
 Total number of cores: NA

Hole U1370B

Latitude: 41°51.1285'S
 Longitude: 153°6.3953'W (20 m west of Hole U1370A)
 Time on hole (h): 3.75
 Seafloor (drill pipe measurement below rig floor, m DRF): 5085.7
 Distance between rig floor and sea level (m): 11.2
 Water depth (drill pipe measurement from sea level, mbsl): 5074.6
 Total penetration (drilling depth below seafloor, m DSF): 7.8
 Total length of cored section (m): 7.8
 Total core recovered (m): 7.81
 Core recovery (%): 100.1
 Total number of cores: 1 (hole terminated after failure to take additional cores)

Hole U1370C

Latitude: 41°51.1171'S
 Longitude: 153°6.3975'W (20 m north of Hole U1370B)
 Time on hole (h): 10
 Seafloor (drill pipe measurement below rig floor, m DRF): 5085.7
 Distance between rig floor and sea level (m): 11.2
 Water depth (drill pipe measurement from sea level, mbsl): 5074.6 (offset depth from Hole U1370B)
 Total penetration (drilling depth below seafloor, m DSF): 7.8
 Total length of cored section (m): 0.0
 Total core recovered (m): NA
 Core recovery (%): NA
 Total number of cores: NA

Hole U1370D

Latitude: 41°51.1156'S
 Longitude: 153°6.3812'W (20 m east of Hole U1370C)
 Time on hole (h): 16.75
 Seafloor (drill pipe measurement below rig floor, m DRF): 5084.7
 Distance between rig floor and sea level (m): 11.2
 Water depth (drill pipe measurement from sea level, mbsl): 5073.6
 Total penetration (drilling depth below seafloor, m DSF): 68.2
 Total length of cored section (m): 68.2
 Total core recovered (m): 70.26
 Core recovery (%): 103
 Total number of cores: 8



Table T1 (continued). (Continued on next page.)

Hole U1370E

Latitude: 41°51.1158'S
 Longitude: 139°6.3668'W (20 m east of Hole U1370D)
 Time on hole (h): 20.25
 Seafloor (drill pipe measurement below rig floor, m DRF): 5085.3
 Distance between rig floor and sea level (m): 11.2
 Water depth (drill pipe measurement from sea level, mbsl): 5074.2
 Total penetration (drilling depth below seafloor, m DSF): 65.6
 Total length of cored section (m): 65.6
 Total core recovered (m): 70.2
 Core recovery (%): 107
 Total number of cores: 9

Hole U1370F

Latitude: 41°51.1267'S
 Longitude: 139°6.3674'W (20 m south of Hole U1370E)
 Time on hole (h): 21
 Seafloor (drill pipe measurement below rig floor, m DRF): 5084.8
 Distance between rig floor and sea level (m): 11.2
 Water depth (drill pipe measurement from sea level, mbsl): 5073.6
 Total penetration (drilling depth below seafloor, m DSF): 64.7
 Total length of cored section (m): 64.7
 Total core recovered (m): 66.32
 Core recovery (%): 102.5
 Total number of cores: 8

Core	Date (2010)	Time (h)	Depth DSF (m)		Interval advanced (m)	Depth CSF (m)		Length of core recovered (m)	Recovery (%)	Sections (N)	Coring shoe type	Remarks
			Top of cored interval	Bottom of cored interval		Top of cored interval	Bottom of cored interval					
329-U1370A-11	27 Nov	1545										Basement contact @ 64.8 mbsf
*****Drilled from 0.0 to 66.7 m DSF*****												
329-U1370B-1H	27 Nov	1815	0.0	7.8	7.8	0.0	7.81	7.81	100	7	Non-mag core barrel	Mudline core only
329-U1370C-11	28 Nov	0430										2 shear pins could not fire 2H
*****Drilled from 0.0 to 7.8 m DSF*****												
329-U1370D-1H	28 Nov	0800	0.0	8.8	8.8	0.0	8.75	8.75	99	7	Non-mag core barrel	
2H	28 Nov	1005	8.8	18.3	9.5	8.8	18.43	9.63	101	8	Non-mag core barrel	
3H	28 Nov	1215	18.3	25.0	6.7	18.3	25.05	6.75	101	6	Non-mag core barrel	
4H	28 Nov	1425	25.0	34.5	9.5	25.0	31.45	6.45	68	6	Non-mag core barrel	
5H	28 Nov	1620	34.5	44.0	9.5	34.5	43.40	8.90	94	7	Non-mag core barrel	
6H	28 Nov	1805	44.0	53.5	9.5	44.0	53.88	9.88	104	8	STD	
7H	28 Nov	1955	53.5	63.0	9.5	53.5	63.30	9.80	103	8	STD	
8H	28 Nov	2150	63.0	68.2	5.2	63.0	73.10	10.10	194	8	STD	Drilled down and tagged basement after last core
329-U1370E-1H	29 Nov	0130	0.0	6.2	6.2	0.0	6.20	6.20	100	5	Non-mag core barrel	
2H	29 Nov	0335	6.2	15.7	9.5	6.2	15.62	9.64	101	8	Non-mag core barrel	
3H	29 Nov	0555	15.7	25.2	9.5	15.7	24.19	8.49	89	7	APCT-3	
4H	29 Nov	0805	25.2	34.7	9.5	25.2	33.43	8.23	87	7	Non-mag core barrel	
5H	29 Nov	1010	34.7	44.2	9.5	34.7	43.54	8.84	93	8	APCT-3	



Table T1 (continued).

Core	Date (2010)	Time (h)	Depth DSF (m)			Depth CSF (m)		Length of core recovered (m)	Recovery (%)	Sections (N)	Coring shoe type	Remarks
			Top of cored interval	Bottom of cored interval	Interval advanced (m)	Top of cored interval	Bottom of cored interval					
6H	29 Nov	1210	44.2	53.7	9.5	44.2	51.56	7.36	77	6	APCT-3	
7H	29 Nov	1410	53.7	56.1	2.4	53.7	56.13	2.43	101	3	STD	
8H	29 Nov	1620	56.1	62.1	6.0	56.1	65.35	9.25	154	8	STD	
9H	29 Nov	1805	62.1	65.6	3.5	62.1	71.86	9.76	279	8	STD	Drilled down and tagged basement after last core
329-U1370F-												
1H	29 Nov	2020	0.0	6.7	6.7	0.0	6.73	6.73	100	6	Non-mag core barrel	
2H	29 Nov	2200	6.7	16.2	9.5	6.7	14.12	7.42	78	6	Non-mag core barrel	
3H	29 Nov	2310	16.2	25.7	9.5	16.2	23.94	7.74	81	7	Non-mag core barrel	
4H	30 Nov	0030	25.7	35.2	9.5	25.7	33.68	7.98	84	7	Non-mag core barrel	
5H	30 Nov	0200	35.2	44.7	9.5	35.2	44.19	8.99	95	7	Non-mag core barrel	
6H	30 Nov	0340	44.7	54.2	9.5	44.7	53.90	9.20	97	7	STD	
7H	30 Nov	0450	54.2	63.7	9.5	54.2	64.08	9.88	104	8	STD	
8H	30 Nov	0600	63.7	64.7	1.0	63.7	72.08	8.38	838	8	STD	Drilled down and tagged basement after last core
Advanced total:					280.8			214.59	104	181		
Total interval cored:					206.3							

NA = not applicable. DSF = drilling depth below seafloor, CSF = core depth below seafloor. H = APC core, 1 = drilled interval. Non-mag = nonmagnetic, STD = standard, APCT-3 = advanced piston corer temperature tool. Time is UTC.

Table T2. Distribution and overall and relative abundance of planktonic foraminifers, Site U1370.

Core, section, interval (cm)	Depth (mbsf)	Planktonic foraminifer zone	Preservation	Overall abundance										Number of taxa	Comments
				<i>Chiloguembelina midwayensis</i> (Cushman, 1940)	<i>Chiloguembelina morsei</i> (Kline, 1943)	<i>Eoglobigerina edita</i> (Subbotina, 1953)	<i>Eoglobigerina eobulloides</i> Morozova, 1959	<i>Guembelitra cretacea</i> (Cushman, 1933)	<i>Parasubbotina pseudobulloides</i> (Plummer, 1926)	<i>Parasubbotina</i> aff. <i>pseudobulloides</i> (Plummer, 1926)	<i>Subbotina triloculinoides</i> (Plummer, 1926)	<i>Subbotina trivialis</i> (Subbotina, 1953)			
329-U1370D-7H-6, 97-99	62.01	P1b	VG	A	P	P	P	P			P	P	P	6	Taxa not older than Zone P1b
7H-CC	63.28	P1a/P1b	VG	A	P	P	P	P			P	P	P	5	
8H-1, 147-149	64.47	P1a	G	C		P	P		P		P	P	P	6	

Preservation: VG = very good, G = good. Abundance: A = abundant, C = common, P = present. For more specific preservation and abundance definitions, refer to **“Paleontology and biostratigraphy”** in the “Methods” chapter (Expedition 329 Scientists, 2011a).

Table T3. Distribution and overall and relative abundance of benthic foraminifers and ostracods, Site U1370.

Core, section, interval (cm)	Depth (mbsf)	Preservation	Overall abundance	Relative abundance																			Number of foraminifer taxa	Ostracods						
				<i>Anomalina</i> sp.	<i>Aragonia</i> spp.	<i>Bulimina midwayensis</i>	<i>Bulimina trihedra</i>	<i>Bulimina trinitaensis</i>	<i>Buliminella grata</i>	<i>Cibicides</i> sp.	<i>Dorothyia trochoides</i>	<i>Gyroidinoides globosus</i>	<i>Lagena</i> spp	<i>Lenticulina</i> spp.	<i>Nodosaria limbata</i>	<i>Nodosaria</i> sp.	<i>Nonion havanense</i>	<i>Nuttallides truempyi</i>	<i>Oridorsalis umbonatus</i>	<i>Osangularia velascoensis</i>	<i>Spiroplectammia</i> spp.	<i>Stilostomella midwayensis</i>			<i>Stilostomella subspinosa</i>	<i>Tappanina selmensis</i>	<i>Vulvulina spinosa</i>	<i>Vulvulina</i> sp.		
329-U1370D-7H-6, 97-99	62.01	M	C	R	A	A			R	R	F	R	R	R	R	R	R	F	A	A	R	R	R	R	R	R	R	R	19	
7H-CC	63.28	M	C	R	A		R		R	R	F	R	R	A		F	R	A	A	R	R	R	R		R		R	17	P	
8H-1, 147-149	64.47																													

Preservation: M = moderate. Abundance: A = abundant, C= common, F = few, R = rare. For more specific preservation and abundance definitions, refer to **“Paleontology and biostratigraphy”** in the “Methods” chapter (Expedition 329 Scientists, 2011a).

Table T4. Electrical conductivity measurements of surface seawater, Site U1370. (Continued on next page.)

Measurement number	Electrical conductivity (mS/cm)	Temperature (°C)	Correction factor at 20°C (mS/cm)	Seawater electrical conductivity at 20°C (mS/cm)
1	51.38	21.9	49.84	49.37
9	51.03	21.8	49.74	49.14
10	51.10	21.8	49.74	49.21
18	51.06	21.8	49.74	49.17
27	51.03	21.7	49.63	49.24
34	51.02	21.5	49.43	49.44
43	51.02	21.9	49.84	49.03
50	50.75	21.5	49.43	49.17
51	50.83	21.0	48.91	49.77
52	50.68	21.0	48.91	49.62
61	51.16	21.2	49.12	49.88



Table T4 (continued).

Measurement number	Electrical conductivity (mS/cm)	Temperature (°C)	Correction factor at 20°C (mS/cm)	Seawater electrical conductivity at 20°C (mS/cm)
68	51.07	21.4	49.32	49.59
77	51.07	21.5	49.43	49.48
84	51.04	21.5	49.43	49.46
95	51.30	21.5	49.43	49.71
96	51.15	22.2	50.15	48.85
102	51.40	21.7	49.63	49.60
109	51.40	21.8	49.74	49.50
116	51.57	21.9	49.84	49.56
125	51.64	21.7	49.63	49.83
132	51.63	21.8	49.74	49.72
141	51.26	21.8	49.74	49.36
148	51.30	21.7	49.63	49.50
156	51.11	21.2	49.12	49.83
164	51.21	21.6	49.53	49.52
172	50.21	21.4	49.32	48.75
180	50.15	21.2	49.12	48.90
188	51.42	21.5	49.43	49.82
189	50.99	21.5	49.43	49.41
190	50.93	21.4	49.32	49.45
196	50.98	21.3	49.22	49.60
204	50.83	21.3	49.22	49.46
212	50.86	21.4	49.32	49.38
220	50.87	21.4	49.32	49.39
221	51.61	22.0	49.94	49.49
229	51.43	21.8	49.74	49.52
237	51.45	21.8	49.74	49.54
246	51.39	21.8	49.74	49.49
254	51.29	21.9	49.84	49.29
259	51.26	21.7	49.63	49.46
266	51.23	21.7	49.63	49.43
277	51.23	21.6	49.53	49.54
290	50.94	21.2	49.12	49.67
291	50.91	21.2	49.12	49.64
292	51.36	22.0	49.94	49.25
302	51.33	21.9	49.84	49.33
311	51.33	21.8	49.74	49.43
319	51.37	21.8	49.74	49.47
327	51.28	21.7	49.63	49.48
336	51.29	21.7	49.63	49.49
345	51.23	21.7	49.63	49.43
352	51.22	21.7	49.63	49.42
360	51.34	21.8	49.74	49.44
368	51.34	21.6	49.53	49.64
380	51.33	21.7	49.63	49.53
381	50.87	22.0	49.94	48.78
395	51.21	22.0	49.94	49.11
410	51.24	21.7	49.63	49.44
425	50.21	21.7	49.63	48.45
440	51.44	22.2	50.15	49.13
455	50.85	21.7	49.63	49.07
470	51.35	21.7	49.63	49.55
477	50.87	21.5	49.43	49.29
478	50.37	22.3	50.25	48.01
493	49.77	21.8	49.74	47.93
508	49.91	21.6	49.53	48.26
523	49.59	21.4	49.32	48.15
538	49.35	21.1	49.02	48.22
553	49.37	21.5	49.43	47.84
568	49.35	21.4	49.32	47.92
573	49.34	21.4	49.32	47.91
574	48.89	22.0	49.94	46.88
575	48.86	22.0	49.94	46.86
583	49.52	21.9	49.84	47.59
598	49.57	21.8	49.74	47.73
613	49.45	21.8	49.74	47.62
628	49.31	22.0	49.94	47.29
633	49.29	21.9	49.84	47.37

Table T5. Formation factor measurements, Site U1370. (Continued on next eight pages.)

Core, section, interval (cm)	Depth (mbsf)	Measurement number	Temperature-corrected seawater conductivity (mS/cm)	Sediment temperature (°C)	Sediment electrical conductivity (mS/cm)	Correction factor at 20°C (mS/cm)	Sediment electrical conductivity at 20°C (mS/cm)	Drift-corrected sediment electrical conductivity at 20°C (mS/cm)	Formation factor
329-U1370D-									
1H-1, 10	0.10	2	49.43	21.50	34.10	49.43	33.04	33.04	1.50
1H-1, 20	0.20	3	49.43	21.50	33.60	49.43	32.56	32.56	1.52
1H-1, 30	0.30	4	49.43	21.50	33.01	49.43	31.99	31.99	1.55
1H-1, 40	0.40	5	49.43	21.40	33.64	49.32	32.66	32.66	1.51
1H-1, 50	0.50	6	49.43	21.40	31.33	49.32	30.42	30.42	1.63
1H-1, 60	0.60	7	49.43	21.40	31.52	49.32	30.61	30.61	1.62
1H-1, 70	0.70	8	49.43	21.40	34.94	49.32	33.93	33.93	1.46
1H-1, 80	0.80	11	49.43	21.40	33.50	49.32	32.53	32.53	1.52
1H-1, 90	0.90	12	49.43	21.40	33.25	49.32	32.29	32.29	1.53
1H-1, 100	1.00	13	49.43	21.40	32.57	49.32	31.62	31.62	1.56
1H-1, 110	1.10	14	49.43	21.40	32.51	49.32	31.57	31.57	1.57
1H-1, 120	1.20	15	49.43	21.50	29.73	49.43	28.81	28.81	1.72
1H-1, 130	1.30	16	49.43	21.40	32.63	49.32	31.68	31.68	1.56
1H-1, 140	1.40	17	49.43	21.40	33.20	49.32	32.24	32.24	1.53
1H-2, 10	1.62	19	49.43	21.10	33.84	49.02	33.06	33.06	1.50
1H-2, 20	1.72	20	49.43	21.10	34.37	49.02	33.58	33.58	1.47
1H-2, 30	1.82	21	49.43	21.10	34.61	49.02	33.82	33.82	1.46
1H-2, 40	1.92	22	49.43	21.10	35.28	49.02	34.47	34.47	1.43
1H-2, 50	2.02	23	49.43	21.10	34.88	49.02	34.08	34.08	1.45
1H-2, 60	2.12	24	49.43	21.10	34.83	49.02	34.03	34.03	1.45
1H-2, 70	2.22	25	49.43	21.10	34.06	49.02	33.28	33.28	1.49
1H-2, 80	2.32	26	49.43	21.10	34.25	49.02	33.46	33.46	1.48
1H-2, 90	2.42	28	49.43	21.10	34.67	49.02	33.88	33.88	1.46
1H-2, 100	2.52	29	49.43	21.10	34.10	49.02	33.32	33.32	1.48
1H-2, 110	2.62	30	49.43	21.10	33.13	49.02	32.37	32.37	1.53
1H-2, 120	2.72	31	49.43	21.10	34.00	49.02	33.22	33.22	1.49
1H-2, 130	2.82	32	49.43	21.20	33.29	49.12	32.46	32.46	1.52
1H-2, 140	2.92	33	49.43	21.20	33.36	49.12	32.53	32.53	1.52
1H-3, 10	3.12	35	49.43	21.20	30.14	49.12	29.39	29.39	1.68
1H-3, 20	3.22	36	49.43	21.20	33.52	49.12	32.68	32.68	1.51
1H-3, 30	3.32	37	49.43	21.20	32.68	49.12	31.86	31.86	1.55
1H-3, 40	3.42	38	49.43	21.20	32.88	49.12	32.06	32.06	1.54
1H-3, 50	3.52	39	49.43	21.30	32.59	49.22	31.71	31.71	1.56
1H-3, 60	3.62	40	49.43	21.30	32.80	49.22	31.91	31.91	1.55
1H-3, 70	3.72	41	49.43	21.30	32.73	49.22	31.85	31.85	1.55
1H-3, 80	3.82	42	49.43	21.30	31.87	49.22	31.01	31.01	1.59
1H-3, 90	3.92	44	49.43	21.10	32.08	49.02	31.34	31.34	1.58
1H-3, 100	4.02	45	49.43	21.10	32.74	49.02	31.99	31.99	1.55
1H-3, 110	4.12	46	49.43	21.10	33.22	49.02	32.46	32.46	1.52
1H-3, 120	4.22	47	49.43	21.10	32.28	49.02	31.54	31.54	1.57
1H-3, 130	4.32	48	49.43	21.10	31.76	49.02	31.03	31.03	1.59
1H-3, 140	4.42	49	49.43	21.10	32.07	49.02	31.33	31.34	1.58
1H-4, 10	4.62	53	49.43	21.50	31.75	49.43	30.76	30.76	1.61
1H-4, 20	4.72	54	49.43	21.50	32.10	49.43	31.10	31.10	1.59
1H-4, 30	4.82	55	49.43	21.50	30.53	49.43	29.58	29.58	1.67
1H-4, 40	4.92	56	49.43	21.50	31.44	49.43	30.46	30.46	1.62
1H-4, 50	5.02	57	49.43	21.50	32.79	49.43	31.77	31.77	1.56
1H-4, 60	5.12	58	49.43	21.50	31.65	49.43	30.67	30.67	1.61
1H-4, 70	5.22	59	49.43	21.50	31.69	49.43	30.71	30.71	1.61
1H-4, 80	5.32	60	49.43	21.50	30.95	49.43	29.99	29.99	1.65
1H-4, 90	5.42	62	49.43	21.20	33.86	49.12	33.01	33.02	1.50
1H-4, 100	5.52	63	49.43	21.20	32.03	49.12	31.23	31.23	1.58
1H-4, 110	5.62	64	49.43	21.20	28.16	49.12	27.46	27.46	1.80
1H-4, 120	5.72	65	49.43	21.10	33.20	49.02	32.44	32.44	1.52
1H-4, 130	5.82	66	49.43	21.10	32.60	49.02	31.85	31.85	1.55
1H-4, 140	5.92	67	49.43	21.10	33.48	49.02	32.71	32.71	1.51
1H-5, 10	6.12	69	49.43	21.20	31.54	49.12	30.75	30.75	1.61
1H-5, 20	6.22	70	49.43	21.20	30.97	49.12	30.20	30.20	1.64
1H-5, 30	6.32	71	49.43	21.20	30.07	49.12	29.32	29.32	1.69
1H-5, 40	6.42	72	49.43	21.20	30.80	49.12	30.03	30.03	1.65
1H-5, 50	6.52	73	49.43	21.20	31.04	49.12	30.27	30.27	1.63
1H-5, 60	6.62	74	49.43	21.20	30.30	49.12	29.54	29.54	1.67
1H-5, 70	6.72	75	49.43	21.20	30.43	49.12	29.67	29.67	1.67
1H-5, 80	6.82	76	49.43	21.20	31.07	49.12	30.29	30.29	1.63
1H-5, 90	6.92	78	49.43	21.20	31.17	49.12	30.39	30.39	1.63

Table T5 (continued). (Continued on next page.)

Core, section, interval (cm)	Depth (mbsf)	Measurement number	Temperature-corrected seawater conductivity (mS/cm)	Sediment temperature (°C)	Sediment electrical conductivity (mS/cm)	Correction factor at 20°C (mS/cm)	Sediment electrical conductivity at 20°C (mS/cm)	Drift-corrected sediment electrical conductivity at 20°C (mS/cm)	Formation factor
1H-5, 100	7.02	79	49.43	21.20	28.85	49.12	28.13	28.13	1.76
1H-5, 110	7.12	80	49.43	21.20	30.53	49.12	29.77	29.77	1.66
1H-5, 120	7.22	81	49.43	21.20	29.61	49.12	28.87	28.87	1.71
1H-5, 130	7.32	82	49.43	21.20	27.24	49.12	26.56	26.56	1.86
1H-5, 140	7.42	83	49.43	21.20	27.49	49.12	26.80	26.80	1.84
1H-6, 10	7.61	85	49.43	21.20	29.89	49.12	29.14	29.14	1.70
1H-6, 20	7.71	86	49.43	21.20	27.77	49.12	27.08	27.08	1.83
1H-6, 30	7.81	87	49.43	21.20	28.57	49.12	27.86	27.86	1.77
1H-6, 40	7.91	88	49.43	21.10	30.40	49.02	29.70	29.70	1.66
1H-6, 50	8.01	89	49.43	21.10	30.91	49.02	30.20	30.20	1.64
1H-6, 60	8.11	90	49.43	21.10	27.22	49.02	26.60	26.60	1.86
1H-6, 70	8.21	91	49.43	21.10	29.32	49.02	28.65	28.65	1.73
1H-6, 80	8.31	92	49.43	21.10	26.75	49.02	26.14	26.14	1.89
1H-6, 90	8.41	93	49.43	21.10	28.93	49.02	28.27	28.27	1.75
1H-6, 100	8.51	94	49.43	21.10	21.82	49.02	21.32	21.32	2.32
2H-1, 10	8.90	97	49.43	21.40	29.70	49.32	28.84	28.84	1.71
2H-1, 20	9.00	98	49.43	21.40	33.57	49.32	32.60	32.60	1.52
2H-1, 30	9.10	99	49.43	21.40	34.18	49.32	33.19	33.19	1.49
2H-1, 40	9.20	100	49.43	21.40	33.45	49.32	32.48	32.48	1.52
2H-1, 50	9.30	101	49.43	21.40	34.06	49.32	33.07	33.07	1.49
2H-2, 10	9.51	103	49.43	21.50	31.52	49.43	30.54	30.54	1.62
2H-2, 20	9.61	104	49.43	21.50	30.14	49.43	29.20	29.21	1.69
2H-2, 30	9.71	105	49.43	21.50	31.49	49.43	30.51	30.51	1.62
2H-2, 40	9.81	106	49.43	21.50	32.49	49.43	31.48	31.48	1.57
2H-2, 65	10.06	107	49.43	21.50	30.01	49.43	29.08	29.08	1.70
2H-2, 85	10.26	108	49.43	21.50	28.16	49.43	27.29	27.29	1.81
2H-2, 90	10.31	110	49.43	21.30	28.78	49.22	28.00	28.00	1.77
2H-2, 100	10.41	111	49.43	21.30	27.20	49.22	26.47	26.47	1.87
2H-2, 110	10.51	112	49.43	21.30	27.02	49.22	26.29	26.29	1.88
2H-2, 120	10.61	113	49.43	21.30	27.02	49.22	26.29	26.29	1.88
2H-2, 130	10.71	114	49.43	21.30	27.88	49.22	27.13	27.13	1.82
2H-2, 140	10.81	115	49.43	21.30	28.76	49.22	27.98	27.98	1.77
2H-3, 10	11.01	117	49.43	21.40	28.23	49.32	27.41	27.41	1.80
2H-3, 20	11.11	118	49.43	21.40	26.29	49.32	25.53	25.53	1.94
2H-3, 30	11.21	119	49.43	21.40	25.97	49.32	25.22	25.22	1.96
2H-3, 40	11.31	120	49.43	21.40	24.83	49.32	24.11	24.11	2.05
2H-3, 50	11.41	121	49.43	21.40	26.05	49.32	25.29	25.29	1.95
2H-3, 60	11.51	122	49.43	21.40	26.22	49.32	25.46	25.46	1.94
2H-3, 70	11.61	123	49.43	21.30	26.88	49.22	26.15	26.16	1.89
2H-3, 80	11.71	124	49.43	21.30	27.44	49.22	26.70	26.70	1.85
2H-3, 90	11.81	126	49.43	21.40	27.62	49.32	26.82	26.82	1.84
2H-3, 100	11.91	127	49.43	21.40	26.83	49.32	26.05	26.05	1.90
2H-3, 110	12.01	128	49.43	21.40	27.08	49.32	26.29	26.29	1.88
2H-3, 120	12.11	129	49.43	21.40	26.03	49.32	25.27	25.28	1.96
2H-3, 130	12.21	130	49.43	21.40	26.58	49.32	25.81	25.81	1.92
2H-3, 140	12.31	131	49.43	21.40	25.98	49.32	25.23	25.23	1.96
2H-4, 10	12.52	133	49.43	21.40	25.60	49.32	24.86	24.86	1.99
2H-4, 20	12.62	134	49.43	21.40	23.97	49.32	23.27	23.28	2.12
2H-4, 30	12.72	135	49.43	21.40	25.52	49.32	24.78	24.78	1.99
2H-4, 40	12.82	136	49.43	21.40	24.03	49.32	23.33	23.33	2.12
2H-4, 50	12.92	137	49.43	21.40	24.77	49.32	24.05	24.05	2.06
2H-4, 60	13.02	138	49.43	21.30	24.16	49.22	23.51	23.51	2.10
2H-4, 70	13.12	139	49.43	21.30	22.70	49.22	22.09	22.09	2.24
2H-4, 80	13.22	140	49.43	21.30	24.34	49.22	23.68	23.68	2.09
2H-4, 90	13.32	142	49.43	21.10	24.90	49.02	24.33	24.33	2.03
2H-4, 100	13.42	143	49.43	21.10	23.80	49.02	23.25	23.26	2.13
2H-4, 110	13.52	144	49.43	21.20	22.96	49.12	22.39	22.39	2.21
2H-4, 120	13.62	145	49.43	21.20	24.51	49.12	23.90	23.90	2.07
2H-4, 130	13.72	146	49.43	21.20	24.44	49.12	23.83	23.83	2.07
2H-4, 140	13.82	147	49.43	21.20	24.97	49.12	24.35	24.35	2.03
2H-5, 10	14.02	149	49.43	21.30	25.05	49.22	24.37	24.37	2.03
2H-5, 20	14.12	150	49.43	21.30	24.90	49.22	24.23	24.23	2.04
2H-5, 30	14.22	151	49.43	21.30	24.22	49.22	23.57	23.57	2.10
2H-5, 40	14.32	152	49.43	21.30	24.52	49.22	23.86	23.86	2.07
2H-5, 50	14.42	153	49.43	21.30	24.33	49.22	23.67	23.67	2.09
2H-5, 60	14.52	154	49.43	21.30	23.80	49.22	23.16	23.16	2.13
2H-5, 70	14.62	155	49.43	21.20	23.13	49.12	22.55	22.55	2.19

Table T5 (continued). (Continued on next page.)

Core, section, interval (cm)	Depth (mbsf)	Measurement number	Temperature-corrected seawater conductivity (mS/cm)	Sediment temperature (°C)	Sediment electrical conductivity (mS/cm)	Correction factor at 20°C (mS/cm)	Sediment electrical conductivity at 20°C (mS/cm)	Drift-corrected sediment electrical conductivity at 20°C (mS/cm)	Formation factor
2H-5, 80	14.72	157	49.43	21.10	22.90	49.02	22.37	22.38	2.21
2H-5, 90	14.82	158	49.43	21.10	23.87	49.02	23.32	23.32	2.12
2H-5, 100	14.92	159	49.43	21.10	23.76	49.02	23.22	23.22	2.13
2H-5, 110	15.02	160	49.43	21.10	23.92	49.02	23.37	23.37	2.11
2H-5, 120	15.12	161	49.43	21.10	23.26	49.02	22.73	22.73	2.17
2H-5, 130	15.22	162	49.43	21.10	21.34	49.02	20.85	20.85	2.37
2H-5, 140	15.32	163	49.43	21.10	23.80	49.02	23.25	23.26	2.13
2H-6, 10	15.52	165	49.43	20.80	23.68	48.71	23.28	23.28	2.12
2H-6, 20	15.62	166	49.43	20.80	24.05	48.71	23.65	23.65	2.09
2H-6, 30	15.72	167	49.43	20.80	21.82	48.71	21.45	21.46	2.30
2H-6, 40	15.82	168	49.43	20.80	23.39	48.71	23.00	23.00	2.15
2H-6, 50	15.92	169	49.43	20.80	23.05	48.71	22.66	22.66	2.18
2H-6, 60	16.02	170	49.43	20.80	22.92	48.71	22.54	22.54	2.19
2H-6, 70	16.12	171	49.43	20.80	22.19	48.71	21.82	21.82	2.27
2H-6, 80	16.22	173	49.43	21.00	23.50	48.91	23.01	23.01	2.15
2H-6, 90	16.32	174	49.43	21.00	22.35	48.91	21.88	21.88	2.26
2H-6, 100	16.42	175	49.43	21.00	23.30	48.91	22.81	22.81	2.17
2H-6, 110	16.52	176	49.43	21.00	23.02	48.91	22.54	22.54	2.19
2H-6, 120	16.62	177	49.43	21.00	23.07	48.91	22.59	22.59	2.19
2H-6, 130	16.72	178	49.43	21.00	22.24	48.91	21.78	21.78	2.27
2H-6, 140	16.82	179	49.43	21.00	21.68	48.91	21.23	21.23	2.33
2H-7, 10	17.01	181	49.43	20.50	23.99	48.40	23.74	23.74	2.08
2H-7, 20	17.11	182	49.43	20.50	24.20	48.40	23.95	23.95	2.06
2H-7, 30	17.21	183	49.43	20.50	22.07	48.40	21.84	21.84	2.26
2H-7, 80	17.71	184	49.43	20.50	23.91	48.40	23.66	23.66	2.09
2H-7, 102	17.93	185	49.43	20.50	23.56	48.40	23.31	23.31	2.12
2H-7, 110	18.01	186	49.43	20.50	22.63	48.40	22.39	22.39	2.21
2H-7, 120	18.11	187	49.43	20.50	21.80	48.40	21.57	21.57	2.29
3H-3, 105	22.17	191	49.43	20.90	31.33	48.81	30.74	30.74	1.61
3H-3, 110	22.22	192	49.43	20.90	31.15	48.81	30.56	30.56	1.62
3H-3, 120	22.32	193	49.43	20.80	31.04	48.71	30.52	30.52	1.62
3H-3, 130	22.42	194	49.43	20.80	29.83	48.71	29.33	29.33	1.69
3H-3, 140	22.52	195	49.43	20.80	29.30	48.71	28.81	28.81	1.72
3H-4, 10	22.73	197	49.43	21.10	28.03	49.02	27.39	27.39	1.80
3H-4, 20	22.83	198	49.43	21.10	27.20	49.02	26.58	26.58	1.86
3H-4, 30	22.93	199	49.43	21.10	27.36	49.02	26.73	26.73	1.85
3H-4, 40	23.03	200	49.43	21.10	26.97	49.02	26.35	26.35	1.88
3H-4, 50	23.13	201	49.43	21.10	26.82	49.02	26.21	26.21	1.89
3H-4, 60	23.23	202	49.43	21.10	27.16	49.02	26.54	26.54	1.86
3H-4, 70	23.33	203	49.43	21.10	26.92	49.02	26.30	26.30	1.88
3H-4, 80	23.43	205	49.43	20.80	27.77	48.71	27.30	27.31	1.81
3H-4, 90	23.53	206	49.43	20.80	27.73	48.71	27.27	27.27	1.81
3H-4, 102	23.65	207	49.43	20.80	27.92	48.71	27.45	27.45	1.80
3H-4, 111	23.74	208	49.43	20.80	27.75	48.71	27.28	27.29	1.81
3H-4, 120	23.83	209	49.43	20.80	27.61	48.71	27.15	27.15	1.82
3H-4, 130	23.93	210	49.43	20.80	27.75	48.71	27.28	27.29	1.81
3H-4, 140	24.03	211	49.43	20.80	27.71	48.71	27.25	27.25	1.81
3H-5, 5	24.16	213	49.43	20.70	27.37	48.61	26.97	26.97	1.83
3H-5, 17	24.28	214	49.43	20.70	27.67	48.61	27.26	27.26	1.81
3H-5, 28	24.39	215	49.43	20.70	27.55	48.61	27.15	27.15	1.82
3H-5, 39	24.50	216	49.43	20.70	27.04	48.61	26.64	26.64	1.86
3H-5, 50	24.61	217	49.43	20.60	27.10	48.51	26.76	26.76	1.85
3H-5, 60	24.71	218	49.43	20.60	27.57	48.51	27.22	27.22	1.82
3H-5, 70	24.81	219	49.43	20.60	27.64	48.51	27.29	27.29	1.81
4H-1, 10	25.10	222	49.43	21.20	28.15	49.12	27.45	27.45	1.80
4H-1, 20	25.20	223	49.43	21.20	26.50	49.12	25.84	25.84	1.91
4H-1, 30	25.30	224	49.43	21.20	26.05	49.12	25.40	25.40	1.95
4H-1, 40	25.40	225	49.43	21.20	26.74	49.12	26.07	26.07	1.90
4H-1, 50	25.50	226	49.43	21.20	26.36	49.12	25.70	25.70	1.92
4H-1, 60	25.60	227	49.43	21.20	25.22	49.12	24.59	24.59	2.01
4H-1, 70	25.70	228	49.43	21.20	25.70	49.12	25.06	25.06	1.97
4H-1, 80	25.80	230	49.43	21.30	25.43	49.22	24.74	24.74	2.00
4H-1, 90	25.90	231	49.43	21.30	26.87	49.22	26.14	26.15	1.89
4H-1, 100	26.00	232	49.43	21.30	26.65	49.22	25.93	25.93	1.91
4H-1, 110	26.10	233	49.43	21.30	24.88	49.22	24.21	24.21	2.04
4H-1, 120	26.20	234	49.43	21.30	25.58	49.22	24.89	24.89	1.99
4H-1, 130	26.30	235	49.43	21.30	26.64	49.22	25.92	25.92	1.91

Table T5 (continued). (Continued on next page.)

Core, section, interval (cm)	Depth (mbsf)	Measurement number	Temperature-corrected seawater conductivity (mS/cm)	Sediment temperature (°C)	Sediment electrical conductivity (mS/cm)	Correction factor at 20°C (mS/cm)	Sediment electrical conductivity at 20°C (mS/cm)	Drift-corrected sediment electrical conductivity at 20°C (mS/cm)	Formation factor
4H-1, 140	26.40	236	49.43	21.30	26.83	49.22	26.11	26.11	1.89
4H-2, 10	26.61	238	49.43	21.20	25.97	49.12	25.32	25.32	1.95
4H-2, 20	26.71	239	49.43	21.20	26.62	49.12	25.96	25.96	1.90
4H-2, 30	26.81	240	49.43	21.20	26.23	49.12	25.58	25.58	1.93
4H-2, 40	26.91	241	49.43	21.20	26.25	49.12	25.59	25.60	1.93
4H-2, 50	27.01	242	49.43	21.10	26.52	49.02	25.91	25.91	1.91
4H-2, 60	27.11	243	49.43	21.10	26.50	49.02	25.89	25.89	1.91
4H-2, 70	27.21	244	49.43	21.10	24.57	49.02	24.01	24.01	2.06
4H-2, 80	27.31	245	49.43	21.10	25.93	49.02	25.34	25.34	1.95
4H-2, 88	27.39	247	49.43	21.00	26.68	48.91	26.12	26.12	1.89
4H-2, 99	27.50	248	49.43	21.00	26.67	48.91	26.11	26.11	1.89
4H-2, 110	27.61	249	49.43	21.00	25.49	48.91	24.96	24.96	1.98
4H-2, 120	27.71	250	49.43	21.00	25.47	48.91	24.94	24.94	1.98
4H-2, 130	27.81	251	49.43	21.00	25.96	48.91	25.42	25.42	1.94
4H-2, 140	27.91	252	49.43	21.00	25.47	48.91	24.94	24.94	1.98
4H-2, 145	27.96	253	49.43	21.00	24.78	48.91	24.26	24.26	2.04
4H-3, 10	28.11	255	49.43	21.00	25.65	48.91	25.11	25.12	1.97
4H-3, 20	28.21	256	49.43	21.00	24.74	48.91	24.22	24.22	2.04
4H-3, 30	28.31	257	49.43	21.00	24.94	48.91	24.42	24.42	2.02
4H-3, 40	28.41	258	49.43	21.00	24.63	48.91	24.12	24.12	2.05
4H-3, 50	28.51	260	49.43	21.00	25.14	48.91	24.62	24.62	2.01
4H-3, 60	28.61	261	49.43	21.00	25.10	48.91	24.58	24.58	2.01
4H-3, 70	28.71	262	49.43	21.00	24.67	48.91	24.15	24.16	2.05
4H-3, 80	28.81	263	49.43	21.00	24.70	48.91	24.18	24.19	2.04
4H-3, 90	28.91	264	49.43	21.00	23.85	48.91	23.35	23.35	2.12
4H-3, 100	29.01	265	49.43	21.00	24.86	48.91	24.34	24.34	2.03
4H-3, 110	29.11	267	49.43	20.90	25.37	48.81	24.89	24.89	1.99
4H-3, 120	29.21	268	49.43	20.90	23.61	48.81	23.17	23.17	2.13
4H-3, 130	29.31	269	49.43	20.90	24.83	48.81	24.36	24.36	2.03
4H-3, 140	29.41	270	49.43	20.80	25.18	48.71	24.76	24.76	2.00
4H-3, 148	29.49	271	49.43	20.80	25.14	48.71	24.72	24.72	2.00
4H-4, 10	29.61	272	49.43	20.80	24.61	48.71	24.20	24.20	2.04
4H-4, 20	29.71	273	49.43	20.80	24.12	48.71	23.72	23.72	2.08
4H-4, 30	29.81	274	49.43	20.80	23.55	48.71	23.16	23.16	2.13
4H-4, 40	29.91	275	49.43	20.80	24.37	48.71	23.96	23.96	2.06
4H-4, 50	30.01	276	49.43	20.80	24.74	48.71	24.33	24.33	2.03
4H-4, 60	30.11	278	49.43	20.70	25.15	48.61	24.78	24.78	1.99
4H-4, 70	30.21	279	49.43	20.70	24.82	48.61	24.46	24.46	2.02
4H-4, 80	30.31	280	49.43	20.70	25.02	48.61	24.65	24.65	2.00
4H-4, 90	30.41	281	49.43	20.70	23.44	48.61	23.10	23.10	2.14
4H-4, 98	30.49	282	49.43	20.70	23.98	48.61	23.63	23.63	2.09
4H-5, 10	30.60	283	49.43	20.70	24.47	48.61	24.11	24.11	2.05
4H-5, 20	30.70	284	49.43	20.70	23.71	48.61	23.36	23.36	2.12
4H-5, 30	30.80	285	49.43	20.70	23.82	48.61	23.47	23.47	2.11
4H-5, 40	30.90	286	49.43	20.70	23.42	48.61	23.08	23.08	2.14
4H-5, 50	31.00	287	49.43	20.70	23.92	48.61	23.57	23.57	2.10
4H-5, 60	31.10	288	49.43	20.70	23.48	48.61	23.13	23.14	2.14
4H-5, 70	31.20	289	49.43	20.70	23.15	48.61	22.81	22.81	2.17
5H-1, 70	35.20	293	49.43	21.30	24.38	49.22	23.72	23.72	2.08
5H-1, 80	35.30	294	49.43	21.30	23.68	49.22	23.04	23.04	2.15
5H-1, 90	35.40	295	49.43	21.30	23.65	49.22	23.01	23.01	2.15
5H-1, 100	35.50	296	49.43	21.30	23.97	49.22	23.32	23.32	2.12
5H-1, 110	35.60	297	49.43	21.30	23.78	49.22	23.14	23.14	2.14
5H-1, 120	35.70	298	49.43	21.30	24.07	49.22	23.42	23.42	2.11
5H-1, 130	35.80	299	49.43	21.30	23.88	49.22	23.24	23.24	2.13
5H-1, 140	35.90	300	49.43	21.30	23.84	49.22	23.20	23.20	2.13
5H-1, 147	35.97	301	49.43	21.30	23.46	49.22	22.83	22.83	2.17
5H-2, 10	36.10	303	49.43	21.30	23.21	49.22	22.58	22.59	2.19
5H-2, 20	36.20	304	49.43	21.30	22.72	49.22	22.11	22.11	2.24
5H-2, 30	36.30	305	49.43	21.30	23.11	49.22	22.49	22.49	2.20
5H-2, 40	36.40	306	49.43	21.30	23.49	49.22	22.86	22.86	2.16
5H-2, 50	36.50	307	49.43	21.30	23.55	49.22	22.91	22.92	2.16
5H-2, 60	36.60	308	49.43	21.30	23.61	49.22	22.97	22.97	2.15
5H-2, 70	36.70	309	49.43	21.30	23.44	49.22	22.81	22.81	2.17
5H-2, 80	36.80	310	49.43	21.30	23.15	49.22	22.53	22.53	2.19
5H-2, 90	36.90	312	49.43	21.20	23.66	49.12	23.07	23.07	2.14
5H-2, 100	37.00	313	49.43	21.20	23.44	49.12	22.85	22.86	2.16

Table T5 (continued). (Continued on next page.)

Core, section, interval (cm)	Depth (mbsf)	Measurement number	Temperature-corrected seawater conductivity (mS/cm)	Sediment temperature (°C)	Sediment electrical conductivity (mS/cm)	Correction factor at 20°C (mS/cm)	Sediment electrical conductivity at 20°C (mS/cm)	Drift-corrected sediment electrical conductivity at 20°C (mS/cm)	Formation factor
5H-2, 110	37.10	314	49.43	21.20	23.72	49.12	23.13	23.13	2.14
5H-2, 120	37.20	315	49.43	21.20	23.13	49.12	22.55	22.55	2.19
5H-2, 130	37.30	316	49.43	21.20	23.38	49.12	22.80	22.80	2.17
5H-2, 140	37.40	317	49.43	21.20	23.55	49.12	22.96	22.96	2.15
5H-2, 148	37.48	318	49.43	21.20	23.33	49.12	22.75	22.75	2.17
5H-3, 10	37.62	320	49.43	21.10	23.21	49.02	22.68	22.68	2.18
5H-3, 20	37.72	321	49.43	21.10	23.60	49.02	23.06	23.06	2.14
5H-3, 30	37.82	322	49.43	21.10	23.61	49.02	23.07	23.07	2.14
5H-3, 40	37.92	323	49.43	21.10	23.41	49.02	22.87	22.88	2.16
5H-3, 50	38.02	324	49.43	21.10	22.44	49.02	21.93	21.93	2.25
5H-3, 60	38.12	325	49.43	21.10	22.81	49.02	22.29	22.29	2.22
5H-3, 70	38.22	326	49.43	21.10	23.02	49.02	22.49	22.49	2.20
5H-3, 80	38.32	328	49.43	20.90	22.43	48.81	22.01	22.01	2.25
5H-3, 90	38.42	329	49.43	20.90	23.00	48.81	22.57	22.57	2.19
5H-3, 100	38.52	330	49.43	20.90	23.91	48.81	23.46	23.46	2.11
5H-3, 110	38.62	331	49.43	20.90	23.72	48.81	23.27	23.28	2.12
5H-3, 120	38.72	332	49.43	20.90	23.41	48.81	22.97	22.97	2.15
5H-3, 130	38.82	333	49.43	20.90	23.48	48.81	23.04	23.04	2.15
5H-3, 140	38.92	334	49.43	20.90	23.67	48.81	23.22	23.23	2.13
5H-3, 148	39.00	335	49.43	20.90	23.27	48.81	22.83	22.83	2.16
5H-4, 10	39.11	337	49.43	20.90	23.24	48.81	22.80	22.80	2.17
5H-4, 20	39.21	338	49.43	20.90	23.38	48.81	22.94	22.94	2.15
5H-4, 30	39.31	339	49.43	20.90	23.10	48.81	22.67	22.67	2.18
5H-4, 40	39.41	340	49.43	20.90	23.26	48.81	22.82	22.82	2.17
5H-4, 50	39.51	341	49.43	20.90	23.11	48.81	22.67	22.68	2.18
5H-4, 60	39.61	342	49.43	20.90	22.87	48.81	22.44	22.44	2.20
5H-4, 70	39.71	343	49.43	20.90	23.34	48.81	22.90	22.90	2.16
5H-4, 80	39.81	344	49.43	20.90	23.21	48.81	22.77	22.77	2.17
5H-4, 90	39.91	346	49.43	20.90	22.88	48.81	22.45	22.45	2.20
5H-4, 100	40.01	347	49.43	20.90	22.66	48.81	22.23	22.24	2.22
5H-4, 110	40.11	348	49.43	20.90	23.18	48.81	22.74	22.75	2.17
5H-4, 120	40.21	349	49.43	20.90	22.91	48.81	22.48	22.48	2.20
5H-4, 130	40.31	350	49.43	20.90	22.38	48.81	21.96	21.96	2.25
5H-4, 140	40.41	351	49.43	20.90	22.77	48.81	22.34	22.34	2.21
5H-5, 10	40.61	353	49.43	20.90	22.76	48.81	22.33	22.33	2.21
5H-5, 20	40.71	354	49.43	20.90	22.75	48.81	22.32	22.32	2.21
5H-5, 30	40.81	355	49.43	20.90	22.63	48.81	22.20	22.21	2.23
5H-5, 40	40.91	356	49.43	20.90	22.54	48.81	22.12	22.12	2.23
5H-5, 50	41.01	357	49.43	20.90	22.76	48.81	22.33	22.33	2.21
5H-5, 60	41.11	358	49.43	20.90	22.31	48.81	21.89	21.89	2.26
5H-5, 70	41.21	359	49.43	20.90	22.46	48.81	22.04	22.04	2.24
5H-5, 80	41.31	361	49.43	20.90	23.04	48.81	22.61	22.61	2.19
5H-5, 90	41.41	362	49.43	20.90	22.98	48.81	22.55	22.55	2.19
5H-5, 100	41.51	363	49.43	20.90	22.30	48.81	21.88	21.88	2.26
5H-5, 110	41.61	364	49.43	20.90	22.46	48.81	22.04	22.04	2.24
5H-5, 120	41.71	365	49.43	20.90	22.19	48.81	21.77	21.77	2.27
5H-5, 130	41.81	366	49.43	20.90	22.62	48.81	22.19	22.20	2.23
5H-5, 140	41.91	367	49.43	20.90	21.77	48.81	21.36	21.36	2.31
5H-6, 10	42.07	369	49.43	20.90	22.36	48.81	21.94	21.94	2.25
5H-6, 20	42.17	370	49.43	20.90	22.65	48.81	22.22	22.23	2.22
5H-6, 30	42.27	371	49.43	20.90	22.50	48.81	22.08	22.08	2.24
5H-6, 40	42.37	372	49.43	20.90	22.56	48.81	22.14	22.14	2.23
5H-6, 50	42.47	373	49.43	20.90	22.66	48.81	22.23	22.24	2.22
5H-6, 60	42.57	374	49.43	20.90	21.91	48.81	21.50	21.50	2.30
5H-6, 70	42.67	375	49.43	20.90	21.99	48.81	21.58	21.58	2.29
5H-6, 80	42.77	376	49.43	20.90	22.17	48.81	21.75	21.75	2.27
5H-6, 90	42.87	377	49.43	20.90	21.77	48.81	21.36	21.36	2.31
5H-6, 100	42.97	378	49.43	20.90	22.35	48.81	21.93	21.93	2.25
5H-6, 110	43.07	379	49.43	20.90	22.57	48.81	22.15	22.15	2.23
6H-1, 10	44.10	382	49.43	21.80	27.16	49.74	26.15	26.16	1.89
6H-1, 20	44.20	383	49.43	21.80	27.14	49.74	26.13	26.14	1.89
6H-1, 30	44.30	384	49.43	21.80	27.65	49.74	26.63	26.63	1.86
6H-1, 40	44.40	385	49.43	21.70	27.96	49.63	26.98	26.98	1.83
6H-1, 50	44.50	386	49.43	21.70	27.33	49.63	26.37	26.37	1.87
6H-1, 60	44.60	387	49.43	21.70	25.56	49.63	24.66	24.67	2.00
6H-1, 80	44.80	388	49.43	21.50	26.47	49.43	25.65	25.65	1.93
6H-1, 94	44.94	389	49.43	21.50	23.05	49.43	22.33	22.34	2.21

Table T5 (continued). (Continued on next page.)

Core, section, interval (cm)	Depth (mbsf)	Measurement number	Temperature-corrected seawater conductivity (mS/cm)	Sediment temperature (°C)	Sediment electrical conductivity (mS/cm)	Correction factor at 20°C (mS/cm)	Sediment electrical conductivity at 20°C (mS/cm)	Drift-corrected sediment electrical conductivity at 20°C (mS/cm)	Formation factor
6H-1, 100	45.00	390	49.43	21.50	22.42	49.43	21.72	21.73	2.28
6H-1, 110	45.10	391	49.43	21.50	21.77	49.43	21.09	21.10	2.34
6H-1, 120	45.20	392	49.43	21.50	22.24	49.43	21.55	21.55	2.29
6H-1, 130	45.30	393	49.43	21.40	21.99	49.32	21.35	21.35	2.31
6H-1, 140	45.40	394	49.43	21.40	21.62	49.32	20.99	20.99	2.35
6H-2, 10	45.62	396	49.43	21.40	22.26	49.32	21.61	21.62	2.29
6H-2, 20	45.72	397	49.43	21.40	21.87	49.32	21.24	21.24	2.33
6H-2, 30	45.82	398	49.43	21.40	21.53	49.32	20.91	20.91	2.36
6H-2, 40	45.92	399	49.43	21.40	21.69	49.32	21.06	21.06	2.35
6H-2, 50	46.02	400	49.35	21.40	20.20	49.32	19.61	21.02	2.35
6H-2, 60	46.12	401	49.34	21.40	20.78	49.32	20.18	21.63	2.28
6H-2, 70	46.22	402	49.33	21.40	20.80	49.32	20.20	21.65	2.28
6H-2, 80	46.32	403	49.32	21.10	21.47	49.02	20.98	22.49	2.19
6H-2, 90	46.42	404	49.31	21.10	21.60	49.02	21.10	22.63	2.18
6H-2, 100	46.52	405	49.30	21.10	21.24	49.02	20.75	22.26	2.21
6H-2, 110	46.62	406	49.29	21.10	21.07	49.02	20.59	22.09	2.23
6H-2, 120	46.72	407	49.29	21.10	20.34	49.02	19.87	21.32	2.31
6H-2, 130	46.82	408	49.28	21.10	20.40	49.02	19.93	21.39	2.30
6H-2, 140	46.92	409	49.27	21.10	20.10	49.02	19.64	21.08	2.34
6H-3, 10	47.10	411	49.25	21.10	22.42	49.02	21.91	23.52	2.09
6H-3, 20	47.20	412	49.24	21.10	22.33	49.02	21.82	23.43	2.10
6H-3, 30	47.30	413	49.23	21.10	21.80	49.02	21.30	22.88	2.15
6H-3, 40	47.40	414	49.22	21.10	21.49	49.02	21.00	22.56	2.18
6H-3, 50	47.50	415	49.21	21.10	21.11	49.02	20.63	22.16	2.22
6H-3, 60	47.60	416	49.20	21.10	20.88	49.02	20.40	21.92	2.24
6H-3, 70	47.70	417	49.19	21.10	20.88	49.02	20.40	21.93	2.24
6H-3, 80	47.80	418	49.18	20.80	20.48	48.71	20.14	21.65	2.27
6H-3, 90	47.90	419	49.17	20.80	20.60	48.71	20.25	21.78	2.26
6H-3, 100	48.00	420	49.16	20.80	20.49	48.71	20.15	21.66	2.27
6H-3, 110	48.10	421	49.15	20.80	20.47	48.71	20.13	21.65	2.27
6H-3, 120	48.20	422	49.14	20.80	19.91	48.71	19.58	21.06	2.33
6H-3, 130	48.30	423	49.13	20.80	19.65	48.71	19.32	20.79	2.36
6H-3, 140	48.40	424	49.12	20.80	19.98	48.71	19.65	21.14	2.32
6H-4, 10	48.62	426	49.10	21.10	21.08	49.02	20.60	22.17	2.21
6H-4, 20	48.72	427	49.09	21.10	20.37	49.02	19.90	21.43	2.29
6H-4, 30	48.82	428	49.08	21.00	20.40	48.91	19.97	21.51	2.28
6H-4, 40	48.92	429	49.08	21.00	20.23	48.91	19.81	21.33	2.30
6H-4, 50	49.02	430	49.07	21.00	20.50	48.91	20.07	21.62	2.27
6H-4, 60	49.12	431	49.06	21.00	20.19	48.91	19.77	21.30	2.30
6H-4, 70	49.22	432	49.05	21.00	20.43	48.91	20.00	21.55	2.28
6H-4, 80	49.32	433	49.04	20.70	19.97	48.61	19.68	21.20	2.31
6H-4, 90	49.42	434	49.03	20.70	19.36	48.61	19.08	20.56	2.38
6H-4, 100	49.52	435	49.02	20.70	20.07	48.61	19.78	21.32	2.30
6H-4, 110	49.62	436	49.01	20.70	20.07	48.61	19.78	21.32	2.30
6H-4, 120	49.72	437	49.00	20.70	20.13	48.61	19.83	21.39	2.29
6H-4, 130	49.82	438	48.99	20.70	20.38	48.61	20.08	21.66	2.26
6H-4, 140	49.92	439	48.98	20.70	20.10	48.61	19.80	21.36	2.29
6H-5, 10	50.12	441	48.96	20.90	20.47	48.81	20.08	21.67	2.26
6H-5, 20	50.22	442	48.95	20.90	19.69	48.81	19.32	20.85	2.35
6H-5, 30	50.32	443	48.94	20.90	20.22	48.81	19.84	21.42	2.29
6H-5, 40	50.42	444	48.93	20.80	19.99	48.71	19.65	21.22	2.31
6H-5, 50	50.52	445	48.92	20.80	20.49	48.71	20.15	21.75	2.25
6H-5, 60	50.62	446	48.91	20.80	19.97	48.71	19.64	21.21	2.31
6H-5, 70	50.72	447	48.90	20.80	19.37	48.71	19.05	20.57	2.38
6H-5, 80	50.82	448	48.89	20.60	20.00	48.51	19.75	21.33	2.29
6H-5, 90	50.92	449	48.88	20.60	20.36	48.51	20.10	21.72	2.25
6H-5, 100	51.02	450	48.87	20.60	19.50	48.51	19.25	20.81	2.35
6H-5, 110	51.12	451	48.87	20.60	19.99	48.51	19.74	21.33	2.29
6H-5, 120	51.22	452	48.86	20.50	20.31	48.40	20.10	21.73	2.25
6H-5, 130	51.32	453	48.85	20.50	19.26	48.40	19.06	20.61	2.37
6H-5, 140	51.42	454	48.84	20.50	19.63	48.40	19.42	21.01	2.32
6H-6, 10	51.62	456	48.82	20.90	19.73	48.81	19.36	20.94	2.33
6H-6, 20	51.72	457	48.81	20.80	20.19	48.71	19.85	21.48	2.27
6H-6, 30	51.82	458	48.80	20.80	19.60	48.71	19.27	20.85	2.34
6H-6, 40	51.92	459	48.79	20.80	20.00	48.71	19.66	21.28	2.29
6H-6, 50	52.02	460	48.78	20.80	19.82	48.71	19.49	21.10	2.31
6H-6, 60	52.12	461	48.77	20.90	20.31	48.81	19.93	21.58	2.26

Table T5 (continued). (Continued on next page.)

Core, section, interval (cm)	Depth (mbsf)	Measurement number	Temperature-corrected seawater conductivity (mS/cm)	Sediment temperature (°C)	Sediment electrical conductivity (mS/cm)	Correction factor at 20°C (mS/cm)	Sediment electrical conductivity at 20°C (mS/cm)	Drift-corrected sediment electrical conductivity at 20°C (mS/cm)	Formation factor
6H-6, 70	52.22	462	48.76	20.90	20.46	48.81	20.07	21.74	2.24
6H-6, 80	52.32	463	48.75	20.60	19.76	48.51	19.51	21.13	2.31
6H-6, 90	52.42	464	48.74	20.60	19.67	48.51	19.42	21.04	2.32
6H-6, 100	52.52	465	48.73	20.60	20.13	48.51	19.88	21.53	2.26
6H-6, 110	52.62	466	48.72	20.60	20.03	48.51	19.78	21.43	2.27
6H-6, 120	52.72	467	48.71	20.60	19.88	48.51	19.63	21.27	2.29
6H-6, 130	52.82	468	48.70	20.60	20.10	48.51	19.85	21.51	2.26
6H-6, 140	52.92	469	48.69	20.60	20.34	48.51	20.08	21.77	2.24
6H-7, 10	53.10	471	48.67	20.90	20.40	48.81	20.02	21.71	2.24
6H-7, 20	53.20	472	48.67	20.90	19.92	48.81	19.54	21.20	2.30
6H-7, 30	53.30	473	48.66	20.90	19.24	48.81	18.88	20.48	2.38
6H-7, 40	53.40	474	48.65	20.90	20.12	48.81	19.74	21.42	2.27
6H-7, 55	53.55	475	48.64	20.90	19.03	48.81	18.67	20.26	2.40
6H-7, 61	53.61	476	48.63	20.90	19.67	48.81	19.30	20.95	2.32
7H-1, 10	53.60	479	48.60	21.90	25.78	49.84	24.77	26.90	1.81
7H-1, 20	53.70	480	48.59	21.90	25.61	49.84	24.61	26.73	1.82
7H-1, 30	53.80	481	48.58	21.90	26.29	49.84	25.26	27.44	1.77
7H-1, 40	53.90	482	48.57	21.90	20.52	49.84	19.72	21.42	2.27
7H-1, 50	54.00	483	48.56	21.90	19.42	49.84	18.66	20.28	2.39
7H-1, 60	54.10	484	48.55	21.80	19.07	49.74	18.36	19.96	2.43
7H-1, 70	54.20	485	48.54	21.80	18.67	49.74	17.98	19.54	2.48
7H-1, 80	54.30	486	48.53	21.80	18.82	49.74	18.12	19.70	2.46
7H-1, 90	54.40	487	48.52	21.80	18.31	49.74	17.63	19.17	2.53
7H-1, 100	54.50	488	48.51	21.80	17.63	49.74	16.98	18.46	2.63
7H-1, 110	54.60	489	48.50	21.80	18.29	49.74	17.61	19.16	2.53
7H-1, 120	54.70	490	48.49	21.80	18.05	49.74	17.38	18.91	2.56
7H-1, 130	54.80	491	48.48	21.80	18.06	49.74	17.39	18.92	2.56
7H-1, 140	54.90	492	48.47	21.80	17.97	49.74	17.30	18.83	2.57
7H-2, 10	55.10	494	48.46	21.40	18.47	49.32	17.93	19.52	2.48
7H-2, 20	55.20	495	48.45	21.40	18.44	49.32	17.90	19.49	2.49
7H-2, 30	55.30	496	48.44	21.40	18.46	49.32	17.92	19.52	2.48
7H-2, 40	55.40	497	48.43	21.40	18.00	49.32	17.48	19.04	2.54
7H-2, 50	55.50	498	48.42	21.40	18.21	49.32	17.68	19.26	2.51
7H-2, 60	55.60	499	48.41	21.40	18.22	49.32	17.69	19.27	2.51
7H-2, 70	55.70	500	48.40	21.40	17.93	49.32	17.41	18.97	2.55
7H-2, 80	55.80	501	48.39	21.40	17.58	49.32	17.07	18.60	2.60
7H-2, 90	55.90	502	48.38	21.40	17.70	49.32	17.19	18.73	2.58
7H-2, 100	56.00	503	48.37	21.40	17.76	49.32	17.24	18.80	2.57
7H-2, 110	56.10	504	48.36	21.40	17.63	49.32	17.12	18.67	2.59
7H-2, 120	56.20	505	48.35	21.40	17.78	49.32	17.26	18.83	2.57
7H-2, 130	56.30	506	48.34	21.30	17.30	49.22	16.83	18.36	2.63
7H-2, 140	56.40	507	48.33	21.30	17.31	49.22	16.84	18.37	2.63
7H-3, 10	56.63	509	48.31	21.10	17.27	49.02	16.87	18.41	2.62
7H-3, 20	56.73	510	48.30	21.10	17.24	49.02	16.84	18.39	2.63
7H-3, 30	56.83	511	48.29	21.10	17.05	49.02	16.66	18.19	2.66
7H-3, 40	56.93	512	48.28	21.10	17.32	49.02	16.92	18.48	2.61
7H-3, 50	57.03	513	48.27	21.10	17.31	49.02	16.91	18.47	2.61
7H-3, 60	57.13	514	48.26	21.10	16.85	49.02	16.46	17.98	2.68
7H-3, 70	57.23	515	48.25	21.10	16.86	49.02	16.47	18.00	2.68
7H-3, 80	57.33	516	48.25	21.10	16.85	49.02	16.46	17.99	2.68
7H-3, 90	57.43	517	48.24	21.10	17.12	49.02	16.73	18.28	2.64
7H-3, 100	57.53	518	48.23	21.10	17.56	49.02	17.16	18.75	2.57
7H-3, 110	57.63	519	48.22	21.10	18.26	49.02	17.84	19.50	2.47
7H-3, 120	57.73	520	48.21	21.10	18.52	49.02	18.10	19.78	2.44
7H-3, 130	57.83	521	48.20	21.10	19.47	49.02	19.02	20.80	2.32
7H-3, 140	57.93	522	48.19	21.10	19.78	49.02	19.33	21.14	2.28
7H-4, 10	58.12	524	48.17	21.20	17.12	49.12	16.69	18.26	2.64
7H-4, 20	58.22	525	48.16	21.20	16.05	49.12	15.65	17.12	2.81
7H-4, 30	58.32	526	48.15	21.20	15.89	49.12	15.49	16.96	2.84
7H-4, 40	58.42	527	48.14	21.20	16.00	49.12	15.60	17.08	2.82
7H-4, 50	58.52	528	48.13	21.20	15.82	49.12	15.43	16.89	2.85
7H-4, 60	58.62	529	48.12	21.20	15.80	49.12	15.41	16.87	2.85
7H-4, 70	58.72	530	48.11	21.20	15.15	49.12	14.77	16.18	2.97
7H-4, 80	58.82	531	48.10	21.20	15.01	49.12	14.64	16.03	3.00
7H-4, 90	58.92	532	48.09	21.20	16.10	49.12	15.70	17.20	2.80
7H-4, 100	59.02	533	48.08	21.20	15.05	49.12	14.67	16.08	2.99
7H-4, 110	59.12	534	48.07	21.20	15.00	49.12	14.63	16.03	3.00

Table T5 (continued). (Continued on next page.)

Core, section, interval (cm)	Depth (mbsf)	Measurement number	Temperature-corrected seawater conductivity (mS/cm)	Sediment temperature (°C)	Sediment electrical conductivity (mS/cm)	Correction factor at 20°C (mS/cm)	Sediment electrical conductivity at 20°C (mS/cm)	Drift-corrected sediment electrical conductivity at 20°C (mS/cm)	Formation factor
7H-4, 120	59.22	535	48.06	21.20	14.53	49.12	14.17	15.53	3.10
7H-4, 130	59.32	536	48.05	21.20	14.53	49.12	14.17	15.53	3.09
7H-4, 140	59.42	537	48.05	21.20	15.01	49.12	14.64	16.05	2.99
7H-5, 10	59.63	539	48.03	20.90	15.47	48.81	15.18	16.65	2.89
7H-5, 20	59.73	540	48.02	21.10	15.88	49.02	15.52	17.02	2.82
7H-5, 30	59.83	541	48.01	21.10	15.71	49.02	15.35	16.84	2.85
7H-5, 40	59.93	542	48.00	21.10	15.83	49.02	15.47	16.97	2.83
7H-5, 50	60.03	543	47.99	21.10	16.13	49.02	15.76	17.30	2.77
7H-5, 60	60.13	544	47.98	21.10	16.35	49.02	15.98	17.53	2.74
7H-5, 70	60.23	545	47.97	21.10	17.16	49.02	16.77	18.41	2.61
7H-5, 80	60.33	546	47.96	21.10	16.64	49.02	16.26	17.85	2.69
7H-5, 90	60.43	547	47.95	21.10	16.71	49.02	16.33	17.93	2.67
7H-5, 100	60.53	548	47.94	21.10	16.93	49.02	16.54	18.17	2.64
7H-5, 110	60.63	549	47.93	21.10	16.64	49.02	16.26	17.86	2.68
7H-5, 120	60.73	550	47.92	21.10	17.30	49.02	16.90	18.57	2.58
7H-5, 130	60.83	551	47.91	21.10	17.13	49.02	16.74	18.39	2.61
7H-5, 140	60.93	552	47.90	21.10	17.56	49.02	17.16	18.86	2.54
7H-6, 10	61.13	554	47.88	21.00	19.20	48.91	18.80	20.67	2.32
7H-6, 20	61.23	555	47.87	21.00	20.61	48.91	20.18	22.19	2.16
7H-6, 30	61.33	556	47.86	21.00	21.57	48.91	21.12	23.23	2.06
7H-6, 40	61.43	557	47.85	21.00	20.84	48.91	20.40	22.44	2.13
7H-6, 50	61.53	558	47.84	21.00	20.92	48.91	20.48	22.53	2.12
7H-6, 60	61.63	559	47.84	21.00	22.24	48.91	21.78	23.96	2.00
7H-6, 70	61.73	560	47.83	21.00	22.36	48.91	21.89	24.09	1.99
7H-6, 80	61.83	561	47.82	21.00	23.79	48.91	23.29	25.64	1.87
7H-6, 90	61.93	562	47.81	21.00	20.57	48.91	20.14	22.17	2.16
7H-6, 100	62.03	563	47.80	21.00	16.38	48.91	16.04	17.66	2.71
7H-6, 110	62.13	564	47.79	21.00	16.45	48.91	16.11	17.74	2.69
7H-6, 120	62.23	565	47.78	21.00	16.05	48.91	15.71	17.31	2.76
7H-6, 130	62.33	566	47.77	21.00	17.23	48.91	16.87	18.58	2.57
7H-6, 140	62.43	567	47.76	21.00	15.53	48.91	15.21	16.75	2.85
7H-7, 10	62.63	569	47.74	20.90	18.17	48.81	17.83	19.65	2.43
7H-7, 20	62.73	570	47.73	20.90	16.49	48.81	16.18	17.83	2.68
7H-7, 30	62.83	571	47.72	20.90	12.44	48.81	12.21	13.46	3.55
7H-7, 40	62.93	572	47.71	20.90	15.56	48.81	15.27	16.83	2.83
8H-1, 10	63.10	576	47.67	21.50	20.34	49.43	19.71	21.75	2.19
8H-1, 60	63.60	577	47.66	21.50	20.40	49.43	19.77	21.81	2.19
8H-1, 75	63.75	578	47.65	21.50	19.42	49.43	18.82	20.77	2.29
8H-1, 100	64.00	579	47.64	21.40	16.91	49.32	16.42	18.12	2.63
8H-1, 120	64.20	580	47.64	21.40	20.87	49.32	20.26	22.37	2.13
8H-1, 130	64.30	581	47.63	21.40	20.87	49.32	20.26	22.38	2.13
8H-1, 140	64.40	582	47.62	21.40	19.46	49.32	18.90	20.87	2.28
8H-2, 10	64.61	584	47.60	21.40	19.30	49.32	18.74	20.70	2.30
8H-2, 20	64.71	585	47.59	21.40	17.92	49.32	17.40	19.23	2.48
8H-2, 30	64.81	586	47.58	21.40	19.03	49.32	18.48	20.42	2.33
8H-2, 40	64.91	587	47.57	21.30	18.88	49.22	18.37	20.30	2.34
8H-2, 50	65.01	588	47.56	21.30	18.82	49.22	18.31	20.24	2.35
8H-2, 60	65.11	589	47.55	21.30	19.08	49.22	18.56	20.53	2.32
8H-2, 70	65.21	590	47.54	21.30	18.72	49.22	18.21	20.14	2.36
8H-2, 80	65.31	591	47.53	21.30	18.97	49.22	18.46	20.41	2.33
8H-2, 90	65.41	592	47.52	21.30	18.90	49.22	18.39	20.34	2.34
8H-2, 100	65.51	593	47.51	21.30	18.77	49.22	18.26	20.21	2.35
8H-2, 110	65.61	594	47.50	21.20	18.42	49.12	17.96	19.87	2.39
8H-2, 120	65.71	595	47.49	21.20	17.80	49.12	17.36	19.21	2.47
8H-2, 130	65.81	596	47.48	21.20	18.04	49.12	17.59	19.47	2.44
8H-2, 140	65.91	597	47.47	21.20	16.81	49.12	16.39	18.15	2.62
8H-3, 10	66.11	599	47.45	21.30	22.74	49.22	22.13	24.50	1.94
8H-3, 20	66.21	600	47.44	21.30	23.90	49.22	23.25	25.76	1.84
8H-3, 30	66.31	601	47.43	21.30	24.36	49.22	23.70	26.26	1.81
8H-3, 40	66.41	602	47.43	21.30	24.67	49.22	24.00	26.60	1.78
8H-3, 50	66.51	603	47.42	21.20	25.53	49.12	24.89	27.59	1.72
8H-3, 60	66.61	604	47.41	21.20	24.80	49.12	24.18	26.80	1.77
8H-3, 70	66.71	605	47.40	21.20	25.89	49.12	25.24	27.98	1.69
8H-3, 80	66.81	606	47.39	21.20	24.72	49.12	24.10	26.72	1.77
8H-3, 90	66.91	607	47.38	21.20	24.70	49.12	24.08	26.71	1.77
8H-3, 100	67.01	608	47.37	21.20	24.06	49.12	23.46	26.02	1.82
8H-3, 110	67.11	609	47.36	21.20	24.22	49.12	23.62	26.20	1.81

Table T5 (continued).

Core, section, interval (cm)	Depth (mbsf)	Measurement number	Temperature-corrected seawater conductivity (mS/cm)	Sediment temperature (°C)	Sediment electrical conductivity (mS/cm)	Correction factor at 20°C (mS/cm)	Sediment electrical conductivity at 20°C (mS/cm)	Drift-corrected sediment electrical conductivity at 20°C (mS/cm)	Formation factor
8H-3, 120	67.21	610	47.35	21.20	21.20	49.12	20.67	22.93	2.06
8H-3, 130	67.31	611	47.34	21.20	20.34	49.12	19.83	22.01	2.15
8H-3, 140	67.41	612	47.33	21.20	20.50	49.12	19.99	22.18	2.13
8H-4, 10	67.62	614	47.31	21.30	25.22	49.22	24.54	27.24	1.74
8H-4, 20	67.72	615	47.30	21.30	24.78	49.22	24.11	26.77	1.77
8H-4, 30	67.82	616	47.29	21.30	25.24	49.22	24.56	27.27	1.73
8H-4, 40	67.92	617	47.28	21.30	25.72	49.22	25.03	27.80	1.70
8H-4, 50	68.02	618	47.27	21.30	26.01	49.22	25.31	28.11	1.68
8H-4, 60	68.12	619	47.26	21.30	24.20	49.22	23.55	26.16	1.81
8H-4, 70	68.22	620	47.25	21.30	27.39	49.22	26.65	29.61	1.60
8H-4, 80	68.32	621	47.24	21.30	26.43	49.22	25.72	28.58	1.65
8H-4, 90	68.42	622	47.23	21.30	27.19	49.22	26.46	29.41	1.61
8H-4, 100	68.52	623	47.22	21.30	25.81	49.22	25.11	27.92	1.69
8H-4, 110	68.62	624	47.22	21.30	26.56	49.22	25.84	28.74	1.64
8H-4, 120	68.72	625	47.21	21.30	26.54	49.22	25.82	28.72	1.64
8H-4, 130	68.82	626	47.20	21.30	26.60	49.22	25.88	28.79	1.64
8H-4, 140	68.92	627	47.19	21.30	26.21	49.22	25.50	28.37	1.66
8H-5, 10	69.12	629	47.17	21.30	28.29	49.22	27.53	30.63	1.54
8H-5, 20	69.22	630	47.16	21.30	27.28	49.22	26.54	29.54	1.60
8H-5, 30	69.32	631	47.15	21.30	27.34	49.22	26.60	29.61	1.59
8H-5, 38	69.40	632	47.14	21.30	27.28	49.22	26.54	29.55	1.60

Table T6. Summary of APCT-3 temperature measurements, Site U1370.

Core	Depth (mbsf)	BWT (°C)	Origin time (s)	Time delay (s)	Start fit (s)	End fit (s)	Measurement time (min)	Equilibrium temperature (°C)	Remark
329-U1370D-									
4H	34.5	1.24	10,039	274	313	581	4.47	4.34	Poor
329-U1370E-									
3H	25.2	1.29	7,773	379.7	465	656	3.18	3.84	Poor
5H	44.3	1.29	10,741	297.3	354	552	3.30	5.65	Poor
6H	53.7	1.28	13,531	89.2	137	531	3.85	6.56	Fair

BWT = bottom water temperature.

Table T7. Dissolved oxygen concentrations determined using electrodes, Holes U1370B and U1370D–U1370F. (Continued on next page.)

Core, section, interval (cm)	Depth (mbsf)	O ₂ (μM)	Core, section, interval (cm)	Depth (mbsf)	O ₂ (μM)	Core, section, interval (cm)	Depth (mbsf)	O ₂ (μM)
329-U1370B-			2H-2, 90	10.30	74.27	6H-3, 30	47.30	10.19
1H-1, 15	0.15	123.44	2H-2, 120	10.60	73.28	6H-3, 80	47.80	4.39
1H-1, 30	0.30	122.05	2H-3, 30	11.20	61.88	6H-3, 110	48.10	4.80
1H-1, 45	0.45	121.00	2H-3, 80	11.70	64.31	6H-4, 30	48.80	4.26
1H-1, 60	0.60	121.88	2H-3, 120	12.10	62.76	6H-4, 80	49.30	4.26
1H-1, 75	0.75	118.27	2H-4, 30	12.70	67.52	6H-4, 110	49.60	3.88
1H-1, 90	0.90	117.90	2H-4, 80	13.20	61.70	6H-5, 30	50.30	5.23
1H-1, 105	1.05	110.78	2H-4, 120	13.60	62.97	6H-5, 80	50.80	4.84
1H-1, 120	1.20	104.45	2H-5, 30	14.20	60.12	6H-5, 110	51.10	4.41
1H-1, 135	1.35	102.53	2H-5, 60	14.50	57.41	6H-6, 30	51.80	4.00
1H-2, 15	1.65	97.24	2H-5, 100	14.90	54.01	6H-6, 80	52.30	3.31
1H-2, 30	1.80	98.91	2H-6, 30	15.70	53.47	6H-6, 110	52.60	4.41
1H-2, 45	1.95	99.29	2H-6, 80	16.20	49.01	6H-7, 20	53.20	3.10
1H-2, 60	2.10	99.44	2H-6, 120	16.60	48.39	7H-1, 80	54.30	13.72
1H-2, 75	2.25	100.80	2H-7, 30	17.20	53.42	7H-1, 120	54.70	10.74
1H-2, 90	2.40	98.20	2H-7, 80	17.70	46.96	7H-2, 30	55.30	6.34
1H-2, 105	2.55	96.51	2H-7, 120	18.10	53.20	7H-2, 80	55.80	4.15
1H-2, 120	2.70	97.62	3H-1, 40	18.70	101.36	7H-2, 120	56.20	3.17
1H-2, 135	2.85	98.98	3H-1, 80	19.10	106.03	7H-3, 30	56.80	4.92
1H-3, 40	3.40	98.12	3H-1, 122	19.52	98.69	7H-3, 80	57.30	4.96
1H-3, 60	3.60	95.90	3H-2, 30	19.97	95.38	7H-3, 120	57.70	4.39
1H-3, 80	3.80	96.11	3H-2, 70	20.37	68.62	7H-4, 30	58.31	3.15
1H-3, 100	4.00	95.22	3H-3, 40	21.51	113.21	7H-4, 80	58.81	2.38
1H-3, 120	4.20	95.37	3H-3, 80	21.91	113.29	7H-4, 120	59.21	3.17
1H-3, 135	4.35	94.85	3H-3, 120	22.31	101.11	7H-5, 30	59.82	9.77
1H-4, 40	4.90	91.20	3H-4, 30	22.91	39.24	7H-5, 80	60.32	2.93
1H-4, 60	5.10	87.89	3H-4, 80	23.41	33.40	7H-5, 120	60.72	2.23
1H-4, 80	5.30	88.80	3H-4, 120	23.81	32.38	7H-6, 30	61.32	4.26
1H-4, 100	5.50	88.89	3H-5, 30	24.41	31.86	7H-6, 80	61.82	1.62
1H-4, 120	5.70	90.07	4H-1, 34	25.34	23.95	7H-7, 40	62.90	1.53
1H-4, 140	5.90	89.00	4H-1, 80	25.80	23.68	7H-7, 80	63.30	1.49
1H-5, 20	6.20	87.57	4H-1, 120	26.20	22.88	8H-1, 30	63.30	1.25
1H-5, 40	6.40	86.64	4H-2, 30	26.80	32.86	8H-1, 80	63.80	1.11
1H-5, 60	6.60	83.49	4H-2, 80	27.30	22.73	8H-1, 110	64.10	0.97
1H-6, 30	7.80	80.87	4H-2, 112	27.70	17.89	8H-2, 30	64.80	0.95
329-U1370D-			4H-2, 130	28.30	17.20	8H-2, 80	65.30	0.83
1H-1, 20	0.20	130.98	4H-3, 80	28.80	17.70	8H-2, 110	65.60	0.45
1H-1, 40	0.40	122.41	4H-3, 112	29.12	19.34	8H-3, 30	66.30	0.69
1H-1, 64	0.64	122.37	4H-3, 130	29.30	19.30	8H-3, 80	66.80	0.48
1H-1, 80	0.80	122.21	4H-3, 30	29.80	15.63	8H-3, 110	67.10	0.18
1H-1, 100	1.00	122.00	4H-4, 50	30.00	16.37	8H-4, 30	67.80	0.31
1H-1, 120	1.20	118.81	4H-4, 20	30.70	18.80	8H-4, 80	68.30	1.97
1H-2, 20	1.70	109.05	4H-5, 50	31.00	16.27	8H-4, 110	68.60	1.68
1H-2, 50	2.00	104.93	4H-5, 80	31.30	16.27	8H-5, 30	69.30	0.56
1H-2, 85	2.35	106.69	4H-5, 80	35.30	11.24	8H-5, 80	69.80	3.51
1H-2, 110	2.60	106.96	5H-1, 110	35.60	11.91	8H-5, 110	70.10	2.48
1H-2, 135	2.85	106.74	5H-1, 138	35.88	14.99	8H-6, 30	70.81	5.19
1H-3, 20	3.20	121.66	5H-1, 30	36.30	12.37	8H-6, 80	71.31	43.92
1H-3, 50	3.50	106.32	5H-2, 60	36.60	12.48	8H-7, 30	72.31	44.77
1H-3, 70	3.70	108.27	5H-2, 90	36.90	10.60	329-U1370E-		
1H-3, 90	3.90	103.51	5H-2, 30	37.80	27.37	2H-1, 22	6.42	79.37
1H-3, 110	4.10	103.61	5H-3, 90	38.40	32.07	2H-1, 42	6.62	83.73
1H-4, 20	4.70	96.19	5H-3, 134	38.84	20.36	2H-1, 77	6.97	84.43
1H-4, 50	5.00	95.12	5H-3, 30	39.30	8.41	2H-1, 110	7.30	90.16
1H-4, 70	5.20	93.85	5H-4, 90	39.90	8.93	2H-2, 20	7.90	88.24
1H-4, 90	5.40	90.87	5H-4, 130	40.30	8.46	2H-2, 85	7.85	84.77
1H-4, 110	5.60	91.40	5H-5, 30	40.80	58.91	2H-3, 15	9.35	91.55
1H-4, 135	5.85	92.18	5H-5, 60	41.10	21.65	2H-3, 90	9.40	73.40
1H-5, 30	6.30	92.17	5H-6, 30	42.27	8.63	2H-4, 90	7.10	64.49
1H-5, 50	6.50	91.06	5H-6, 60	42.57	10.01	2H-4, 110	7.30	68.93
1H-5, 80	6.80	87.64	5H-6, 90	42.87	7.96	2H-5, 15	12.35	62.84
1H-5, 110	7.10	88.89	6H-1, 36	44.36	13.80	2H-5, 90	13.10	55.69
1H-5, 130	7.30	88.91	6H-1, 90	44.90	12.79	2H-5, 110	13.30	58.37
1H-6, 30	7.80	85.49	6H-1, 110	45.10	8.73	2H-6, 20	13.90	58.11
1H-6, 50	8.00	81.82	6H-2, 30	45.80	4.79	2H-6, 40	14.10	55.84
1H-6, 80	8.30	78.53	6H-2, 80	46.30	4.17	2H-6, 85	14.55	52.36
2H-2, 30	9.70	110.77	6H-2, 110	46.60	3.62	2H-6, 100	14.70	47.67

Table T7 (continued).

Core, section, interval (cm)	Depth (mbsf)	O ₂ (μ M)	Core, section, interval (cm)	Depth (mbsf)	O ₂ (μ M)	Core, section, interval (cm)	Depth (mbsf)	O ₂ (μ M)
3H-1, 20	15.90	44.19	5H-4, 110	40.24	10.25	3H-3, 130	20.50	33.98
3H-1, 40	16.10	43.73	5H-5, 15	40.79	11.24	3H-4, 30	21.00	28.37
3H-1, 90	16.60	40.23	5H-5, 30	40.94	25.72	3H-4, 80	21.50	31.03
3H-1, 120	16.90	41.39	5H-5, 98	41.52	7.22	3H-4, 130	22.00	26.95
3H-2, 15	17.35	36.75	5H-5, 116	41.80	10.30	3H-5, 70	22.90	27.57
3H-2, 90	18.10	37.13	5H-6, 30	42.44	11.24	3H-5, 100	23.20	22.93
3H-2, 110	18.30	35.33	6H-1, 110	45.30	6.65	3H-6, 60	24.00	33.06
3H-2, 125	18.45	36.08	6H-1, 130	45.50	14.63	4H-1, 30	26.00	156.22
3H-3, 20	18.90	33.39	6H-2, 94	46.64	6.40	4H-1, 80	26.50	22.28
3H-3, 90	17.40	33.81	6H-2, 114	46.84	6.66	4H-1, 130	27.00	35.66
3H-4, 20	20.40	29.47	6H-3, 100	48.13	7.88	4H-2, 30	27.50	20.77
3H-4, 40	20.60	32.56	6H-3, 120	48.33	6.59	4H-2, 80	28.00	24.77
3H-4, 90	21.10	28.98	6H-4, 95	49.58	6.54	4H-2, 130	28.50	18.84
3H-4, 110	21.30	32.10	6H-4, 120	49.73	6.42	4H-3, 125	29.95	41.58
3H-5, 20	21.90	27.80	6H-5, 20	50.33	6.36	4H-4, 30	30.50	19.32
3H-5, 90	22.60	29.13				4H-4, 80	31.00	33.57
3H-5, 120	22.90	27.61	329-U1370F-			4H-4, 130	31.50	16.20
3H-6, 20	23.40	27.74	1H-1, 30	0.30	144.51	4H-5, 70	32.40	16.91
4H-1, 20	25.40	23.19	1H-1, 60	0.60	142.81	4H-5, 100	32.70	12.54
4H-1, 40	25.60	55.20	1H-3, 120	4.20	111.90	4H-6, 20	33.23	12.73
4H-1, 90	26.10	21.25	1H-3, 140	4.40	121.38	4H-6, 35	33.38	11.05
4H-1, 110	26.30	20.53	1H-4, 81	5.31	94.80	6H-1, 30	45.00	124.95
4H-1, 125	26.45	19.70	1H-4, 141	5.91	96.98	6H-1, 80	45.50	154.46
4H-2, 15	26.85	39.17	1H-5, 21	6.21	98.34	6H-1, 130	46.00	35.66
4H-2, 90	27.60	18.88	1H-5, 41	6.41	97.39	6H-2, 30	46.50	8.46
4H-2, 155	27.85	18.42	2H-1, 30	7.00	83.22	6H-2, 80	47.00	8.71
4H-3, 20	28.40	18.22	2H-1, 50	7.20	82.96	6H-2, 120	47.40	6.90
4H-3, 50	28.70	17.99	2H-1, 115	7.95	79.83	6H-3, 115	48.85	13.90
4H-3, 90	29.10	22.34	2H-1, 140	8.10	81.42	6H-3, 135	49.00	4.39
4H-4, 20	29.90	17.83	2H-2, 30	8.50	79.83	6H-4, 100	50.20	17.30
4H-4, 40	30.10	19.30	2H-2, 80	9.00	72.92	6H-4, 120	50.40	4.87
4H-4, 90	30.613	15.72	2H-2, 130	9.50	74.02	6H-5, 90	51.60	14.90
4H-4, 110	30.813	15.66	2H-3, 105	10.75	65.11	6H-5, 120	51.90	3.21
4H-5, 20	31.40	13.43	2H-4, 30	11.50	65.26	6H-6, 90	53.10	8.52
4H-5, 85	31.45	14.18	2H-4, 80	12.00	59.31	6H-6, 120	53.30	5.50
5H-1, 50	35.20	10.38	2H-4, 130	12.50	62.34	7H-1, 85	55.05	5.88
5H-1, 70	35.40	12.44	2H-5, 60	13.30	39.70	7H-1, 95	55.15	5.84
5H-1, 155	36.28	11.08	2H-5, 100	13.70	50.69	7H-2, 125	56.95	8.01
5H-2, 15	36.35	18.06	3H-1, 30	16.50	39.48	7H-2, 145	57.15	3.93
5H-2, 110	37.30	16.30	3H-1, 80	17.00	42.08	7H-3, 95	58.15	3.46
5H-3, 100	38.64	33.27	3H-1, 130	17.50	58.71	7H-3, 125	58.35	3.29
5H-3, 120	38.84	11.45	3H-2, 110	18.80	41.58	7H-4, 100	59.70	8.33
5H-4, 90	40.04	25.44	3H-3, 30	19.50	40.27	7H-4, 120	59.80	8.48
			3H-3, 80	20.00	33.71			

Table T8. Dissolved oxygen concentrations determined using optodes, Holes U1370B and U1370D–U1370F.

Core, section, interval (cm)	Depth (mbsf)	O ₂ (μM)	Core, section, interval (cm)	Depth (mbsf)	O ₂ (μM)	Core, section, interval (cm)	Depth (mbsf)	O ₂ (μM)
329-U1370B-			2H-3, 50	11.40	71.9	7H-4, 50	58.51	6.62
1H-1, 5	0.05	149.7	2H-3, 125	12.15	93.6	7H-4, 125	59.26	6.45
1H-1, 10	0.10	149.6	2H-4, 50	12.90	66.5	7H-5, 50	60.02	7.07
1H-1, 25	0.25	144.1	2H-4, 125	13.65	63.6	7H-5, 125	60.77	6.29
1H-1, 35	0.35	153.8	2H-5, 50	14.40	60.2	7H-6, 50	61.52	6.73
1H-1, 45	0.45	140.8	2H-5, 125	15.15	56.9	7H-6, 125	62.27	7.58
1H-1, 50	0.50	140.4	2H-6, 50	15.90	55.5	8H-2, 50	65.00	5.79
1H-1, 65	0.65	141.6	2H-6, 125	16.65	68.5	8H-2, 125	65.75	6.30
1H-1, 75	0.75	134.3	3H-2, 50	20.17	111.9	8H-3, 50	66.50	6.72
1H-1, 85	0.85	123.2	3H-2, 50	20.17	116.5	8H-3, 125	67.25	6.14
1H-1, 100	1.00	120.7	3H-3, 125	22.36	88.7	8H-4, 25	67.75	6.12
1H-1, 115	1.15	120.8	3H-4, 50	23.11	37.9	8H-4, 50	68.00	6.20
1H-1, 130	1.30	119.3	3H-4, 125	23.86	37.0	329-U1370E-		
1H-2, 10	1.60	119.0	3H-5, 25	24.36	36.5	1H-3, 75	3.75	115.0
1H-2, 40	1.90	116.3	4H-1, 50	25.50	25.9	2H-1, 30	6.50	84.9
1H-2, 75	2.25	116.0	4H-1, 125	26.25	24.6	2H-5, 110	13.30	56.9
1H-2, 100	2.50	113.3	4H-2, 50	27.00	23.9	3H-1, 110	16.80	40.1
1H-2, 130	2.80	113.2	4H-2, 125	27.75	22.5	3H-3, 25	18.95	35.4
1H-3, 25	3.25	111.2	4H-3, 50	28.50	29.6	3H-5, 110	22.80	27.9
1H-3, 75	3.75	108.5	4H-3, 125	29.25	21.4	4H-1, 110	26.30	21.7
1H-3, 125	4.25	104.8	4H-4, 40	29.90	20.1	4H-3, 95	29.15	18.3
1H-4, 25	4.75	101.9	4H-4, 90	30.40	19.4	4H-4, 100	30.70	16.7
1H-4, 75	5.25	100.2	4H-5, 30	30.80	18.2	4H-5, 90	32.10	15.3
1H-4, 125	5.75	97.9	4H-5, 60	31.10	17.9	5H-1, 60	35.30	16.6
1H-5, 25	6.25	95.8	5H-1, 85	35.35	13.9	5H-3, 110	38.74	7.98
1H-5, 75	6.75	92.6	5H-1, 125	35.75	13.6	5H-6, 35	42.49	10.8
1H-6, 10	7.10	91.5	5H-2, 50	36.50	13.1	6H-1, 40	44.60	8.47
1H-6, 55	7.55	88.3	5H-2, 135	37.35	12.8	6H-1, 55	44.75	9.27
329-U1370D-			5H-3, 50	38.00	12.3	6H-3, 110	48.23	8.02
1H-1, 15	0.15	122.9	5H-3, 125	38.75	12.2	6H-5, 25	50.38	7.95
1H-1, 45	0.45	118.6	5H-4, 50	39.50	11.6	329-U1370F-		
1H-1, 105	1.05	117.7	5H-4, 125	40.25	10.9	1H-3, 125	4.25	105.7
1H-1, 125	1.25	116.1	5H-5, 50	41.00	10.7	1H-4, 100	5.50	100.0
1H-2, 15	1.65	114.5	5H-5, 125	41.75	10.6	1H-5, 30	6.30	96.4
1H-2, 40	1.90	113.3	5H-6, 50	42.47	10.1	2H-2, 135	9.55	80.1
1H-2, 75	2.25	119.5	5H-6, 85	42.82	9.83	2H-3, 130	11.00	67.7
1H-2, 125	2.75	114.3	6H-1, 125	45.25	8.87	2H-5, 75	13.45	58.0
1H-3, 25	3.25	111.6	6H-2, 50	46.00	8.43	3H-1, 75	16.95	43.7
1H-3, 75	3.75	105.0	6H-2, 125	46.75	9.16	3H-3, 75	19.95	36.2
1H-3, 125	4.25	102.8	6H-3, 50	47.50	8.98	3H-5, 75	22.95	29.7
1H-4, 25	4.75	100.3	6H-3, 125	48.25	8.74	4H-2, 25	27.45	21.7
1H-4, 75	5.25	97.8	6H-4, 50	49.00	8.20	4H-3, 120	29.90	18.6
1H-4, 125	5.75	95.5	6H-4, 125	49.75	8.76	4H-5, 75	32.45	16.0
1H-4, 125	5.75	96.0	6H-5, 50	49.00	7.72	6H-4, 100	50.20	7.55
1H-5, 25	6.25	93.3	6H-5, 125	49.75	8.81	6H-5, 100	51.70	8.73
1H-5, 75	6.75	90.7	6H-6, 50	52.00	6.61	7H-1, 90	55.10	8.55
1H-5, 125	7.25	89.2	6H-6, 125	52.75	8.70	7H-2, 20	55.90	7.84
1H-6, 15	7.65	88.4	7H-1, 50	54.00	7.31	7H-3, 90	58.10	6.42
1H-6, 80	8.30	87.7	7H-1, 125	54.75	6.88	7H-4, 110	59.80	7.41
2H-1, 15	8.95	100.4	7H-2, 50	55.50	7.28	7H-5, 110	61.30	6.86
2H-2, 35	9.75	108.8	7H-2, 125	56.25	6.70	7H-6, 50	62.20	6.95
2H-2, 125	10.65	74.9	7H-3, 50	57.01	8.34			
			7H-3, 130	57.81	7.00			

Table T9. Dissolved hydrogen measured by the headspace gas method, Hole U1370E.

Core, section	Depth (mbsf)	H ₂ (nM)	Catwalk sampling	Comment
329-U1370E-				
1H-1	0.40	BD	No	
1H-1	0.90	BD	No	
1H-1	1.40	BD	Yes	
1H-2	1.90	BD	No	
1H-2	2.40	BD	No	
1H-2	2.90	BD	Yes	
1H-3	3.40	BD	No	
1H-3	3.90	BD	Yes	
1H-3	4.30	BD	Yes	
1H-4	6.00	BD	Yes	
2H-1	7.60	BD	Yes	
2H-2	9.10	BD	Yes	
2H-3	10.60	BD	Yes	
2H-4	12.00	BD	Yes	
2H-5	13.60	BD	Yes	
2H-6	14.90	BD	Yes	
3H-1	17.10	BD	Yes	
3H-2	18.60	BD	Yes	
3H-3	20.10	BD	Yes	
3H-4	21.50	BD	Yes	
3H-5	23.10	BD	Yes	
3H-6	23.80	BD	Yes	
4H-1	26.60	BD	Yes	
4H-2	28.10	BD	Yes	
4H-3	29.60	BD	Yes	
4H-4	31.00	BD	Yes	
4H-5	32.60	BD	Yes	
4H-6	33.30	BD	Yes	
5H-1	36.10	BD	Yes	
5H-2	37.50	BD	Yes	
5H-3	39.00	BD	Yes	
5H-4	40.40	BD	Yes	
5H-5	42.00	BD	Yes	
5H-6	42.70	BD	Yes	
6H-1	45.60	BD	Yes	
6H-2	47.00	BD	Yes	
6H-3	48.50	BD	Yes	
6H-4	50.00	BD	Yes	
6H-5	51.10	BD	Yes	
8H-2	58.40	23.2	Yes	Disturbed
8H-3	59.90	BD	Yes	Disturbed
8H-4	61.30	5.4	Yes	Disturbed
8H-5	62.90	10.9	Yes	Disturbed
9H-1	63.50	2.7	Yes	
9H-2	65.00	BD	Yes	
5H-3	39.60	BD	Yes	
5H-4	41.10	BD	Yes	
5H-5	42.60	BD	Yes	
6H-2	47.60	BD	Yes	
6H-3	49.10	BD	Yes	
6H-4	50.60	BD	Yes	
6H-5	52.10	BD	Yes	
7H-1	55.60	BD	Yes	
7H-2	57.10	BD	Yes	
7H-3	58.60	BD	Yes	
7H-4	60.00	BD	Yes	
7H-5	61.60	BD	Yes	
7H-6	63.10	BD	Yes	

BD = below detection (<2.3 nM).

Table T10. Interstitial fluid nitrate in Rhizon samples, Site U1370.

Core, section, interval (cm)	Depth (mbsf)	NO ₃ (μM)	Core, section, interval (cm)	Depth (mbsf)	NO ₃ (μM)
329-U1370B-			3H-5, 60-70	22.35	50.29
1H-1, 40-50	0.45	33.86	3H-6, 40-50	23.65	49.86
1H-1, 95-105	1.00	41.46	4H-1, 60-70	25.85	50.73
1H-1, 140-150	1.45	41.78	4H-2, 60-70	27.35	50.43
1H-2, 20-30	1.75	41.99	4H-3, 60-70	28.85	51.71
1H-2, 80-90	2.35	42.27	4H-4, 60-70	30.35	50.17
1H-2, 125-135	2.80	42.31	4H-5, 60-70	31.85	51.29
1H-3, 15-25	3.20	41.75	4H-6, 10-20	32.85	50.03
1H-3, 65-75	3.70	41.83	5H-1, 80-90	35.55	51.00
1H-3, 110-120	4.15	42.56	5H-2, 60-70	36.85	50.70
1H-4, 15-25	4.70	42.20	5H-3, 60-70	38.29	51.03
1H-4, 65-75	5.20	42.02	5H-4, 60-70	39.79	51.75
1H-4, 110-120	5.65	43.25	5H-5, 60-70	41.29	51.19
1H-5, 40-50	6.45	45.90	5H-6, 50-60	42.69	49.92
1H-5, 85-95	6.90	44.91	6H-1, 70-80	44.95	46.73
1H-6, 40-50	7.45	44.37	6H-2, 60-70	46.35	49.77
329-U1370E-			6H-3, 60-70	47.78	49.55
1H-1, 15-25	0.20	38.51	6H-4, 60-70	49.28	48.13
1H-1, 52.5-62.5	0.58	39.17	6H-5, 60-70	50.78	47.72
1H-1, 100-110	1.05	40.00	9H-1, 60-70	62.75	45.87
1H-2, 0-10	1.55	40.50	9H-2, 60-70	64.25	45.44
1H-2, 50-60	2.05	40.80	9H-2, 120-130	64.85	45.41
1H-2, 100-110	2.55	41.91	329-U1370F-		
1H-3, 0-10	3.05	40.41	5H-3, 60-70	38.85	50.21
1H-3, 50-60	3.55	42.14	5H-4, 60-70	40.35	49.39
1H-3, 100-110	4.05	41.55	5H-5, 60-70	41.85	50.47
1H-4, 60-70	5.15	42.51	5H-6, 40-50	43.15	48.58
2H-1, 60-70	6.85	45.59	6H-3, 80-90	48.55	48.31
2H-2, 60-70	8.35	46.07	6H-4, 60-70	49.85	48.84
2H-3, 60-70	9.85	46.44	6H-5, 60-70	51.35	46.73
2H-4, 60-70	11.35	47.60	6H-6, 60-70	52.85	47.29
2H-5, 60-70	12.85	47.53	7H-1, 60-70	54.85	47.12
2H-6, 60-70	14.35	47.71	7H-2, 70-80	56.45	45.77
3H-1, 60-70	16.35	47.97	7H-3, 60-70	57.85	47.37
3H-2, 60-70	17.85	49.45	7H-4, 70-80	59.45	49.37
3H-3, 60-70	19.35	50.74	7H-5, 70-80	60.95	45.82
3H-4, 60-70	20.85	49.90			



Table T11. Interstitial fluid chemistry, Site U1370. (Continued on next page.)

Core, section, interval (cm)	Catwalk sampling	Depth (m)	pH TITRAUTO	Alkalinity (mM) TITRAUTO	DIC (mM) OI-IC	Cl (mM) M-IC	SO ₄ (mM) M-IC	SO ₄ (%) Calc. anom.	PO ₄ (μM) Spec.	Si (μM) Spec.	Ca (mM) Dx-IC	Mg (mM) Dx-IC	Na (mM) Dx-IC	K (mM) Dx-IC	Ca (mM) ICPAES	Mg (mM) ICPAES	Na (mM) ICPAES	K (mM) ICPAES	B (μM) ICPAES	Fe (μM) ICPAES	Mn (μM) ICPAES	Sr (μM) ICPAES
329-U1370E-																						
1H-1, 5-15	Yes	0.10	7.65	2.49	2.43	553.58	28.23	-1.26	1.94	205	10.56	52.71	483.10	12.17	10.1	52.1	483	12.1	467	9.4	4.0	89.7
1H-1, 42.5-52.5	No	0.48	7.77	2.44	2.47	553.06	28.17	-1.39	2.25	263	10.43	51.86	475.74	12.03	10.2	52.7	482	12.3	448	7.6	3.3	90.1
1H-1, 90-100	No	0.95	7.73	2.43	2.44	553.75	28.11	-1.71	2.51	288	10.49	52.31	478.69	12.16	10.4	53.3	484	12.2	474	9.6	3.7	92.5
1H-1, 140-150	Yes	1.45	7.67	2.44	2.47	554.03	28.08	-1.87	2.43	214	10.43	52.52	480.22	12.10	9.9	51.0	458	11.2	380	6.8	4.4	85.3
1H-2, 40-50	No	1.95	7.76	2.43	2.46	—	—	—	2.70	249	10.42	—	476.54	—	10.3	52.7	472	11.6	449	7.3	3.7	91.8
1H-2, 90-100	No	2.45	7.66	2.46	2.48	553.31	28.07	-1.78	2.57	267	—	—	—	10.2	51.9	471	11.9	437	8.5	4.7	88.8	
1H-2, 140-150	Yes	2.95	7.67	2.45	2.46	554.89	28.11	-1.91	2.75	218	10.57	52.45	482.36	12.21	10.3	51.9	474	11.8	486	9.0	4.3	92.6
1H-3, 40-50	No	3.45	7.76	2.43	2.43	554.75	28.13	-1.82	2.88	253	10.50	52.09	478.15	12.01	10.1	51.5	468	11.6	481	8.9	4.1	92.8
1H-3, 90-100	No	3.95	7.72	2.44	2.44	556.32	28.18	-1.94	2.77	270	10.51	52.59	480.97	11.97	10.2	51.7	470	11.9	496	10.0	3.9	93.1
1H-3, 140-150	Yes	4.45	7.70	2.45	2.50	554.38	28.13	-1.76	2.83	275	10.88	53.12	486.79	12.15	10.2	51.4	466	11.3	466	8.2	4.8	92.0
1H-4, 142-152	Yes	5.97	7.68	2.43	2.42	555.63	28.30	-1.41	2.54	186	—	—	—	10.5	52.4	471	11.7	485	10.1	5.1	92.8	
2H-1, 140-150	Yes	7.65	7.68	2.45	2.45	558.35	28.39	-1.56	2.23	234	—	—	—	10.6	52.5	476	11.6	457	7.2	5.3	91.7	
2H-2, 140-150	Yes	9.15	7.67	2.42	2.49	558.21	28.40	-1.51	2.21	240	10.85	52.61	482.56	11.77	10.3	52.9	492	11.5	483	9.3	5.4	90.6
2H-3, 140-150	Yes	10.65	7.70	2.44	2.51	559.55	28.42	-1.68	1.91	243	10.93	52.27	483.03	11.81	10.6	53.3	488	11.4	507	10.2	7.8	92.7
2H-4, 140-150	Yes	12.15	7.67	2.47	2.51	—	—	—	1.77	241	10.76	52.11	484.52	12.17	10.5	53.1	489	12.3	503	9.2	5.2	91.4
2H-5, 140-150	Yes	13.65	7.69	2.47	2.53	561.14	28.32	-2.29	1.67	244	10.80	52.36	485.93	12.01	10.5	52.7	481	11.5	475	7.3	4.9	91.8
2H-6, 113-123	Yes	14.88	7.71	2.49	2.57	561.58	28.29	-2.49	1.55	269	—	—	—	10.6	52.7	480	11.8	488	7.8	6.4	93.0	
3H-1, 140-150	Yes	17.15	7.70	2.45	2.52	560.56	28.23	-2.51	1.19	229	11.19	53.61	—	—	10.6	52.2	474	11.4	491	9.2	5.3	91.5
3H-2, 140-150	Yes	18.65	7.71	2.45	2.50	563.48	28.36	-2.58	1.20	229	—	—	—	10.8	52.6	479	11.8	492	8.4	4.7	93.1	
3H-3, 140-150	Yes	20.15	7.72	2.45	2.54	—	—	-2.85	1.23	240	11.23	53.93	494.33	12.01	10.5	52.0	471	11.2	497	9.1	4.0	93.3
3H-4, 140-150	Yes	21.65	7.72	2.41	2.49	565.37	28.41	-2.73	1.19	225	10.99	52.95	485.60	11.68	10.9	52.8	480	11.5	502	10.5	5.8	93.1
3H-5, 140-150	Yes	23.15	7.70	2.42	2.51	563.29	28.27	-2.84	0.97	216	11.20	53.08	487.41	11.61	10.5	51.8	473	11.4	485	8.3	4.0	93.0
3H-6, 58-68	Yes	23.83	7.74	2.41	2.49	564.52	28.28	-3.03	1.12	220	11.13	53.10	488.04	11.65	10.7	52.9	475	11.5	506	10.0	5.4	92.0
4H-1, 140-150	Yes	26.65	7.74	2.39	2.46	564.77	28.20	-3.32	0.91	199	11.14	52.93	486.55	11.42	10.8	52.8	482	11.0	460	7.9	5.1	90.5
4H-2, 140-150	Yes	28.15	7.81	2.45	2.42	563.99	28.11	-3.50	0.97	214	11.18	53.63	488.14	11.21	10.8	53.1	495	11.0	507	9.4	5.7	91.0
4H-3, 140-150	Yes	29.65	7.73	2.36	2.42	564.76	28.11	-3.65	0.95	196	11.38	53.08	487.19	11.17	11.0	54.2	498	11.1	499	8.7	5.9	92.6
4H-4, 140-150	Yes	31.15	7.75	2.38	2.42	564.11	27.95	-4.07	1.05	250	11.30	53.69	494.26	11.45	11.0	53.6	489	11.5	478	7.5	5.4	90.6
4H-5, 140-150	Yes	32.65	7.72	2.35	2.41	565.98	28.12	-3.80	0.98	203	11.31	52.90	486.14	11.01	10.9	53.3	483	10.7	493	8.2	4.2	93.0
5H-1, 140-150	Yes	36.15	7.77	2.33	2.36	563.97	27.80	-4.57	0.82	192	11.35	52.55	484.67	10.83	10.9	53.1	480	10.8	503	8.1	5.3	92.5
5H-2, 134-144	Yes	37.59	7.75	2.34	2.35	563.89	27.89	-4.24	0.89	218	11.36	53.57	489.30	10.84	11.3	53.6	483	10.6	520	10.0	5.4	92.4
5H-3, 140-150	Yes	39.09	7.74	2.25	—	—	—	—	1.02	201	11.46	—	—	11.12	11.0	52.3	477	11.0	512	9.4	4.6	93.7
5H-4, 140-150	Yes	40.59	7.76	2.30	2.30	565.94	27.89	-4.58	0.88	185	11.33	53.67	489.03	10.72	11.2	53.1	480	10.7	525	9.9	5.9	93.3
5H-5, 140-150	Yes	42.09	7.77	2.30	2.30	563.16	27.82	-4.38	0.86	210	11.44	52.64	482.64	10.13	11.3	53.3	484	10.6	522	10.6	5.0	93.3
5H-6, 60-70	Yes	42.79	7.76	2.30	2.30	565.53	27.91	-4.45	0.81	192	—	—	—	11.2	52.9	480	10.2	507	8.7	4.2	93.7	
6H-1, 140-150	Yes	45.65	7.78	2.27	2.28	565.19	27.84	-4.65	0.66	204	—	—	—	11.2	53.0	478	10.2	520	9.6	5.7	92.7	
6H-2, 134-144	Yes	47.09	7.76	2.26	2.24	563.79	27.84	-4.39	0.86	208	11.68	53.60	485.68	10.27	11.3	53.1	481	10.4	514	9.6	5.2	92.8
6H-3, 140-150	Yes	48.58	7.79	2.26	2.31	563.94	27.76	-4.71	0.77	190	11.63	53.74	488.89	10.20	11.4	54.3	496	10.2	511	8.4	5.1	90.6
6H-4, 140-150	Yes	50.08	7.87	2.26	2.29	564.25	27.67	-5.05	0.88	226	11.85	53.90	491.19	10.26	11.4	53.9	492	10.1	523	10.1	6.8	93.6
6H-5, 100-110	Yes	51.18	7.86	2.26	2.20	—	—	—	—	—	—	—	—	11.4	53.8	484	11.0	494	9.0	5.1	92.0	
9H-1, 140-150	Yes	63.55	8.07	2.15	2.09	564.04	26.41	-9.35	0.50	199	11.80	50.82	486.47	10.44	11.5	51.7	482	10.1	484	7.6	4.9	92.3
9H-2, 140-150	Yes	65.05	8.07	2.14	2.07	564.46	27.52	-5.61	0.67	228	—	—	—	11.3	52.0	473	10.0	462	7.1	4.7	91.5	
329-U1370F-																						
5H-3, 140-150	Yes	39.65	7.73	2.32	2.36	564.05	27.72	-4.94	0.76	184	11.20	53.65	491.14	11.06	10.7	51.9	475	10.9	512	8.5	4.7	93.0
5H-4, 140-150	Yes	41.15	7.76	2.36	2.34	565.01	27.75	-4.99	0.87	176	11.48	—	—	11.14	10.9	52.3	480	10.6	520	10.4	5.8	93.3
5H-5, 140-150	Yes	42.65	7.74	2.31	2.36	564.64	27.78	-4.84	0.99	173	—	53.22	488.17	10.81	11.2	53.1	483	10.7	516	10.3	6.1	92.2
6H-2, 140-150	Yes	47.65	7.78	2.28	2.28	564.74	27.76	-4.91	0.75	164	11.75	54.15	494.60	10.71	11.0	52.3	477	10.0	519	10.8	6.3	93.5
6H-3, 140-150	Yes	49.15	7.77	2.27	2.25	563.28	27.65	-5.06	0.73	171	11.61	53.57	485.97	10.28	11.2	52.9	479	10.3	521	9.1	5.7	93.5
6H-4, 140-150	Yes	50.65	7.81	2.25	2.26	562.31	27.57	-5.17	0.63	172	11.50	53.23	483.21	10.12	11.3	53.4	481	9.9	465	8.8	5.2	90.6



Table T11 (continued).

Core, section, interval (cm)	Catwalk sampling	Depth (m)	pH TITRAUTO	Alkalinity (mM) TITRAUTO	DIC (mM) OI-IC	Cl (mM) M-IC	SO ₄ (mM) M-IC	SO ₄ (%) Calc. anom.	PO ₄ (μM) Spec.	Si (μM) Spec.	Ca (mM) Dx-IC	Mg (mM) Dx-IC	Na (mM) Dx-IC	K (mM) Dx-IC	Ca (mM) ICPAES	Mg (mM) ICPAES	Na (mM) ICPAES	K (mM) ICPAES	B (μM) ICPAES	Fe (μM) ICPAES	Mn (μM) ICPAES	Sr (μM) ICPAES
6H-5, 140–150	Yes	52.15	7.81	2.27	2.27	562.47	27.59	-5.11	—	—	—	—	—	—	11.4	54.2	496	10.3	498	8.5	4.8	90.2
7H-1, 140–150	Yes	55.65	7.80	2.23	2.18	561.63	27.55	-5.11	0.85	170	11.75	53.95	485.48	9.97	11.6	54.7	492	9.9	521	9.9	5.9	93.7
7H-2, 140–150	Yes	57.15	7.82	2.23	2.15	561.70	27.53	-5.22	0.68	177	11.67	53.98	482.28	9.67	11.5	53.9	481	9.8	511	8.9	5.0	93.4
7H-3, 140–150	Yes	58.65	7.88	2.32	2.21	563.43	26.90	-7.64	0.84	174	11.48	53.18	488.33	10.58	11.1	53.0	481	10.4	496	6.9	4.9	90.6
7H-4, 140–150	Yes	60.15	7.91	2.31	2.19	563.24	26.34	-9.53	0.57	157	11.35	52.16	487.07	11.24	11.0	51.9	477	11.4	505	7.3	4.6	90.0
7H-5, 140–150	Yes	61.65	7.88	2.21	2.12	564.66	26.72	-8.48	0.51	167	11.58	53.02	492.44	11.35	11.2	52.3	480	11.2	515	10.1	4.4	91.5
7H-6, 140–150	Yes	63.15	7.89	2.17	2.11	563.14	27.32	-6.15	0.94	186	11.82	53.22	490.55	10.73	11.2	52.2	479	10.5	480	8.0	4.6	91.8

ISE = ion-selective electrode, TITRAUTO = automated titration, IC = ion chromatography, OI-IC = OI analytical IC, M-IC = Metrohm IC, Calc. anom. = calculated anomaly, Spec. = spectrophotometry, Dx-IC = Dionex IC, ICPAES = inductively coupled plasma–atomic emission spectroscopy. — = no data.

Table T12. Solid-phase carbon and nitrogen, Site U1370.

Core, section, interval (cm)	Depth (mbsf)	TC (wt%)	TN (wt%)	TOC (wt%)	TIC (wt%)	CaCO ₃ (wt%)
329-U1370E-						
1H-1, 5-7	0.06	0.30	0.079	0.25	0.01	0.06
1H-1, 13-15	0.14	0.23	0.069	0.21	0.00	0.04
1H-1, 43-45	0.44	0.19	0.063	0.18	0.01	0.06
1H-1, 50-52	0.51	0.19	0.061	0.16	0.01	0.05
1H-1, 90-92	0.91	0.13	0.055	0.12	0.01	0.05
1H-1, 98-100	0.99	0.13	0.053	0.12	0.01	0.06
1H-1, 140-142	1.41	0.12	0.052	0.11	0.01	0.04
1H-1, 148-150	1.49	0.13	0.052	0.11	0.00	0.03
1H-2, 40-50	1.95	0.11	0.052	0.10	0.01	0.05
1H-2, 90-100	2.45	0.11	0.053	0.10	0.00	0.04
1H-2, 140-150	2.95	0.11	0.052	0.10	0.00	0.04
1H-3, 40-50	3.45	0.10	0.050	0.09	0.00	0.04
1H-3, 90-100	3.95	0.09	0.047	0.09	0.00	0.04
1H-3, 140-150	4.45	0.09	0.042	0.08	0.01	0.05
1H-4, 142-152	5.97	0.07	0.032	0.07	0.01	0.04
2H-1, 140-150	7.65	0.05	0.028	0.05	0.00	0.03
2H-2, 140-150	9.15	0.05	0.028	0.05	0.00	0.03
2H-3, 140-150	10.65	0.05	0.026	0.04	0.01	0.05
2H-4, 140-150	12.15	0.04	0.022	0.04	0.01	0.06
2H-5, 140-150	13.65	0.04	0.023	0.03	0.01	0.05
2H-6, 113-123	14.88	0.04	0.021	0.03	0.01	0.06
3H-1, 140-150	17.15	0.03	0.014	0.02	0.01	0.10
3H-3, 140-150	20.15	0.03	0.013	0.02	0.01	0.09
3H-5, 140-150	23.15	0.02	0.011	0.01	0.01	0.08
4H-1, 140-150	26.65	0.03	0.011	0.03	0.01	0.07
4H-3, 140-150	29.65	0.02	0.010	0.02	0.01	0.12
4H-5, 140-150	32.65	0.02	0.010	0.02	0.01	0.08
5H-2, 134-144	37.59	0.02	0.011	0.02	0.01	0.12
5H-4, 140-150	40.59	0.02	0.011	0.02	0.01	0.12
5H-6, 60-70	42.79	0.02	0.010	0.02	0.01	0.10
6H-1, 140-150	45.65	0.02	0.010	0.02	0.01	0.09
6H-2, 134-144	47.09	0.02	0.010	0.02	0.01	0.08
6H-3, 140-150	48.58	0.02	0.012	0.02	0.01	0.09
6H-4, 140-150	50.08	0.02	0.008	0.02	0.02	0.13
9H-1, 140-150	63.55	0.05	0.002	0.02	0.13	1.12
9H-2, 140-150	65.05	0.03	0.002	0.02	0.05	0.41
329-U1370F-						
5H-3, 140-150	39.65	0.03	0.014	0.02	0.01	0.10
5H-5, 140-150	42.65	0.02	0.014	0.01	0.01	0.09
6H-2, 140-150	47.65	0.02	0.013	0.02	0.01	0.06
6H-4, 140-150	50.65	0.02	0.013	0.01	0.01	0.09
7H-1, 140-150	55.65	0.04	0.007	0.02	0.03	0.28
7H-3, 140-150	58.65	0.07	0.006	0.01	0.08	0.62
7H-5, 140-150	61.65	0.07	0.002	0.01	0.08	0.67
7H-6, 140-150	63.15	0.33	0.005	0.01	0.42	3.47
7H-6, 20-21	61.23	0.06	0.002	0.01	0.08	0.68
7H-6, 134-135	62.37	10.84	BD	0.00	11.29	94.08
7H-7, 44-45	62.97	6.82	BD	0.01	7.02	58.51
7H-CC, 8-9	63.14	10.91	0.006	0.01	11.36	94.62
329-U1370D-						
8H-1, 96-97	63.97	10.37	0.007	0.01	10.98	91.48
8H-2, 96-97	65.47	0.10	0.008	0.02	0.12	1.00
8H-3, 96-97	66.97	0.08	0.004	0.03	0.20	1.67
8H-4, 96-97	68.47	0.06	0.004	0.01	0.17	1.39

TC = total carbon, TN = total nitrogen, TOC = total organic carbon, TIC = total inorganic carbon. BD = below detection.

Table T13. Cell counts by manual microscopy in sediment, Site U1370.

Core, section, interval (cm)	Depth (mbsf)	Cell count (\log_{10} cells/cm ³)					
		Extracted				Nonextracted	
		Count 1	Count 2	Count 3	Count 4	Count 1	Count 2
329-U1370E-							
1H-1, 35-43	0.35	4.5	4.5				
1H-1, 83-90	0.83	4.5	4.5				
1H-1, 135-140	1.35	3.9	3.9	4.0	4.1	5.3	5.0
1H-2, 30-40	1.80						
1H-2, 80-90	2.30						
1H-2, 135-140	2.85					BD	BD
1H-3, 30-40	3.30						
1H-3, 80-90	3.80						
1H-3, 125-130	4.25					BD	BD
1H-4, 147-152	5.97	3.1	3.3				
2H-1, 135-140	7.55	2.8	2.7				
2H-2, 135-140	9.05						
2H-3, 135-140	10.55						
2H-4, 125-130	11.95						
2H-5, 135-140	13.55						
2H-6, 118-123	14.88						
3H-1, 135-140	17.05	2.9	3.1				
3H-2, 135-140	18.55						
3H-3, 135-140	20.05						
3H-4, 125-130	21.45						
3H-5, 135-140	23.05						
3H-6, 53-58	23.73						
4H-1, 135-140	26.55	3.3					
4H-2, 135-140	28.05						
4H-3, 135-140	29.55						
4H-4, 125-130	30.95						
4H-5, 135-140	32.55						
4H-6, 50-56	33.20						
5H-1, 135-140	36.05	3.4	2.9	2.9	2.9		
5H-2, 129-134	37.49						
5H-3, 135-140	38.99						
5H-4, 125-130	40.39						
5H-5, 135-140	41.99						
5H-6, 55-60	42.69						
6H-1, 135-140	45.55						
6H-2, 124-134	46.94						
6H-3, 135-140	48.48						
6H-4, 135-140	49.98						
6H-5, 95-100	51.08						
8H-2, 135-140	58.30						
8H-3, 135-140	59.80						
8H-4, 125-130	61.20						
8H-5, 135-140	62.80						
9H-1, 135-140	63.45						
8H-6, 135-140	64.30						
9H-2, 135-140	64.95						
9H-CC, 29-36	71.79	2.3	2.7				
329-U1370F-							
5H-3, 135-140	39.55						
5H-4, 135-140	41.05						
5H-5, 135-140	42.55						
6H-2, 135-140	47.55	BD					
6H-3, 135-140	49.05						
6H-4, 135-140	50.55						
6H-5, 135-140	52.05						
7H-1, 135-140	55.55	BD	BD	2.6	2.7		
7H-2, 135-140	57.05						
7H-3, 135-140	58.55						
7H-4, 125-130	59.95						
7H-5, 135-140	61.55						
7H-6, 135-140	63.05	BD	BD				

BD = below detection. Blank cells = no count (will be counted postexpedition).

Table T14. Samples to be analyzed postexpedition for virus-like particle counts, Site U1370.

Core, section, interval (cm)	Depth (mbsf)
329-U1370E-	
1H-1, 135-140	1.35
1H-2, 30-40	1.80
1H-2, 80-90	2.30
1H-2, 135-140	2.85
1H-3, 30-40	3.30
1H-3, 80-90	3.80
1H-3, 125-130	4.25
1H-4, 147-152	5.97
2H-1, 135-140	7.55
2H-2, 135-140	9.05
2H-3, 135-140	10.55
2H-4, 125-130	11.95
2H-5, 135-140	13.55
2H-6, 118-123	14.88
3H-1, 135-140	17.05
3H-2, 135-140	18.55
3H-3, 135-140	20.05
3H-4, 125-130	21.45
3H-5, 135-140	23.05
3H-6, 53-58	23.73
4H-1, 135-140	26.55
4H-2, 135-140	28.05
4H-3, 135-140	29.55
4H-4, 125-130	30.95
4H-5, 135-140	32.55
4H-6, 50-56	33.20
5H-1, 135-140	36.05
5H-2, 129-134	37.49
5H-3, 135-140	38.99
5H-4, 125-130	40.39
5H-5, 135-140	41.99
5H-6, 55-60	42.69
6H-1, 135-140	45.55
6H-2, 124-134	46.94
6H-3, 135-140	48.48
6H-4, 135-140	49.98
6H-5, 95-140	51.08
8H-2, 135-140	58.30
8H-3, 135-140	59.80
8H-4, 125-130	61.20
8H-5, 135-140	62.80
9H-1, 135-140	63.45
8H-6, 135-140	64.30
9H-2, 135-140	64.95
329-U1370F-	
1H-2, 30-40	1.80
1H-3, 80-90	3.80
3H-2, 60-70	18.30
5H-2, 60-70	37.30
5H-3, 135-140	39.55
5H-4, 135-140	41.05
5H-5, 135-140	42.55
6H-2, 135-140	47.55
6H-3, 135-140	49.05
6H-4, 135-140	50.55
6H-5, 135-140	52.05
7H-1, 135-140	55.55
7H-2, 135-140	57.05
7H-3, 135-140	58.55
7H-4, 125-130	59.95
7H-5, 135-140	61.55
7H-6, 30-40	62.00
7H-6, 135-140	63.05
8H-1, 20-30	63.90

Table T15. List of samples and culture media used for onboard cultivation experiments, Site U1370.

Core, section	Media used for cultivation
329-U1370F-	
1H-1	SPG-JL
1H-2	Mmm1, Mmm2, SPG-ASW, MA, MB, MR2A, SPG-JL, SLURRY
1H-3	Mmm1, Mmm2, SPG-ASW, MA, MB, MR2A, SPG-JL, SLURRY
1H-4	MA, MB, MR2A, SLURRY
2H-1	MA, MB, MR2A, SLURRY
2H-3	SLURRY
2H-5	SLURRY
3H-2	Mmm1, Mmm2, SPG-ASW, MA, MB, MR2A, SPG-JL, SLURRY
3H-5	SLURRY
4H-3	MA, MB, MR2A, SPG-JL
4H-5	SLURRY
5H-2	Mmm1, Mmm2, SPG-ASW, MA, MB, MR2A, SPG-JL, SLURRY
5H-5	SLURRY
6H-3	MA, MB, MR2A
7H-2	MA, MB, MR2A, SPG-JL, SLURRY
7H-4	MA, MB, MR2A, SPG-JL, SLURRY
7H-5	MA, MB, MR2A, SPG-JL, SLURRY
7H-6	Mmm1, Mmm2, SPG-ASW, MA, MB, MR2A, SPG-JL, SLURRY
8H-1	Mmm1, Mmm2, SPG-ASW, MA, MB, MR2A, SPG-JL

SLURRY = sediment stored anoxically in flushed serum bottles or in syringes kept in sterile foil bags. For more detailed information on the media, see “[Microbiology](#)” in the “Methods” chapter (Expedition 329 Scientists, 2011a).